



University
of Glasgow

<https://theses.gla.ac.uk/>

Theses Digitisation:

<https://www.gla.ac.uk/myglasgow/research/enlighten/theses/digitisation/>

This is a digitised version of the original print thesis.

Copyright and moral rights for this work are retained by the author

A copy can be downloaded for personal non-commercial research or study,
without prior permission or charge

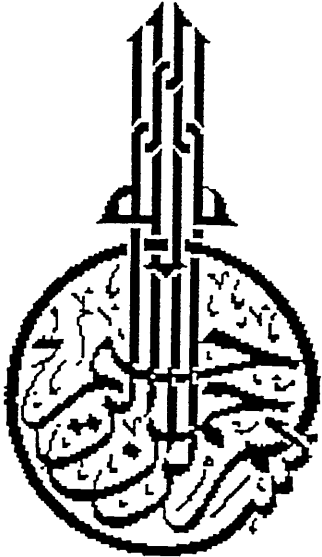
This work cannot be reproduced or quoted extensively from without first
obtaining permission in writing from the author

The content must not be changed in any way or sold commercially in any
format or medium without the formal permission of the author

When referring to this work, full bibliographic details including the author,
title, awarding institution and date of the thesis must be given

Enlighten: Theses

<https://theses.gla.ac.uk/>
research-enlighten@glasgow.ac.uk



In the name of Allah, the Beneficent, the
Merciful.

ProQuest Number: 11011466

All rights reserved

INFORMATION TO ALL USERS

The quality of this reproduction is dependent upon the quality of the copy submitted.

In the unlikely event that the author did not send a complete manuscript and there are missing pages, these will be noted. Also, if material had to be removed, a note will indicate the deletion.



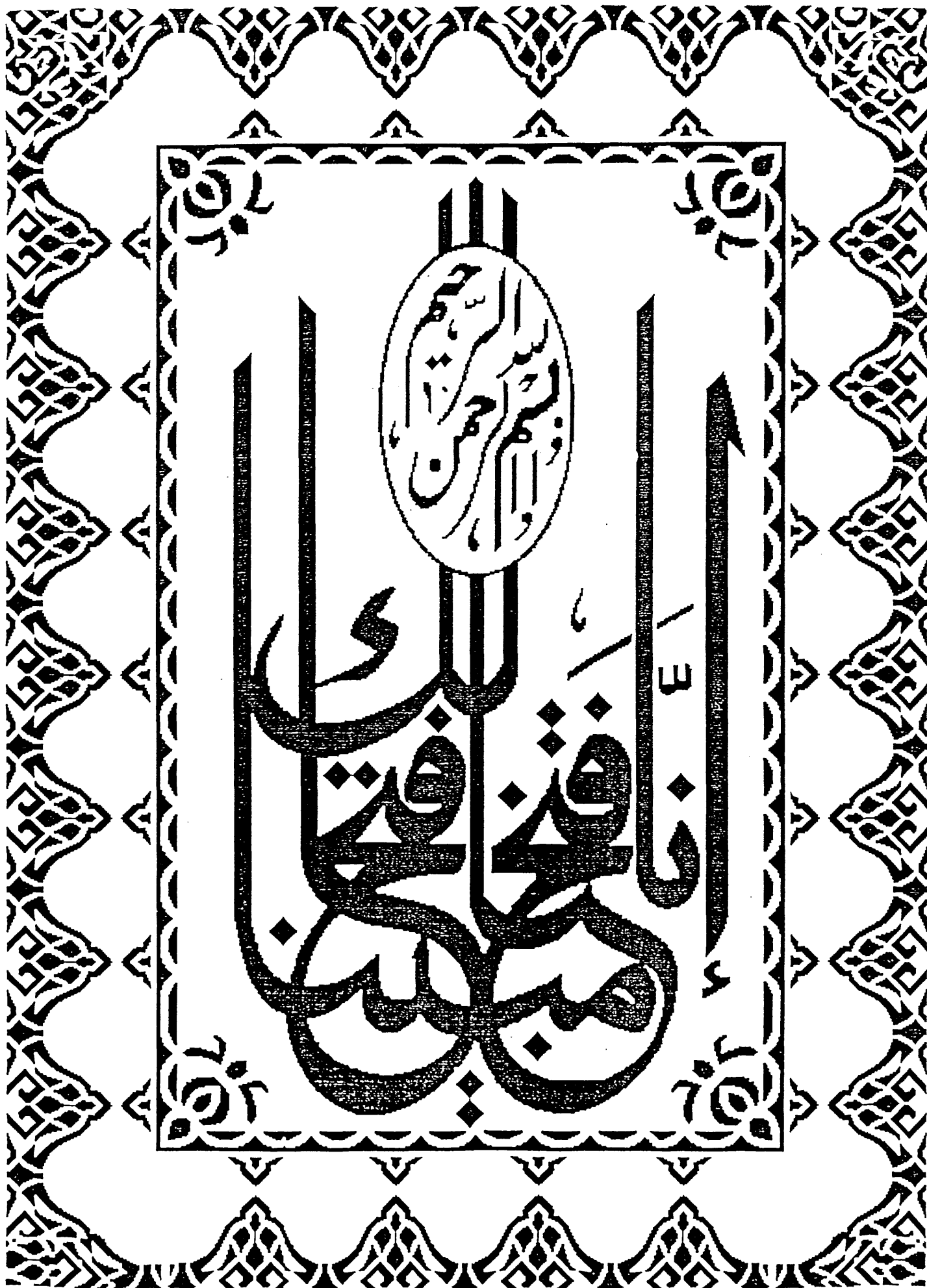
ProQuest 11011466

Published by ProQuest LLC (2018). Copyright of the Dissertation is held by the Author.

All rights reserved.

This work is protected against unauthorized copying under Title 17, United States Code
Microform Edition © ProQuest LLC.

ProQuest LLC.
789 East Eisenhower Parkway
P.O. Box 1346
Ann Arbor, MI 48106 – 1346



DECLARATION

The material presented in this thesis is the result of independent research by the author undertaken between October 1989 and February 1992 at the Department of Geology and Applied Geology, University of Glasgow. Any published papers have been given full acknowledgment in the text.

Fathi M A Ghrouda

Department of Geology and Applied Geology, University of Glasgow.

**SEISMIC INTERPRETATION AND REPROCESSING OVER THE
WADI FIELD NC 149, SIRTE BASIN, LIBYA.**

by

FATHI MOHAMED AHMED GHROUDA

B.Sc. (1980)- Faculty of petroleum and mining Engineering - Tripoli

**Thesis submitted for the Degree of Master of Science (by research) at the
Department of Geology and Applied Geology, University of Glasgow.**

February 1992

Dedicated to my parents and my family

ACKNOWLEDGEMENTS

First, I wish to express my thanks to the management of Sirte Oil Company and in particular the management of the exploration for giving me this opportunity, for the scholarship, and for the release of the data without which this research would not have been possible and. I would like to extend my thanks to the training department for their help and financial support.

I would like to thank my supervisor, Professor Dave K. Smythe, for his guidance and support. Also for his considerable help, constructive advice, and assistance throughout this project.

I am grateful to Dr. Doyle R. Watts for reading the thesis, for his corrections, comments, and suggestions. I also thank Dr. J. J. Doody for his suggestions.

My thanks also go to the people in Sirte Oil Company in Woking office (London), in particular to Dr Reza Sedghat for providing me with the data and to Mr Ahmed Gabaili for his help and understanding. My appreciation goes to the technical staff at the Department of Geology & Applied Geology; in particular to Mr. Robert T. Cumberland, and to Mr. Jim Kavanagh for their computer help.

My especial thanks to postgraduate student friends and colleagues in the Department for their help; in particular to Mohamed Bolfoul and Najim Ben Ayad for their discussions and help.

I would like to take this opportunity to thank my parent, my wife and sons, and daughter patience and understanding.

	Page
Contents	i
List of Figures	v
List of Tables	xi
Summary	xv

Chapter 1 Introduction

1.1 Introduction	2
1.1.1 Wadi field location	2
1.1.2 Exploration history	2
1.2 Geology of Libya	5
1.2.1 Summary of the geology	5
1.2.2 Structural elements of Libya	8
1.2.3 Basins in Libya	9
1.2.4 Geology of Wadi field	13
1.3 Available data	15
1.3.1 Seismic lines	15
1.3.2 Well data	16
1.3.3 Check shot surveys	18
1.3.4 Other data	18
1.4 Aims of the study	24

Chapter 2 Seismic reprocessing

2.1 Introduction	26
2.2 Field parameters	27
2.3 Static corrections	29
2.3.1 Uphole method	30

	Page
2.3.2 Datum plane	32
2.4 Static computation	32
2.5 Processing sequence	33
2.5.1 Introduction	33
2.6 Spherical divergence	37
2.7 AGC (Automatic gain control)	39
2.8 Mute	39
2.9 Deconvolution	42
2.10 Common depth point (CDP)	46
2.11 Applying static correction	47
2.12 Rawstack display	47
2.13 Velocity analysis	49
2.13.1 Continuous velocity estimation	49
2.13.2 Velocity function stack	50
2.14 Residual static correction	52
2.14.1 Introduction	52
2.15 Normal move-out correction	57
2.15.1 NMO stretching	61
2.16 Stacking	61
2.17 Deconvolution and filtering after stack.....	61
2.18 Frequency filttering after stack	64
2.19 Final stack section	66
2.20 Migration	68
2.20.1 Introduction	68

	Page
Chapter 3 Seismic interpretation	
3.1 Seismic interpretation	81
3.1.1 Introduction	81
3.1.2 Definition	81
3.2 Interpretation steps	82
3.2.1 Well tie	82
3.2.2 Closing loops	88
3.2.3 Picking and posting the data	88
3.3 Problems in interpretation of the data	90
3.3.1 Basin style	90
3.3.2 Faulting	92
3.4 Time structure maps	98
3.4.1 Grabens	103
3.4.2 Compaction synclines	103
3.5 Isochron maps	105
3.5.1 Introduction	105
3.5.2 The structure	106
3.6 Hydrocarbon reservoirs	111
3.6.1 Structural traps	111
3.6.2 Stratigraphic traps	111
3.6.4 Reservoir rocks	112
3.5.5 Nubian	112
3.6.6 Meem Member	112
3.7 Hydrocarbon entrapment	113
3.7.1 Source rock and oil migration	113
3.10 Back-stripping	117

	Page
Chapter 4 Velocity and depth conversion	
4.1 Introduction	124
4.2 Check shot survey or well shooting	124
4.3 Seismic velocities	126
4.3.1 Interval velocity	126
4.3.2 Average velocity	132
4.3.3 RMS velocity	132
4.4 Factors effecting velocity	133
3 4.1 Lithology	133
4.4.2 Porosity	133
4.5 Interpretation of velocity data	136
4.6 Depth conversion	138
4.7 Depth maps	147
4.7.1 Nubian structure map	147
4.7.2 Meem structure map	149
Chapter 5 Conclusions	
5.1 Conclusion	152
5.2 Suggestions and recommendations	158
References	160
Appendices	162

List of Figures**Chapter 1**

Fig 1.1	Wadi field location map	3
Fig 1.2	Major tectonic elements of Sirte Basin, Libya	4
Fig 1.3	Shot point map of the Wadi field	6
Fig 1.4a	Map showing the major structural elements of the central Sahara in early Palaeozoic times	10
Fig 1.4b	Map showing the major structural elements of the central Sahara in Late Palaeozoic and Mesozoic times	10
Fig 1.5	The major basins in Libya	11
Fig 1.6	Generalized columnar stratigraphic section in the Hagfa Trough area	14

Chapter 2

Fig 2.1	Source array, receiver array, and spread diagram	28
Fig 2.2a	Uphole shooting	30
Fig 2.2b	Uphole time depth curve showing the weathering and sub weathering velocity (seismic line V07-85 station 440)	31
Fig 2.3	Weathering and sub-weathering velocity for uphole survey along line V07-85	34
Fig 2.4	Shot point gathers showing the effect of wind on the noise content of the data	36
Fig 2.5	Shot gather before and after spherical divergence	38

	Page
Fig 2.6 Shot gather before and after applying automatic gain control (AGC)	40
Fig 2.7 Shot gather before and after applying mute correction	41
Fig 2.8 Frequency analysis on shot point 300, traces 1, 48, and 95	43
Fig 2.9 Shot gather before and after applying deconvolution	45
Fig 2.10 Preliminary processing chart	46
Fig 2.11a Common depth point model for horizontal layer (one layer case)	48
Fig 2.11b Four trace gather for 3 layers before and after NMO correction	48
Fig 2.12 Raw stack section (stacked with one layer velocity picked from the previous processing)	50
Fig 2.13 Velocity spectra for selected CDP gathers	51
Fig 2.14 A constant velocity stack. The horizontal axis is the velocity increasing to the right and decreasing to the left	53
Fig 2.15 Processing flowchart with residual static correction	57
Fig 2.16 Velocity spectra after residual statics are applied	58
Fig 2.17 CDP gathers before and after applying NMO correction	60
Fig 2.18 CDP gather before and after mute correction	62

	Page
Fig 2.19 Part of stacked section before, after deconvolution and band-pass filter	63
Fig 2.20 Stacked data with various band-pass filtered version	65
Fig 2.21 Stacked data with various band-pass filtered version	66
Fig 2.22 Part of stacked section with different filters applied	67
Fig 2.23 Final stack section (no deconvolution applied after stack)	70
Fig 2.24 Final stack section (with deconvolution applied after stack)	70
Fig 4.25 Final stack section (stacked with velocity picked using velocity function)	71
Fig 2.26 Seismic response from syncline	72
Fig 2.27 FK migration section with different migration velo -cities applied	74
Fig 2.28 Migrated final stack section	75
Fig 2.29 Two interpreted seismic sections showing the difference between Western Geophysical section and SierraSEIS section	77
Fig 2.30 Processing flow chart of the reprocessed section	78
Fig 2.31 Label summarizing processing sequence carried out by Western Geophysical in 1985	79

	Page
Chapter 3	
Fig 3.1 Example of normal and reversed polarity minimum phase wavelet	84
Fig 3.2 Examples of the data for different surveys and the events picked for every formation mapped	89
Fig 3.3 Graben hydrocarbon occurrences and structural style	91
Fig 3.4 Seismic line V07-85	93
Fig 3.5 Seismic line V35-85	96
Fig 3.6 Seismic line V13-85	97
Fig 3.7 Time structure map top Gargaf Formation	99
Fig 3.8 Time structure map top Nubian Formation	100
Fig 3.9 Time structure map top Zmam Formation	101
Fig 3.10 Time structure map top Zelten Formation	102
Fig 3.11 Seismic line V11-85	104
Fig 3.12 Isochron map between Gargaf and Nubian	107
Fig 3.13 Isochron map between Nubian and Zmam	108
Fig 3.14 Isochron map between Zmam and Zelten	109
Fig 3.15 Seismic line F41-71	114
Fig 3.16 Seismic line V14-85	115
Fig 3.17 Palinspastic reconstructions across the Wadi field (lower part of the section)	118
Fig 3.17 (continued). Palinspastic reconstructions across the Wadi field (upper part of the section)	119
Fig 3.18 Cross - section through the Wadi field	121

	Page
Fig 3.19 Crosssection showing the relation between the seismic and well data	122
 Chapter 4	
Fig 4.11 Well shooting technique	125
Fig 4.2 (D6-149) Relation between time depth curve, Average velocity, Interval velocity, and RMS velocity	127
Fig 4.3 (D7-149) Relation between time depth curve, Average velocity, Interval velocity, and RMS velocity	128
Fig 4.4 (D8-149) Relation between time depth curve, Average velocity, Interval velocity, and RMS velocity	129
Fig 4.5 (D9-149) Relation between time depth curve, Average velocity, Interval velocity, and RMS velocity	130
Fig 4.6 Relation between time depth curve, Average velocity, Interval velocity, and RMS velocity	131
Fig 4.7 P-wave velocity for various lithologies	134
Fig 4.8 Relation between average velocity calculated from interval velocity and average velocity calculated from wells	140
Fig 4.9 Relation between velocity and depth for all the wells	144
Fig 4.10 Average velocity map top Meem member	145
Fig 4.11 Average velocity map top Nubian	146
Fig 4.12 Structure map top Nubian	148
Fig 4.13 Structure map top Meem member	150

	Page
Chapter 5	
Fig 5.1 Time structure and structure maps top Nubian showing line F27-70 and 88-113	156
Fig 5.2 Structure map top Meem showing location of well D4 and ZZZ1	157

	Page
List of Tables	
Chapter 1	
Table 1.1 Well name, drilling depths and subsea depths	17
Table 1.2 (D6-149) Drilling depth, subsea depth and corresponding time from surface and from datum	17
Table 1.3 (D7-149) Drilling depth, subsea depth and corresponding time from surface and from datum	20
Table 1.4 (D8-149) Drilling depth, subsea depth and corresponding time from surface and from datum	21
Table 1.5 (D9-149) Drilling depth, subsea depth and corresponding time from surface and from datum	22
Table 1.6 (K1-149) Drilling depth, subsea depth and corresponding time from surface and from datum	23
Chapter 2	
Table 2.1 Comparison between static calculated using sabkha and using uphole method	33
Chapter 3	
Table 3.1 Link between wells with check shot survey and seismic data	83
Table 3.2 Type of data and year of acquisition, display polarity and and deconvolution	84
Table 3.3 Well name, seismic line passing through the well	86

	Page
Table 3.4 Formation tops, two-way time in the wells and seismic with the mist-ies	87
Table 3.5 Well names and the formation thicknesses in the Wadi field	110

Chapter 4

Table 4.1 Well name, formation depth, two way time, one way time for Nubian Formation	141
Table 4.2 Well name, formation depth, two way time, one way time for Meem Formation	142

	Page
Appendix 1	
Table 1.1 Shot point number and the edited traces	164
Appendix 2	
Table 2.1 Shot point number and formation tops in ms	167
Table 2.2 Shot point number and isochron time between formation tops calculated using program Isochron	168
Appendix 3	
Table 3.1 (D6-149) Average, interval, and rms velocities calculated formcheck shot survey using program Average Velocity	171
Table 3.2 (D7-149) Average, interval, and rms velocities calculated form check shot survey using program Average Velocity	172
Table 3.3 (D8-149) Average, interval, and rms velocities calculated form check shot survey using program Average Velocity	173
Table 3.4 (D9-149) Average, interval, and rms velocities calculated form check shot survey using program Average Velocity	174
Table 3.5 (K1-149) Average, interval, and rms velocities calculated form check shot survey using program Average Velocity	175

	Page
Appendix 4	
Table 4.1 Time and rms velocity as shown in the seismic section for Nubian formation reflector	180
Table 4.3 Average velocities calculated from the rms velocities for Nubian reflector, calculated using program Avelocity	179

SUMMARY

The Wadi field is located in the Hagfa Trough, where exploration targets are very deep, compared with the other exploration targets on the platform. Seismic data are poor for the deep horizons, and the deepest horizon for reliable mapping is the top Upper Cretaceous Zmam Formation. Twelve wells have been drilled within the Wadi field structure, the main reservoir being penetrated by eleven wells. Five wells have a check shot survey (D6, D7, D8, D9, and K1-149). The field is seismically defined on the basis of a 2-D seismic survey. One line (V07-85) has been reprocessed using the uphole static correction. The uphole static has improved the image in the area where the elevation changes markedly. The check shot surveys from wells D6, D7, D8, D9, and K1-149 are used to identify the reflectors. Eight reflectors have been picked on the seismic sections. Times picked from four horizons (top Gargaf, Nubian, Zmam and Zelten respectively) have been contoured. The maps show that the structure is subdivided into a number of interlinked grabens and half-grabens, separated by structurally high horst or footwall highs formed by normal faults trending NW-SE, with at least one likely growth fault. The isochron maps for the Gargaf-Nubian, Nubian-Zmam and Zmam-Zelten intervals all show thinning on the crest of the structure, and thickening on the flank of the structure towards the grabens.

The tilting is responsible for the entrapment of the oil in the main reservoir (Nubian sandstone) against the Socna shale. To understand the timing of faulting in the study area, the back-stripping technique has been used. Wells D6 and D7-149 show an average velocity decrease with depth at Heira (Palaeocene) and Socna (Upper Cretaceous) horizons. D9-149 shows velocity decrease with depth at the Socna (Upper Cretaceous)

Cretaceous) reflector. The average velocity calculated using the relation between average and interval velocities is unreliable for the depth conversion. All the average velocities calculated using the time from the seismic lines are used for the depth conversion. The structure map for the top Nubian shows the structure subdivided into four blocks (A, B, C, D).

Chapter 1

Introduction and geology of Libya

- 1.1 Introduction
- 1.2 Geology of Libya
- 1.3 Available data
- 1.4 Aims of the study

1.1 INTRODUCTION

1.1.1 Wadi field location

The Wadi field, the subject of this study, is located in the Sirte Basin, in the middle eastern part of concession NC 149, within the Hagfa Trough (Fig 1.1), 24 km southwest of the Nasser oil field in concession 6.

The location and the main structures of the central Sirte Basin are shown in Fig 1.2. A major northwest-trending system of faults traverses the Sirte Basin and controls the trends and linearity of separate sedimentary troughs. These troughs, which measure up to 400 km in length and 150 km in width, are sufficiently large to qualify for the term basin. The term trough has the connotation of marked linearity, commonly resulting from the structural control of elongate graben structures within a linear trend of major faults. Each trough in the Sirte Basin has its own minor structural framework of faults, and the framework of each trough is a part of the major structural framework of the Sirte Basin (Conybeare 1979).

1.1.2 Exploration history

A total of twelve wells have been drilled on the Wadi structure. The main reservoir (Nubian equivalent) was penetrated by eleven wells. Three wells were drilled by Mobil Oil Company in Concession 13. In 1962 Mobil drilled the exploratory well K1-13, followed by two other wells K2-13 and K3-13. These wells were shallow and did not reach the main reservoir in

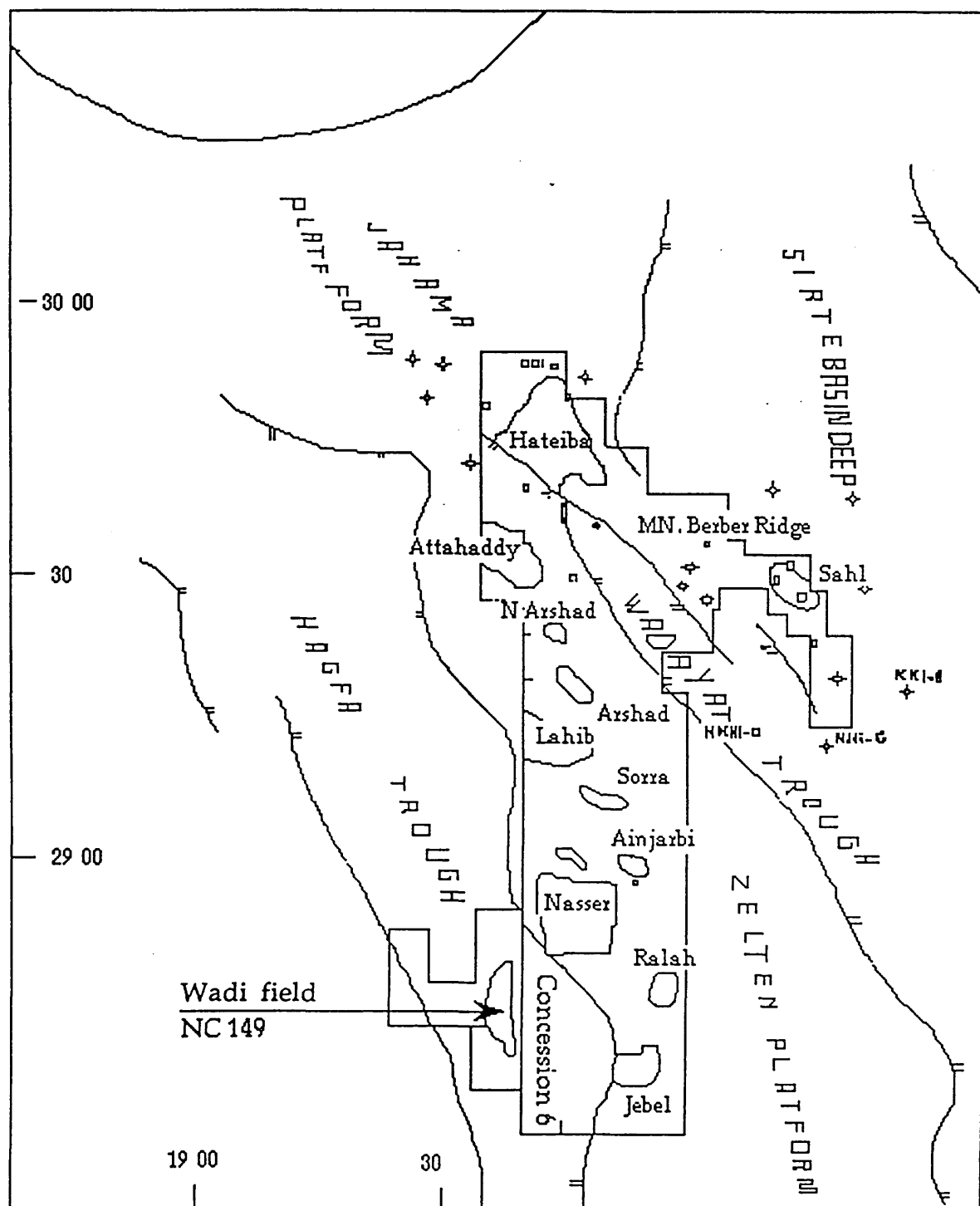


Fig 1.1 Wadi field location map

Scale 1:1,000,000

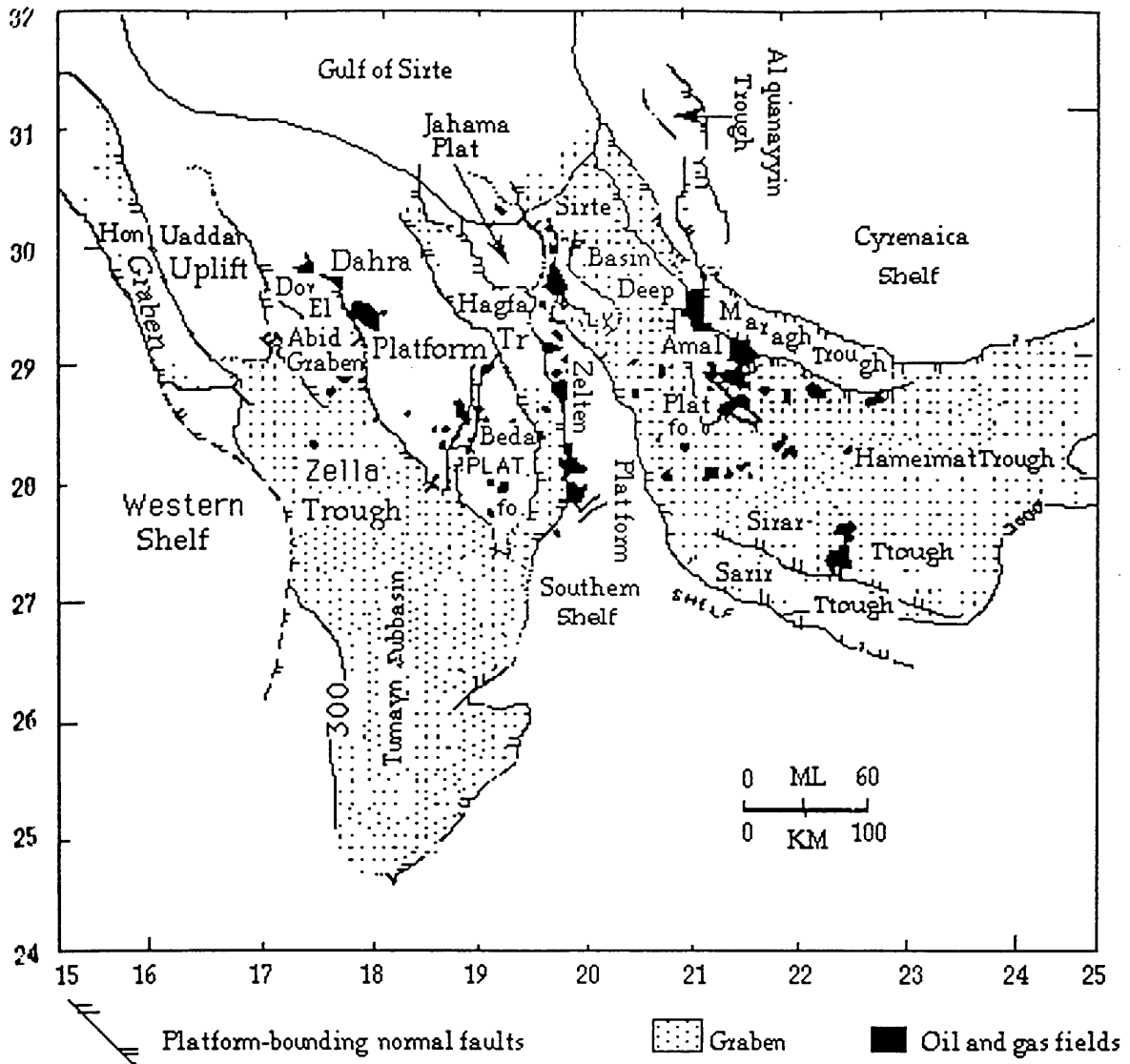


Fig. 1.1 Major tectonic elements of the Sirte Basin, Libya. Five major northwest-trending grabens have formed an unusually wide basin complex in the northwest portion of the basin and provide several sites for maturation of hydrocarbon (after Parson 1980).

the Lower Cretaceous. Aquitaine drilled five wells (D1, D2, D3, D4 and D5-104). D1 was abandoned in the Socna Formation. D2 and D3-104 were tested for oil in the Lower Cretaceous quartzitic sandstone and D4-104 was tested for oil in the Meem member (Palaeocene). Recently, Sirte Oil Company has deepened two wells D1, K1-149 and drilled six more wells (D6, D7, D8, D9, D10, and D11-149). The seismic database consists of 24 2-D seismic lines (484 km length in total), acquired between 1971-1988. Four kinds of 2-D seismic reflection data are available in Wadi and south Wadi field. A shot-point map is presented in Figure 1.3.

1.2 GEOLOGY OF LIBYA

1.2.1 Summary of the geology

Libya is a cratonic basin on the northern fringe of the African shield situated between the stable African shield in the south and the active Mediterranean Tethys area to the north. The cratonic foundation is Precambrian, which crops out north of the Tibesti mountains, around Jebel Auenat, in the centre of the Gargaf uplift, and in some places along the eastern flanks of the Murzuck Basin. There are thick sequences of moderately deformed Palaeozoic rocks, except in the northwest and northeast.

The Mesozoic sedimentary rocks are comparatively thin (approximately 1.2 km in the Sirte embayment and northern Cyrenaica). Tertiary and Quaternary extrusive rocks occupy large areas in south central-Fezzan and north Tripolitania. A continental environment existed in south Libya from Late Palaeozoic time to possibly the middle of Cretaceous time,

during which period several thousand metres of sediment were deposited. The basin was active from Late Cretaceous time to Tertiary time, when several thousand metres of marine sediments were deposited in the Sirte Basin and part of south Cyrenaica. The narrow coastal plains of Libya are generally covered by marine and continental beds of Quaternary age, and the greater part of the Libyan desert is covered by immense gravel plains and sand dune areas which were also formed during Quaternary time.

The Precambrian rocks of Libya are mainly igneous and metamorphic rocks consisting of orthogneisses, schist, phyllite, quartzite, diorite, granodiorite and granite. The metamorphic rocks are intensely folded and intruded by granites. Their most extensive outcrop is in the crest of the Gargaf Arch, where most of the exposed basement rocks are of Precambrian age.

Libya has lain along the margin of numerous transgressions from the north-east and north since the Cambrian. The stratigraphic section in the north and north-western part of the country consists of marine sediment. Cambrian and Ordovician rocks are exposed in many places in the south of the country. The continental conditions were interrupted in western Libya by a brief marine incursion. The presence of an angular unconformity at some places within the sequence has led to the general belief that the lower beds are of Precambrian age. During the Palaeozoic several transgressions inundated all or most of present day Libya. The basement consists chiefly of igneous and metamorphic rocks, but locally sedimentary rocks of probable Cambrian or Ordovician and of Silurian age are known. Whether or not those seas once covered this area, presumably either an Early or Late

Palaeozoic (Hercynian) uplift caused the removal of most of whatever Palaeozoic strata may have been represented.

Transgressions are of special importance. A variety of thick sediments filled the basins in Ordovician-Devonian time. The Devonian in southern Libya is chiefly continental sandstone, through some marine beds are present on the east and west flank of the Murzuk basin.

In the Carboniferous a marine transgression also invaded most of the country, with the exception of the southeastern region. Since the end of the Carboniferous, only continental sediments have been deposited in southern Libya.

During Permian and Mesozoic times, transgressions from the north reached only part of northern Libya. The Upper Palaeozoic rocks of Libya are mainly marine shale, siltstone, sandstone, limestone and continental sandstone. In Fezzan they are mainly marine-continental to predominantly continental facies. In western Libya, Mesozoic strata are chiefly of marine origin, of Triassic and Jurassic age, exposed at the Jebel Nafussa escarpment.

1.2.2 Structural elements of Libya

Intensive folding consolidated the greater part of northern Africa during one or more Precambrian orogenies. Since the Precambrian, epeirogenic movements with block faulting have controlled the structural development.

During Palaeozoic time a system of troughs and uplifts striking NW-SE developed (Fig 1.4a). From the Late Palaeozoic to Early Cretaceous the dominating axes of basin and uplift development were NE-SW and approximately perpendicular to the Early Palaeozoic tectonic trends (Fig 1.4b).

In north Libya these younger elements strike NE-SW. The present shape of the Palaeozoic to Mesozoic basins of Libya is the result of these diverging movements. Finally in Late Cretaceous and Tertiary time, NW-SE striking block faulting accompanied the formation of a system of graben and horsts (Fig 1.1).

During Eocene time subsidence extended across the southern border of the country. Several authors have suggested that during the Palaeocene there was a connection through here between the Mediterranean Sea and Gulf of Guinea.

1.2.3 Basins in Libya

Libya is divided into four basins - the Sirte Basin, Kufra Basin, Ghadames Basin and Murzuk Basin (Fig 1.5).

The Sirte Basin in north-central Libya differs markedly from the neighbouring Murzuk, Kufra, and Ghadames Basins. These basins are broad, essentially unfaulted depressions, that were sites of aggradation throughout much of Mesozoic time. Unlike the latter group, the Sirte Basin is the youngest of the four basins. It formed by large scale subsidence

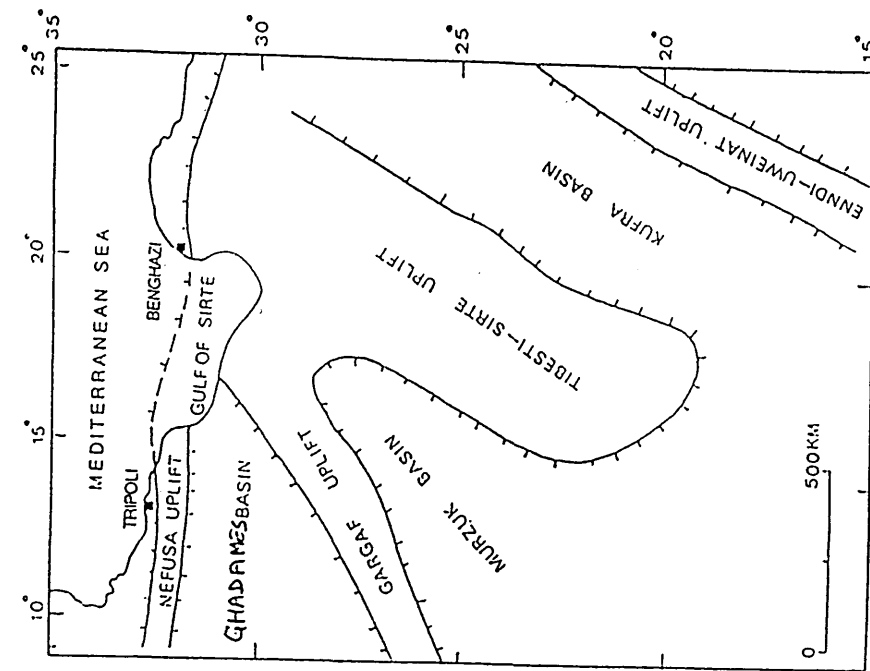


Fig 1.4b Map showing the major structural elements of the central Sahara in Late Palaeozoic and Mesozoic times after Klitzch (1971).

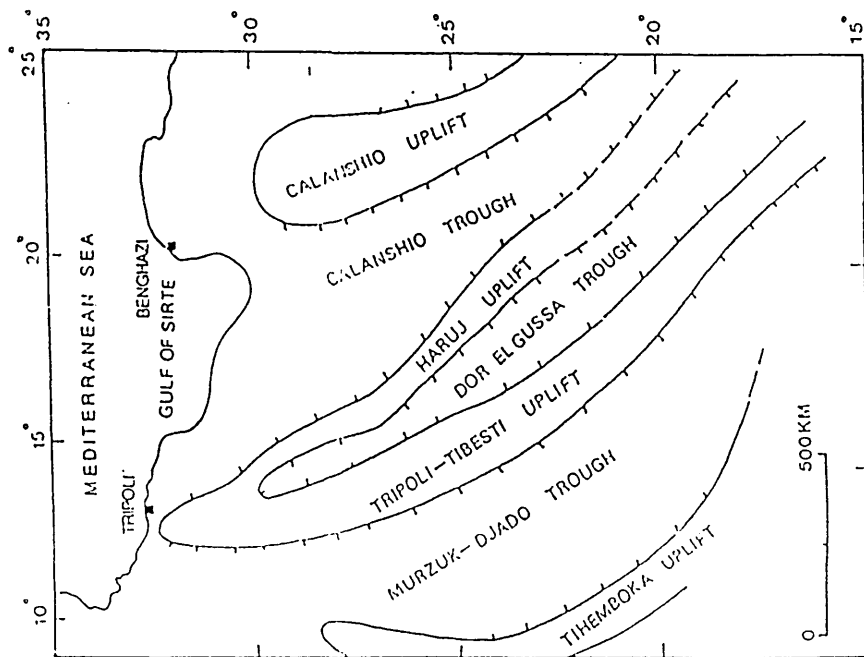


Fig 1.4a Map showing the major structural elements of the central Sahara in Early Palaeozoic times after Klitzch (1971).

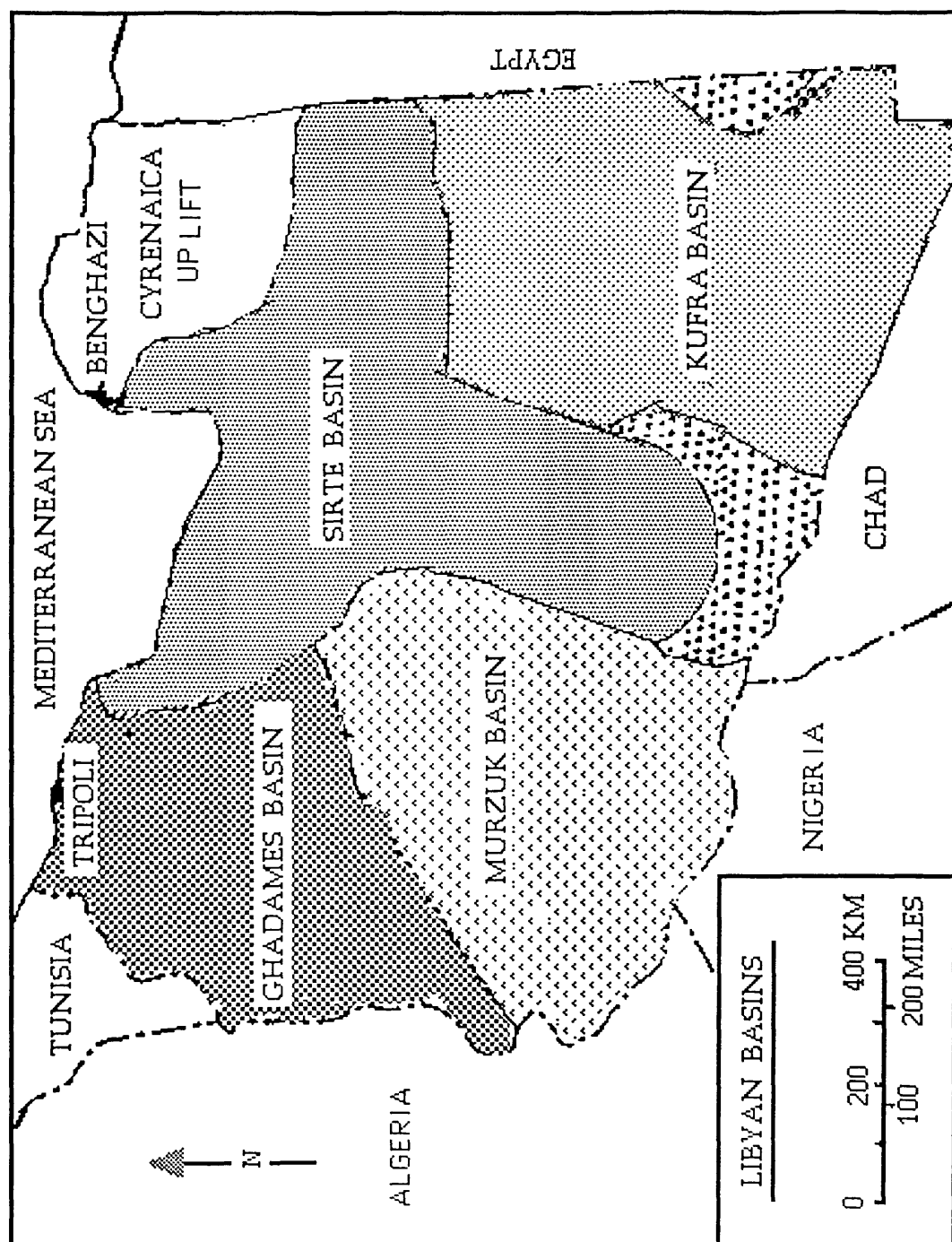


Fig 1.5 The major basins in Libya

and block faulting. Many authors have written about the collapse of the Sirte Basin.

Conant and Goudarzi (1967) suggested that block faulting started in Late Cretaceous time and continued, at least intermittently, to the Miocene and perhaps to the present. Block faulting affected at least the northern part of the Sirte Basin.

Selley (1968) Showed that the complex structural pattern of horsts and grabens in the Sirte Basin began to form in the Late Jurassic-Early Cretaceous, and continued to develop until at least the Miocene and probably into Holocene time.

Burke and Dewey (1974) suggested that the horsts and grabens began to develop during the Early Cretaceous as a result of widespread extension. According to them, this extension developed over a broad zone of strain between two African plates, which led to the collapse of the Sirte Basin arch during the Early Cretaceous.

Parson, Zagaar and Curry (1980) showed that the crustal extension started in the Cretaceous and continued through the Miocene, and has resulted in horsts and grabens as the primary structural form. Van Houten (1983) proposed that it resulted from passage of the area over a fixed mantle hotspot during the early Cretaceous shift in plate motion that presumably produced a change in state of stress within African plate.

Gumati and Kanés (1985) show that the subsidence was continuous throughout Late Cretaceous and Tertiary times, reaching a maximum during the Palaeocene and Eocene, when a major reactivation of the faults occurred.

1.2.4 Geology of the Wadi field

The stratigraphic section of the Wadi field is divided into two major intervals by the intra-Cretaceous unconformity (Fig 1.6). The pre-unconformity sediments of Lower Cretaceous and Cambro-Ordovician age are predominantly non-marine. Above the unconformity, Upper Cretaceous and Tertiary rocks form thick sequences of marine carbonates and shale.

The Wadi field is located within the south central part of the Hagfa Trough near the central part of the palaeo-Sirte Basin arch. As a result, most of the Palaeozoic section of the area was probably eroded (Clifford et al. 1980; Parsons et al., 1980).

The Cretaceous section is divided by the Mid-Cretaceous unconformity into two parts. The lower section represents the lateral equivalent of the Nubian sandstone. In the upper part of the Cretaceous, above the Mid-Cretaceous unconformity (Senonian to Maastrichtian), this section is represented by the thick Socna shale and highly argillaceous Gheriat (Zmam) Formations. Both formations represent deep marine sediment. The Socna shale is the source rock for all the Cretaceous reservoirs and possibly for most of the Tertiary reservoirs.

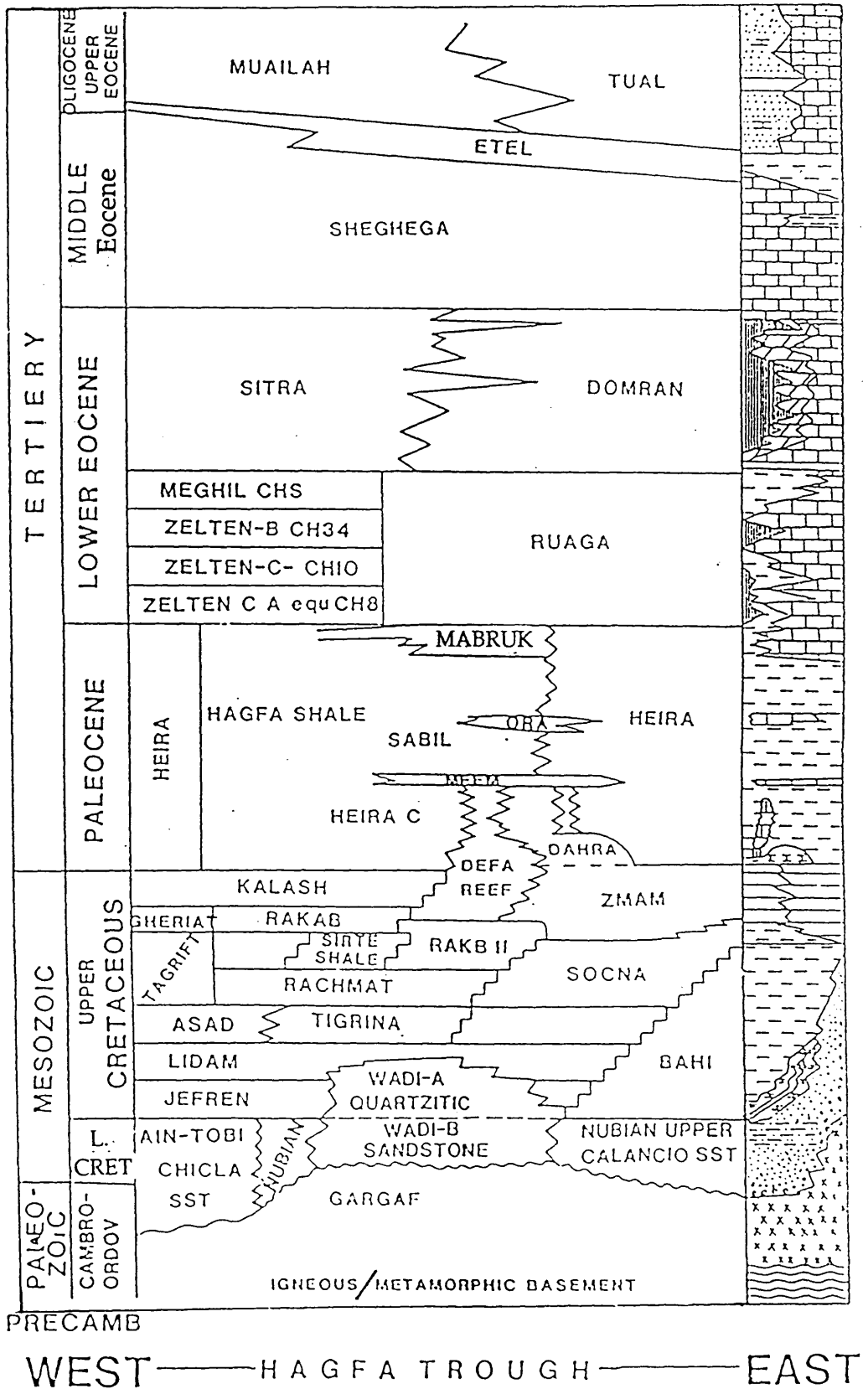


Fig 1.6 Generalized columnar stratigraphic section in the Hagfa Trough area

The Tertiary section is predominantly shale, limestone and dolomite. Sedimentation throughout the section was controlled by mild tectonic movements and gradual subsidence. The depositional environment was mainly deep marine, changing laterally to a shallow marine environment.

The Heira Formation, which underlies the Ruaga limestone, consists of calcareous grey-green shale. Due to facies changes, the formation includes three carbonate members (Mabruk, Ora, Meem). The Heira Formation is a lean source rock in the Wadi field and also forms the seal for the Meem carbonate member.

The Palaeocene to Lower Eocene Ruaga Formation consists of an upper calcareous shale and carbonate called the Megil member and a lower carbonate sequence that includes the Zelten member. The Domran and Sheghega Formations (Lower Eocene to Middle Eocene) rocks consist of dolomitic limestone and limestone.

1.3 AVAILABLE DATA

1.3.1 Seismic lines

In the the study area the following seismic reflection data were available for this study.

a) Six reflection seismic sections, totalling 85 km of 24-fold Dinoseis data, acquired in 1971. These data were shot in southern concession 6. Some of these data are extended to tie the wells in the Wadi field. Quality of the data is fair to good.

b) Four reflection seismic sections, totalling 80 km of 24-fold dynamite data acquired in 1983. These data were shot in southern concession 6. Two of the lines (D75-83 and D76-83) are extended to tie the wells in the Wadi field. Quality of the data is fair to poor.

c) Eleven reflection seismic sections, totalling 234 km of 48-fold Vibroseis (reversed polarity to tie to the other data in the area), acquired in 1985. Quality of the data is fair to good.

d) Five reflection seismic sections, totalling 85 km of 120-fold Vibroseis data, acquired in 1988. Quality of the data is fair to good.

In general the reflection data quality is fair to good in the shallow sedimentary section to the top of the Upper Cretaceous (Zmam Formation), and fair to poor from the Upper Cretaceous (Socna Formation) to deep levels.

A shot-point map (Fig 1.3) shows the entire coverage of the seismic data and the locations of the wells. The survey is basically a 2 * 3 km grid, with more closely spaced lines on the crest of the structure. The other lines shown on the shot-point map were not used because they are not available for this study (some of these data are old and the quality is poor, whereas some of the others were still being processed during the earlier stages of this project).

1.3.2 Well data

Twelve wells have been drilled to date within the field. Table 1.1 shows the formation tops as picked by Sirte Oil Company geologists. Fig 1.3 shows all the wells drilled in the field.

Table 1.1

Well name													
Formation	D1	D2	D3	D4	D5	D6	D7	D8	D9	D10	D11	K1	
Check shot survey available?	NO	NO	NO	NO	NO	YES	YES	YES	YES	NO	NO	YES	
K.B in m	207	188	181	270	170	198	187	230	203	188	224	191	
Sheghega	655 -448	631 -443	639 -458	733 -463	688 -518	636 -438	645 -458	671 -441	646 -443	628 -440	667 -443	639 -448	
Domran	1160 -953	1154 -966	1166 -985	1247 -977	1228 -1058	1154 -956	1168 -981	1183 -953	1168 -965	1153 -965	1173 -949	1168 -977	
Ruaga	1724 -1517	1777 -1589	1762 -1581	1849 -1579	1809 -1639	1698 -1500	1738 -1551	1741 -1511	1761 -1558	1770 -1582	1747 -1523	1773 -1582	
Zelten	1945 -1738	1944 -1756	1980 -1799	2090 -1820	2035 -1865	1917 -1719	1964 -1777	1961 -1731	1654 -1451	1931 -1743	1975 -1751	1952 -1761	
Heira	2094 -1887	2085 -1897	2105 -1924	2259 -1989	2173 -2003	2068 -1870	2102 -1915	2112 -1882	2106 -1903	2051 -1863	2129 -1905	2084 -1893	
Meem	2436 -2229	2347 -2159	2384 -2203	2638 -2368	2560 -2390	2402 -2204	2447 -2260	2446 -2216	2458 -2255	2353 -2165	F	2375 -2184	
Zmam	F	2591 -2403	2633 -2452	2947 -2677	2873 -2703	2665 -2467	2725 -2538	2713 -2483	2633 -2430	2594 -2406	2622 -2398	2620 -2429	
Socna	2766 -2559	2771 -2583	2818 -2637	3236 -2966	3104 -2934	2750 -2552	2910 -2723	2904 -2674	2823 -2620	2775 -2587	2810 -2586	2817 -2626	
Nubian	3242 -3035	3405 -3217	3647 -3466	NP	F	3101 -2903	3469 -3282	3465 -3235	3784 -3581	3458 -3270	3525 -3301	3591 -3400	
Gargaf	3779 -3572	3904 -3716	NP	NP	4065 -3895	3669 -3471	3947 -3760	3600 -3370	NP	4025 -3837	NP	4156 -3965	

Table 1.1 Drilling depths (+) and subsea depths (-) in metres to formation tops as determined by Sirte geologists. Kelly bushing is in metres above sea-level.

NP: well did not penetrate the formation.

F: Formation absent due to fault.

1.3.3 Check shot surveys

Five tables were provided by Sirte Oil Company, showing the depth from the Kelly Bushing (K.B) and the corresponding one-way times from surface for the following wells: D6, D7, D8, D9, K1-149. The depths times and corrected times are shown in Tables 1.2 to 1.6, where:

K.B is the elevation between rotary table and datum plane (sea level).

Subsurface is the drilling depth - KB.

Static is the static correction calculated using the Sabkha formula:-

$$\text{Static} = \text{Elevation}/1500 + 0.012 \text{ (see chapter 2).}$$

1.3.4 Other data

Magnetic tapes for seismic line V07-85, covering shot points 104 to 470 were supplied for the project. They comprise demultiplexed unfiltered shot gather vibroseis data shot in 1985, in SEG-Y format. Six tables show the station elevations. Observer reports record the terrain (rough or flat), direction of shooting, record number, sweep point, and recording stations.

Uphole data are available for stations 165, 296, 385, and 440, showing the subsurface velocity, average velocity to datum, and the static correction to the datum. A Sirte Oil Company internal geological report of the Wadi field was also supplied.

Table 1.2

Well D6-149		KB=197m		Static=0.141 ms
Depth in m	Time in seconds	Subsea depth in metres	Corrected time in seconds	
313.42	0.1902	116.42	0.0492	
394.20	0.2290	197.20	0.0880	
613.07	0.3210	416.07	0.1800	
635.54	0.3324	438.54	0.1914	
730.36	0.3556	533.36	0.2146	
837.32	0.3862	640.32	0.2452	
1153.67	0.4720	956.67	0.3310	
1406.68	0.5350	1209.68	0.3940	
1698.35	0.6047	1501.35	0.4637	
1801.67	0.6361	1604.67	0.4951	
1891.28	0.6610	1694.28	0.5200	
2068.37	0.7026	1871.37	0.5616	
2116.84	0.7149	1919.84	0.5739	
2159.81	0.7286	1962.81	0.5876	
2213.46	0.7454	2016.46	0.6044	
2287.52	0.7695	2090.52	0.6285	
2401.82	0.8041	2204.82	0.6631	
2453.64	0.8187	2256.64	0.6777	
2593.32	0.8602	2396.32	0.7192	
2665.48	0.8856	2468.48	0.7446	
2691.38	0.8910	2494.38	0.7500	
2749.30	0.9020	2552.30	0.7610	
2791.36	0.9267	2594.36	0.7857	
2827.63	0.9267	2630.63	0.7857	
2880.36	0.9455	2683.36	0.8045	
2984.91	0.9803	2787.91	0.8393	
3039.47	0.9969	2842.47	0.8559	
3059.58	1.0030	2862.58	0.8620	
3159.53	1.0192	2962.53	0.8782	
3245.48	1.0313	3048.48	0.8903	
3338.44	1.0465	3141.44	0.9055	
3384.80	1.0552	3187.80	0.9142	
3443.33	1.0617	3246.33	0.9207	
3547.87	1.0823	3350.87	0.9413	
3643.88	1.1051	3446.88	0.9641	
3825.85	1.1362	3628.85	0.9952	

Table 1.2 Drilling depth, subsea depth in metres and corresponding time in seconds from surface and from datum.

Table 1.3

Well D7-149		KB=186 m		Static=0.133 ms
Depth in m	Time in seconds	Subsea depth in metres	Corrected time in seconds	
197.51	0.1662	11.51	0.0332	
343.90	0.2344	157.90	0.1014	
460.25	0.2834	274.25	0.1504	
643.21	0.3654	457.21	0.2324	
918.06	0.4356	732.06	0.3026	
1171.04	0.5040	985.04	0.3710	
1524.00	0.5954	1338.00	0.4624	
1737.36	0.6465	1551.36	0.5135	
1846.17	0.6822	1660.17	0.5492	
1937.61	0.7020	1751.61	0.5690	
2101.60	0.7369	1915.60	0.6039	
2286.00	0.7894	2100.00	0.6564	
2446.02	0.8426	2260.02	0.7096	
2631.95	0.8957	2445.95	0.7627	
2721.25	0.9320	2535.25	0.7990	
2910.23	0.9924	2724.23	0.8594	
3136.39	1.0403	2950.39	0.9073	
3447.29	1.1524	3261.29	1.0194	
3727.70	1.1880	3541.70	1.0550	
3823.19	1.2000	3637.19	1.0670	
3947.16	1.2246	3761.16	1.0916	

Table 1.3 Drilling depth, subsea depth in metres and corresponding time in seconds from surface and from datum.

Table 1.4

Well D8-149		KB=230 m		Static=0.162 ms
Depth in m	Time in seconds	Subsea depth in metres	Corrected time in seconds	
411.48	0.2765	181.48	0.1145	
536.45	0.3286	306.45	0.1666	
673.08	0.3866	443.08	0.2246	
818.69	0.4226	588.69	0.2606	
980.85	0.4656	750.85	0.3036	
1183.62	0.5236	953.62	0.3616	
1310.64	0.5608	1080.64	0.3988	
1427.68	0.5895	1197.68	0.4275	
1553.35	0.6155	1323.35	0.4535	
1758.70	0.6635	1528.70	0.5015	
1846.48	0.6886	1616.48	0.5266	
1959.86	0.7216	1729.86	0.5596	
2111.65	0.7545	1881.65	0.5925	
2211.63	0.7856	1981.63	0.6236	
2286.00	0.8065	2056.00	0.6445	
2346.96	0.8285	2116.96	0.6665	
2445.72	0.8566	2215.72	0.6946	
2636.52	0.9145	2406.52	0.7525	
2713.72	0.9415	2483.72	0.7795	
2850.49	0.9714	2620.49	0.8094	
2917.85	0.9866	2687.85	0.8246	
2977.29	1.0016	2747.29	0.8396	
3040.38	1.0305	2810.38	0.8685	
3108.96	1.0526	2878.96	0.8906	
3159.86	1.0676	2929.86	0.9056	
3261.36	1.0994	3031.36	0.9374	
3347.31	1.1197	3117.31	0.9577	
3383.28	1.1360	3153.28	0.9740	
3463.14	1.1486	3233.14	0.9866	
3596.64	1.1706	3366.64	1.0086	
3718.56	1.1915	3488.56	1.0295	
3807.56	1.2106	3577.56	1.0486	

Table 1.4 Drilling depth, subsea depth in metres and corresponding time in seconds from surface and from datum.

Table 1.5

Well D9-149		KB=202 m		Static=0.143 ms
Depth in m	Time in seconds	Subsea depth in metres	Corrected time in seconds	
365.76	0.2574	163.76	0.1144	
643.43	0.3780	441.43	0.2350	
649.53	0.3800	447.53	0.2370	
807.72	0.4200	605.72	0.2770	
1165.25	0.5180	963.25	0.3750	
1463.04	0.5960	1261.04	0.4530	
1758.09	0.6590	1556.09	0.5160	
1963.30	0.7170	1761.30	0.5740	
2103.42	0.7430	1901.42	0.6000	
2286.00	0.8020	2084.00	0.6590	
2456.69	0.8520	2254.69	0.7090	
2636.52	0.9111	2434.52	0.7681	
2819.70	0.9533	2617.70	0.8103	
3483.86	1.1702	3281.86	1.0272	
3604.56	1.2040	3403.56	1.0610	
3767.63	1.2500	3565.63	1.1070	
3800.86	1.2560	3598.86	1.1130	
3874.01	1.2700	3672.01	1.1270	
3947.16	1.2800	3745.16	1.1370	
3983.74	1.2860	3781.74	1.1430	
4056.89	1.2964	3854.89	1.1534	
4093.46	1.3030	3891.46	1.1600	
4166.62	1.3180	3964.62	1.1750	

Table 1.5 Drilling depth, subsea depth in metres and corresponding time in seconds from surface and from datum.

Table 1.6

Well K1-149		KB=191m		Static=0.136
Depth in m	Time in seconds	Subsea depth in metres	Corrected time in seconds	
621.88	0.3567	430.88	0.2207	
1173.66	0.5065	982.66	0.3705	
1569.93	0.6080	1378.93	0.4720	
1755.89	0.6475	1564.89	0.5115	
1938.80	0.6950	1747.80	0.5590	
2118.57	0.7335	1927.57	0.5975	
2146.07	0.7403	1955.07	0.6043	
2191.73	0.7501	2000.73	0.6141	
2344.19	0.8002	2153.19	0.6642	
2539.20	0.8636	2348.20	0.7276	
2633.72	0.8924	2442.72	0.7564	
2810.47	0.9285	2619.47	0.7925	
2893.83	0.9575	2702.83	0.8215	
3014.69	0.9975	2823.69	0.8615	
3468.59	1.1499	3277.59	1.0139	
3617.95	1.1814	3426.95	1.0454	
3706.28	1.1972	3515.28	1.0612	
3809.94	1.2166	3618.94	1.0806	
3907.51	1.2350	3716.51	1.0990	
4020.22	1.2516	3829.22	1.1156	
4078.16	1.2603	3887.16	1.1243	
4213.34	1.2885	4022.34	1.1525	

Table 1.6 Drilling depth, subsea depth in metres and corresponding time in seconds from surface and from datum.

1.4 AIMS OF THE STUDY

The aims of the study were to:

- (1) Reprocess line V07-85 using the static correction from the uphole surveys, to see whether it is an improvement on the original processed section using a formula for static correction.
- (2) Remap the structure and construct a cross section over the Wadi field using all the existing data (provided by Sirte Oil Company).
- (3) Study the faults of the field, and how they relate to the hydrocarbon occurrences.
- (4) Use maps and the back-stripping technique (with decompaction ignored) to clarify the timing of faulting in the study area.
- (5) Study the average velocity calculated from the wells, and compare it with the average velocity calculated from the interval velocity derived from the velocity tabulations on the seismic sections.

Chapter 2

Seismic reprocessing

- 2.1 Introduction
- 2.2 Field parameters
- 2.3 Static corrections
- 2.4 Static computations
- 2.5 Processing sequence
- 2.6 Spherical divergence
- 2.7 AGC (Automatic gain control)
- 2.8 Mute
- 2.9 Deconvolution
- 2.10 Common depth point (CDP) gather
- 2.11 Applying static correction
- 2.12 Raw stack display
- 2.13 Velocity analysis
- 2.14 Residual static correction
- 2.15 Normal move-out correction
- 2.16 Stacking
- 2.17 Deconvolution after stack
- 2.18 Frequency filtering after stack
- 2.18 Final stack section
- 2.19 Migration

2.1 INTRODUCTION

Seismic data processing strategies and results are strongly affected by the field acquisition parameters. The common-mid point (CMP) recording is the most widely used seismic data acquisition technique. By providing redundancy (measured as the fold of coverage) in the seismic experiment, we can improve signal quality. Surface conditions have a lot to do with the quality of data collected in the field. Other factors, such as weather conditions, care taken during recording, and condition of the recording equipment, also influence data quality. Seismic data are often collected in less than ideal conditions, so we can only hope to suppress the noise and enhance the signal in processing to the extent allowed by the quality of the data (Yilmaz 1987).

In the study area line V07-85 from shot point 104 to 470 was selected for reprocessing using uphole statics. The processing sequence began by reading correlated demultiplexed tape (SEG-Y format) using the SierraSEIS package on the sun computer network in the Geology and Applied Geology Department Glasgow University. The main objective of reprocessing line V07-85 were to use different processing techniques than was used by Western Geophysical. These include:

- a) Using uphole statics to see if we can solve the static problems evident on Western Geophysical sections at shot point 360 (see fig 3.4).
- b) Using deconvolution after stack to get rid of the multiple reflections on the commercial section.
- c) Applying migration to the data.

2.2 FIELD PARAMETERS

The data shot in 1985 were recorded by the Bulgarian Oil Company (BOCO) party 9. Four trucks generate an upsweep (increasing frequency). The vibrators sweep simultaneously in source arrays designed to attenuate surface noise and improve signal to noise ratio. All the geophone arrays are special filters that have directional properties which make the array more sensitive to the upward-travelling energy (reflection) than to horizontally-travelling energy (ground-roll). The field acquisition parameters were based on the results of a noise study carried out in the area. Figures 2.1a, b, and c show the source array, receiver array (24 geophones weighted 1, 2 and 3) and spread diagram respectively, which were chosen for this particular survey from the noise test results. Four seconds of two-way time were recorded using the following parameters:-

Number of vibrators	4.
Number of sweeps	8.
V.P interval	50 m
Sweep patch pattern	118.5 m
Number of sweeps per V.P	4*8 = 32
Horizontal distance between the vibrators	6.25 m
Cross-line offset between the vibrators	8.0 m
Sweep frequency	08-48 Hz.
Geophone frequency	10 Hz
Sweep length	10 s.
Recording length	14 s.
Sample interval	4 ms.
Geophone group interval	50 m.

2.3 STATIC CORRECTIONS

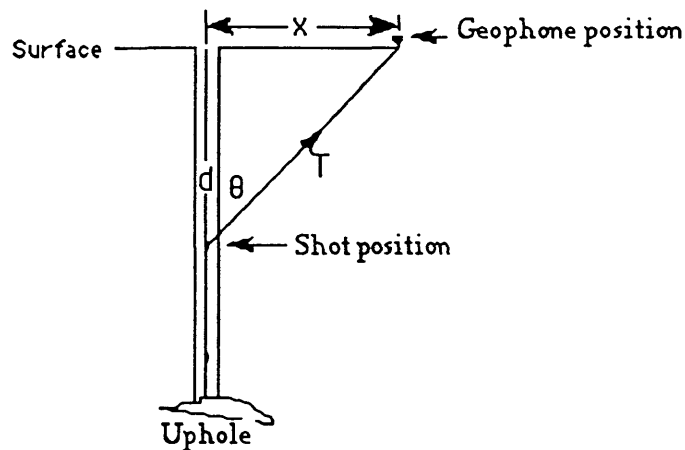
One of the most important steps in land processing is the static correction calculation, especially in areas of rough terrain, and in areas where the near surface velocity is highly variable in either the vertical or horizontal direction. Static corrections are required by changes in surface elevation and thickness or velocity of the weathering layer (low velocity layer, LVL). The LVL is unconsolidated material between surface and bedrock. Corrections must be applied to remove the effects of changes in elevation and the influence of the LVL. These corrections are known as static corrections because the time shift applied is constant for an entire trace. This is achieved by stripping away the upper surface above a datum plane. The static shift should produce the same results as if the source and receiver were both placed at the datum. Static anomalies may be classified as:-

High frequency (short wavelength) static or low-frequency (long wavelength) static anomalies. There is no clear distinction between short and long wavelength static corrections. Generally a short wavelength static is smaller than a spread length for the survey being evaluated, and long wavelength is about a spread length or larger. The short wavelength static errors degrade the CDP stack, and the long wavelength static error moves the data in time, generating an anomaly. It has very little effect on CDP stack response. The long wavelength static error indicates a gradual change in velocity. Two sets of static corrections are computed, one showing shot statics and other showing the receiver static, both as a function of location.

In order to correct for the travel time through the low velocity layer, information is needed about the depth and velocity of this layer. The two commonly used methods of deriving this information are the uphole and the refraction methods.

2.3.1 Uphole method

Uphole surveys provide the most direct measurement of near-surface properties. In this method a geophone known as an "uphole phone" is planted near the top of the hole, and small charges are detonated at different depths in the hole as shown in Figure 2.2a. The arrival times after a correction for slant travel path are plotted against shot depth. Straight lines are fitted to the plotted points. The slopes of these lines indicate the velocity, while the point of change in slope (knee) marks the depth of the weathering zone, as shown in Figure 2.2b.



X is the offset d is the depth of the shot

T is the travel time from shot to the receiver

$\theta = \arctan x/d$ The vertical time = $T \cos \theta$

Fig 2.2a Uphole shooting

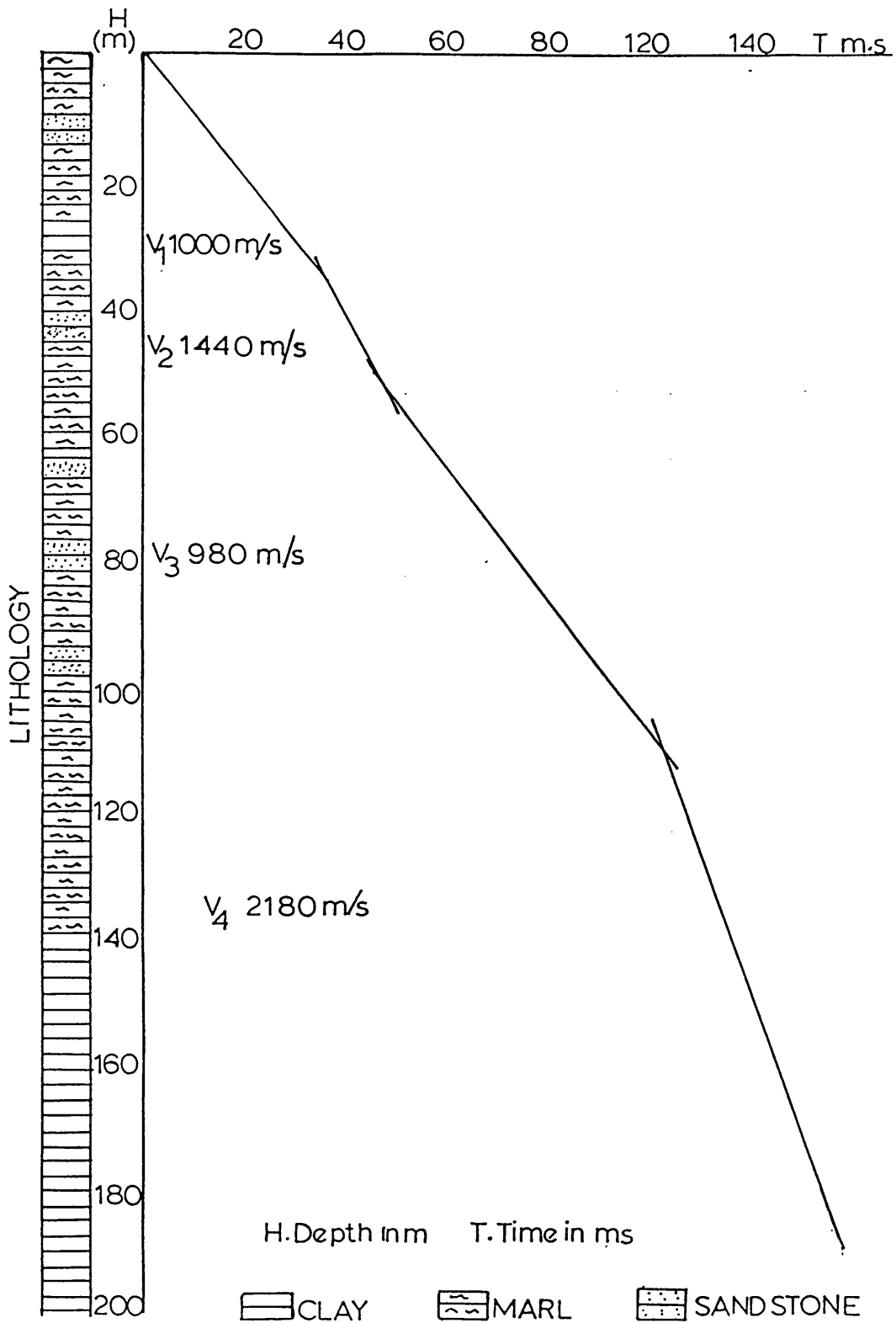


Fig 2.2b Uphole time depth curve showing the weathering and sub-weathering velocity (seismic line V07-85, station 440).

2.3.2 Datum Plane

In order to compute and apply static corrections, an elevation known as the datum plane is used. After applying the static correction, the record appears as though the energy source and geophone were situated on the datum plane rather than on surface of the earth. The datum always corresponds to the zero time on the seismic section.

2.4 STATIC COMPUTATION

The static correction for the old version of processing has been calculated using a formula (Sabkha formula) for both shot and receiver.

$$\text{Trace static} = (\text{ELE} / V) + 0.012 \quad \dots\dots\dots 2.1$$

where:

ELE is the elevation in metres above the datum.

V is the velocity above the datum, set here to 1500 m/s.

0.012 is a constant time in seconds.

For this study the static correction is calculated for line V07-85 using the upholes by considering the correction for both low velocity and elevation. Table 2.1 Show a comparison between static calculated using Sabkha formula and static calculated using upholes at the position of the uphole.

$$\text{Trace static} = \text{Shot static (SPstatic)} + \text{geophone group static (GPstatic)}$$

$$\text{SP static} = (\text{Datum} - \text{GPELE} + \text{SPD}) / \text{Dvel}$$

$$\text{GPstatic} = (\text{Datum} - \text{GPele} + \text{SPD}) / \text{Dvel} - \text{TUH}$$

Where:

- Datum is the datum plane.
- Dvel is the datum velocity.
- SPD is the shot point depth.
- SPELE is the shot point elevation.
- GPELE is the geophone elevation.
- TUH is the uphole time.

Note: The uphole time and the shot point depth are zero because the source and the receiver are both on the surface. Fig 2.3 shows the model used for the weathering and sub-weathering velocity.

SP	Elevation in metres	Static using formula	Static using uphole	Difference in ms
165	284	201	217	+16
296	274	195	193	-02
385	206	158	137	-21
440	187	137	150	+13

Table 2.1 Comparison between static calculated using Sabkha formula and static calculated using upholes at the position of the uphole determinations. The computer will interpolate between the upholes and extrapolate to each end of the line.

2.5 PROCESSING SEQUENCE

2.5.1 Introduction

The objective of seismic reflection data processing is to produce a visual display in the form of a seismic section, showing subsurface ref-

lection patterns that can depict the geological subsurface. Noise in seismic work is defined as unwanted signal. The noise may be classified as random or coherent. Random noise comprises events whose amplitudes and phases are randomly distributed. Random noise has various sources, e.g. a poorly planted geophone, wind motion, transient movements in the vicinity of recording cable, etc. Coherent noise exhibits a pattern, such as multiple reflections, ghosts, and bubble oscillations. Data processing attempts to suppress both types of noise and to present reflections on the seismic section with the greatest possible resolution. Seismic data processing provides the interpreter with seismic cross-sections amenable to geological interpretation for locating hydrocarbon accumulations. Therefore the geological section from the processing stage should be free of random and coherent noise and show only reflection events. Fig 2.4 illustrates three shot point gathers that illustrate the effect of wind on the data. Shots a and b were shot on a windy day, shot c on a quiet day.

The processing begins with the arrival of the tapes from the field crew, and are accompanied by the observer's reports, in which details of line and shot geometry, field settings and problems are given. A second report describes elevation and computed field static correction to be applied to the data. The processing sequence may be divided into three stages.

1) Preprocessing:

The objective of preprocessing is to edit and prepare data for processing analysis. Appendix 1 shows all the editing of the traces.

2) Processing analysis:

Processing analysis involves experiments whereby optimum parameters are selected for use in the processing stage.

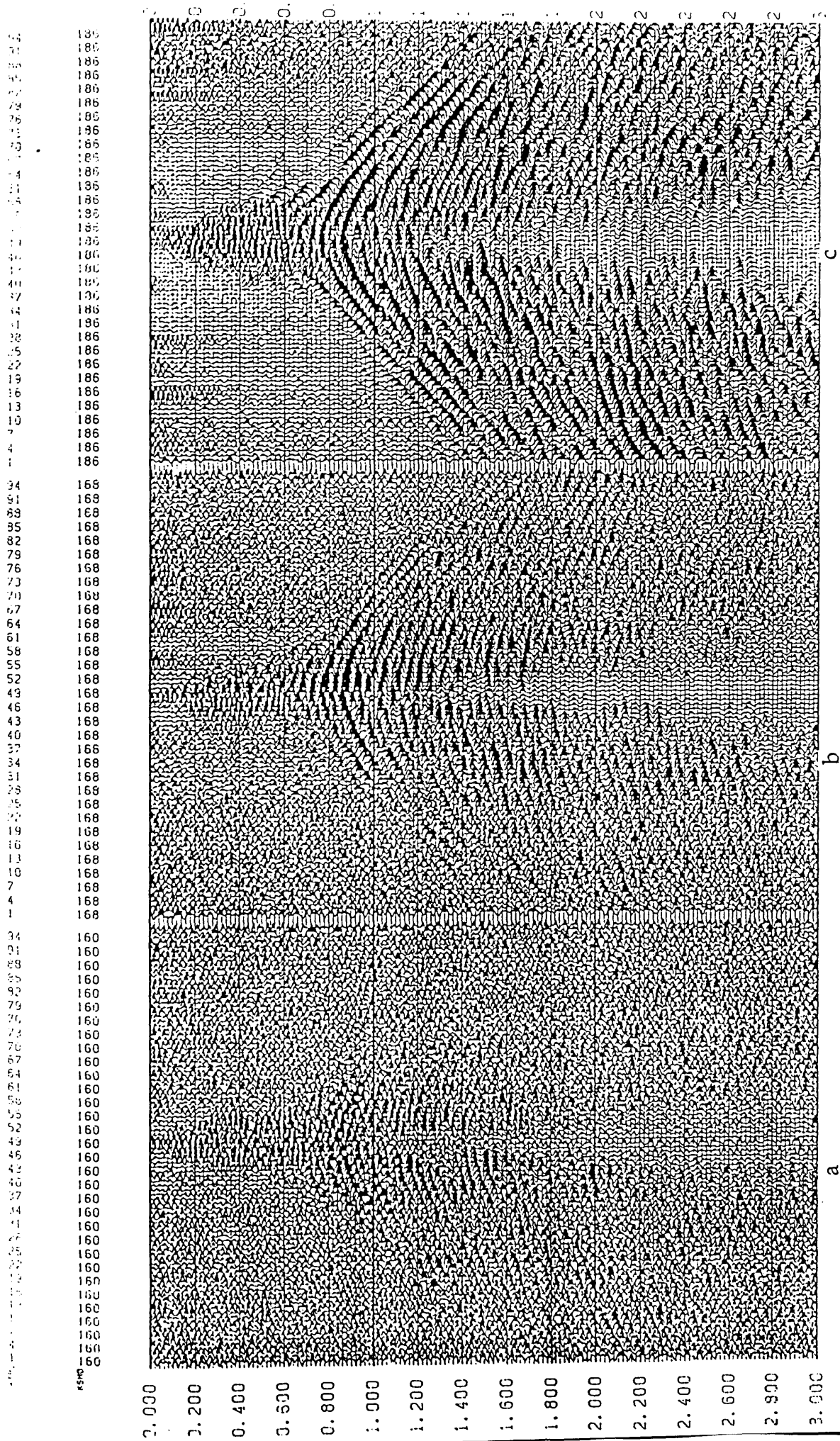


Fig 2.4a, b, c Shot point gathers showing the effect of wind on the noise content of the data.

3) Processing:

This is simply applying the chosen parameters. The product of processing is a final stack.

The field tape is recorded in a multiplexed format. Multiplexing is the arrangement of data in a compact form, involving scanning the data from different channels, which are sent to a single file in multiplexed form for storage. This is done in the field by recording the first sample of each channel, followed by the second sample of each channel, and so on. Before the data can be read in a trace-sequential form, demultiplexing must be carried out.

2.6 SPHERICAL DIVERGENCE

Spherical divergence amplitude attenuation is due to the spreading of the wavefront as it travels away from the source. Amplitude attenuation (A) is inversely proportional to distance travelled: $A \propto 1/r$ where r is the distance travelled, or $A \propto 1/VT$ where V is the average velocity. It follows that correcting for spherical divergence requires multiplying the data by a time-varying function of VT , or adding the VT in decibels ($20 \log VT$) (Morgan 1985).

A shot record before and after geometric spreading correction is shown in Figure 2.5. While the reflections have been enhanced, noise in the data has also been boosted. This is one undesirable aspect of any type of gain application. Besides ambient noise, coherent noise in the data may be boosted. By using the primary velocity function in correcting for geometric

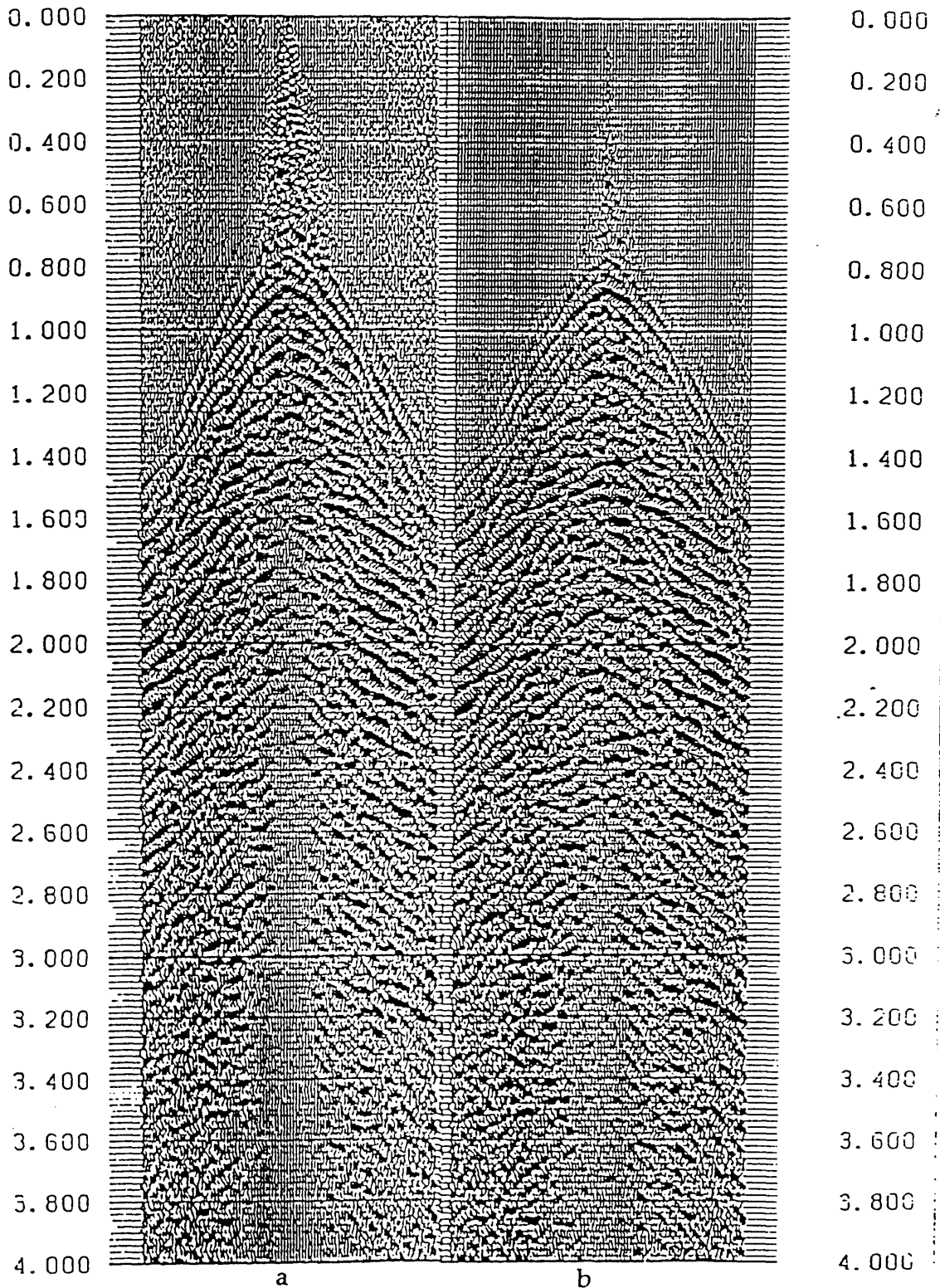


Fig 2.5a, b Shot gather before and after applying spherical divergence correction

spreading, the amplitudes of the dispersive coherent noise and multiples have been over - emphasised (Yilmaz 1987).

2.7 AGC (Automatic gain control)

Automatic gain control (AGC) is applied to the data to enhance weak signals (Yilmaz 1983). AGC has been applied to the traces in the shot gathers. Time variable gain can be used to suppress the gain when strong signals are being received and to increase the gain in the later part of the recording, when the seismic signal has reduced to a very low level (Kearey & Brooks 1991). Automatic gain control has been applied to the traces in the shot gathers. Tests were carried out on the shot gathers with different window lengths, after which a window of 400 ms was chosen to be applied to the data. AGC was run as a test to see the effect on the data before stack (Figure 2.6 shows a shot record before and after AGC application), but is not included in the processing sequence here. The automatic gain control is applied to the stacked section using a 500 ms window.

2.8 MUTE

Muting is applied to suppress unwanted data from the shot gather traces, mainly first breaks. This process zeroes the data samples at either ends of the input traces. This is useful when devising a reliable deconvolution filter and avoids stacking in noise during later processing. Figure 2.7 shows a shot point gather before and after applying mute correction.

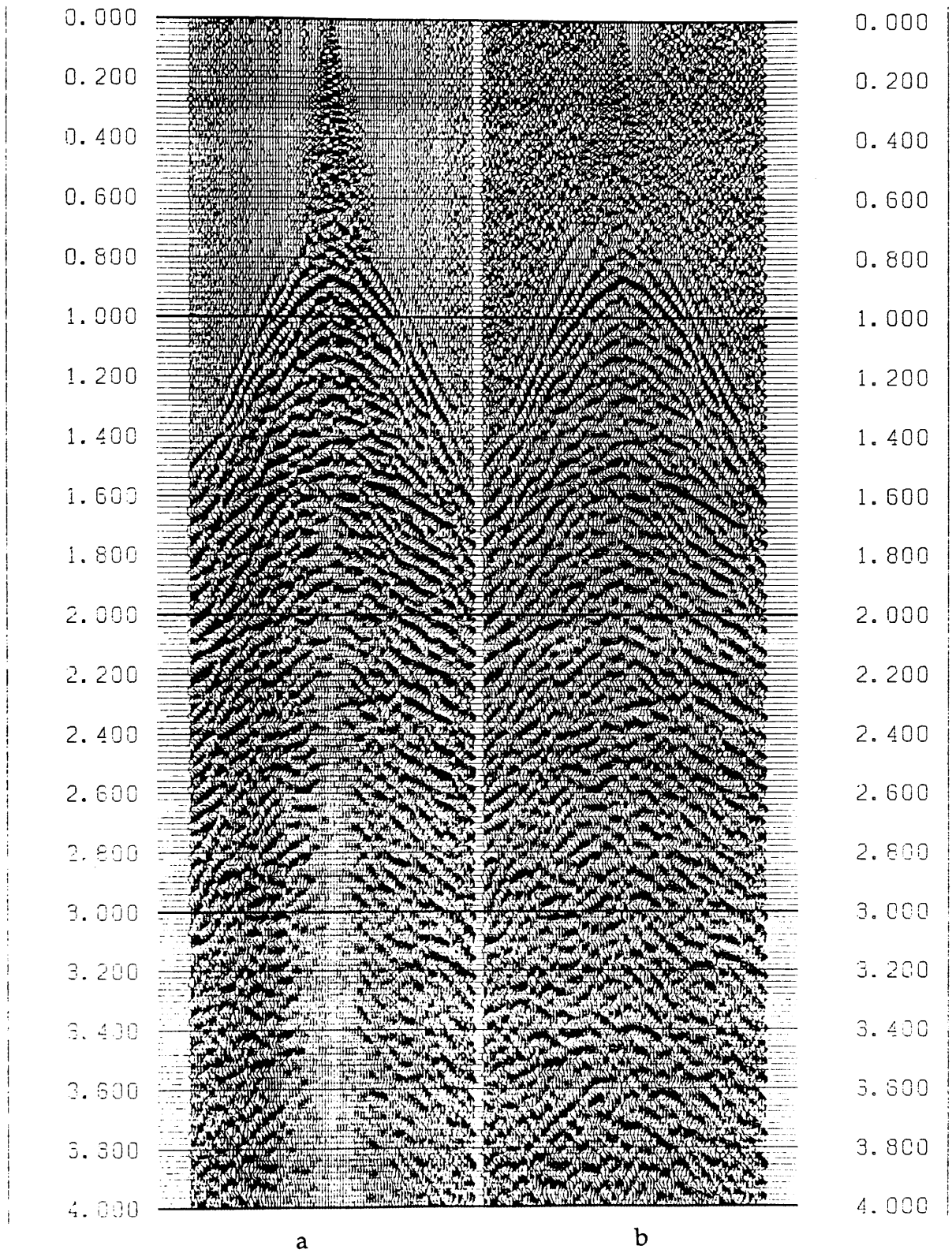


Fig 2.6 a, b Shot gather before and after applying automatic gain control (AGC)

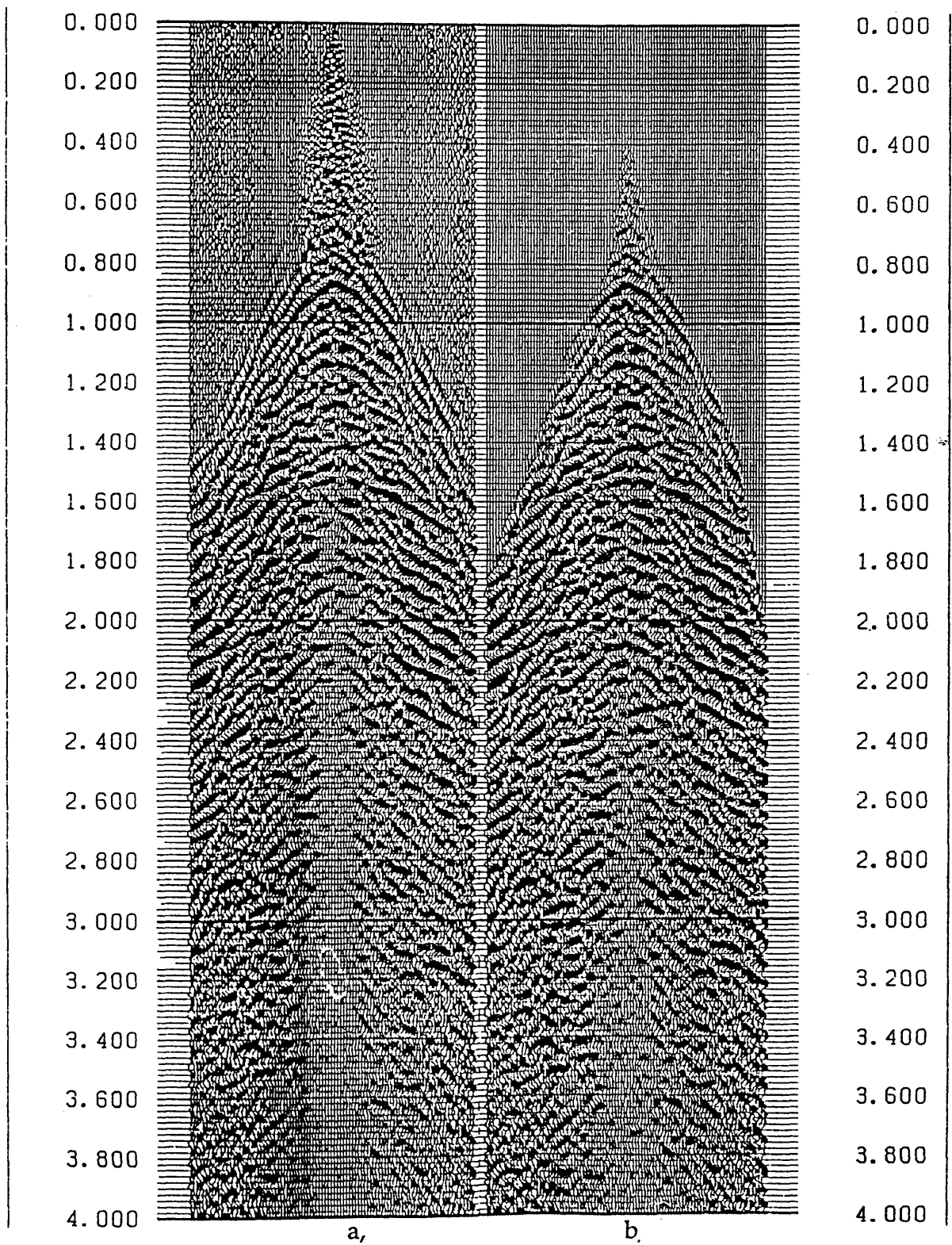


Fig 2.7a, b Shot gather before mute correction and spherical divergence (a) and after mute correction and spherical divergence (b).

2.9 DECONVOLUTION

All the processing techniques may be considered secondary in that they help improve the effectiveness of the primary processes, for example:

- 1) Dip filtering may need to be applied before deconvolution to remove coherent noise, so that the autocorrelation estimate is based on reflection energy that is free from such noise.
- 2) Before deconvolution, a correction for geometric spreading is necessary to compensate for loss of amplitude due to wavefront divergence (as shown in Section 2.6 and Fig 2.5).
- 3) Wide band-pass filtering also may be needed to remove very low and high-frequency noise. Since spiking deconvolution broadens the spectrum of seismic data, traces containing much more high-frequency noise and signal are boosted. The data often need filtering with a wide band-pass filter after deconvolution to bring the data to a common root-mean squared (rms) level. Fig 2.8 shows a frequency analysis of shot point 300 for traces 1, 48 and 96. It shows that the dominant frequencies are from 10 to 50 Hz. The data were filtered with a band-pass filtered 10/18-50/36 Hz where

10 is the low cut frequency.	50 is the high cut frequency
18 is the low cut slope (dB/oct).	36 is the high cut slope (dB/oct).

In exploration seismology, the seismic wavelet generated by the seismic source travels through different strata to reach the receiver. Because of the many distorting effects encountered, the wavelet reaching the receiver is by no means similar to the wavelet produced by the source. Decon-

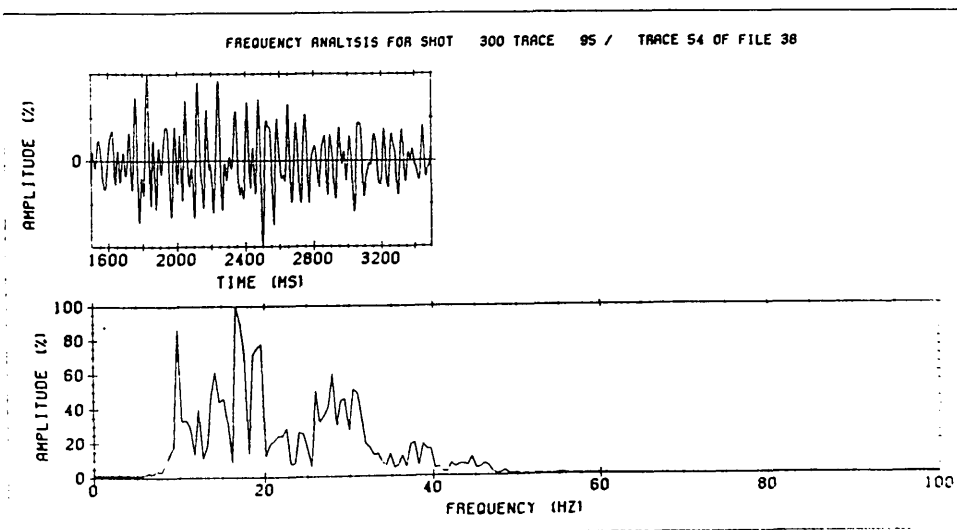
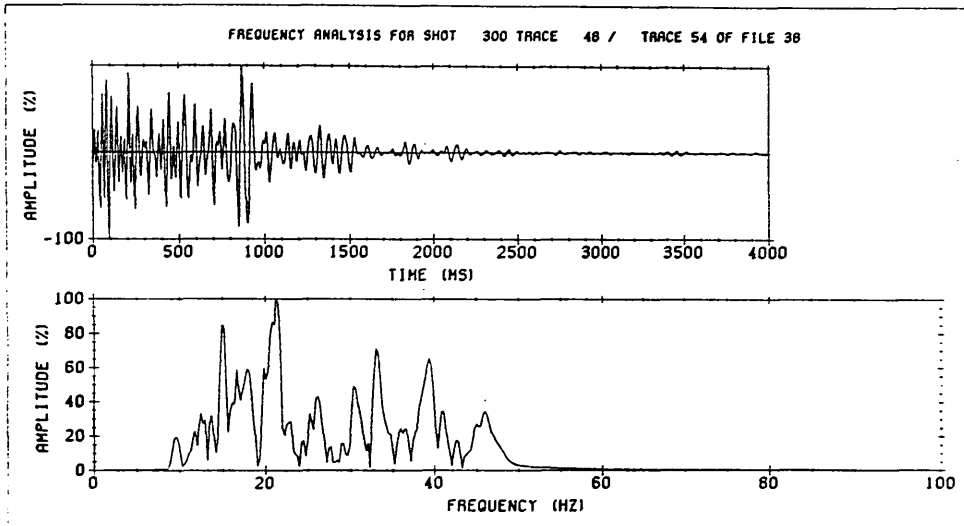
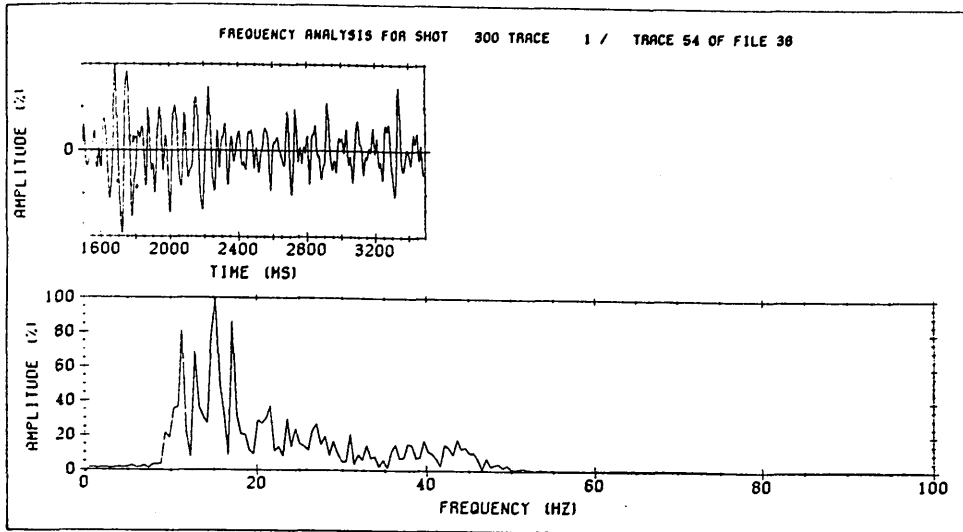


Fig 2.8 Frequency analysis on shot point 300, traces 1,48, and 95.

volution is the process of undoing this filtering. It may be considered as the inverse of convolution(Morgan 1985).

Deconvolution means removing, through data processing, undesirable effects which have occurred in the earth, by collapsing the seismic wavelet to approximately a spike (Yilmaz 1987). Figure 2.9 shows the application and the effect of deconvolution on the data. After deconvolution the traces contain much more high frequency energy, some of which will be noise.

The following variables are used to define and compute the deconvolution operators:

- 1) Start time of autocorrelation window.
- 2) Length of the autocorrelation window.
- 3) Maximum lag for the deconvolution operator.
- 4) Prediction lag for the operator.
- 5) Start time for the application of the operator.

Figure 2.10 shows the preliminary processing steps.

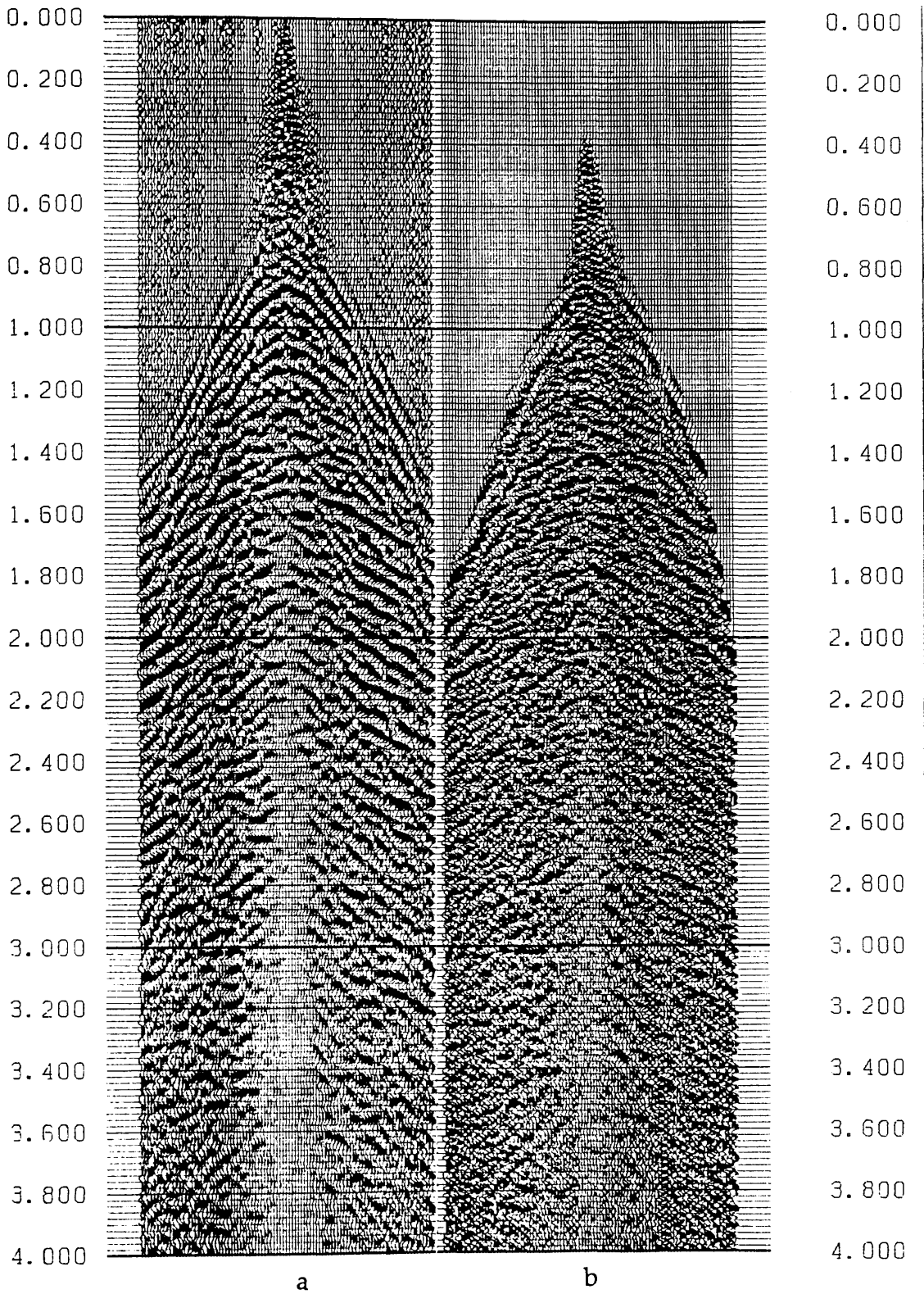


Fig 2.9a, b Shot gather before and after applying deconvolution. Note that muting has also been applied

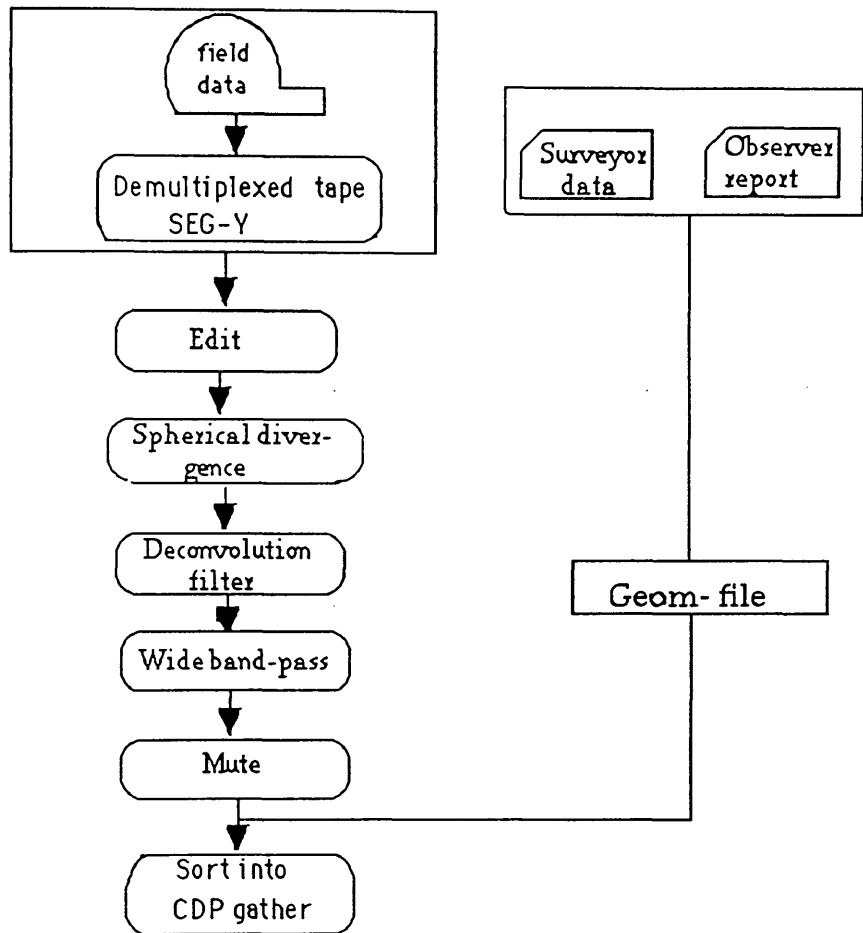


Fig 2.10 Preliminary processing chart

2.10 COMMON DEPTH POINT (CDP) SORTING

After the initial signal processing, the data are re-ordered from shot to common midpoint (CMP) gathers. This is commonly called CDP (common depth point) gather sorting, which requires field geometry information. The CMP gather is equivalent to a CDP gather only when the reflectors are horizontal and velocity does not vary horizontally. However, when there

are dipping reflectors in the subsurface, these two gathers are not equivalent and strictly only the term CMP gather should be used.

Seismic data acquisition with multifold coverage is done in shot receiver (S, G) coordinates. The required coordinate transformation is achieved by sorting the data into CDP gathers. Each individual trace is assigned to the midpoint between the shot and receiver locations associated with that trace, as shown in Figure 2.11a. Those traces with the same midpoint location are grouped together, making up a CDP gather. Figure 2.11a shows ray paths for one layer in a CDP gather.

2.11 APPLYING STATIC CORRECTIONS

The computed statics corrections are applied to the CDPs gather using the statics process command (STATAPLY). Two types of static correction can be applied using this processor:-

- a) Geometry static (surface consistent) including shot static and receiver static.
- b) Residual static.

2.12 RAW STACK DISPLAY

A raw stack display is often the earliest opportunity to observe the geological structure along the line with any certainty, and as such may indicate that a previous parameter selection, such as deconvolution window, timing or velocity analysis was unsatisfactory. For this reason in poor data quality areas, the brute stack using a representative velocity profile is

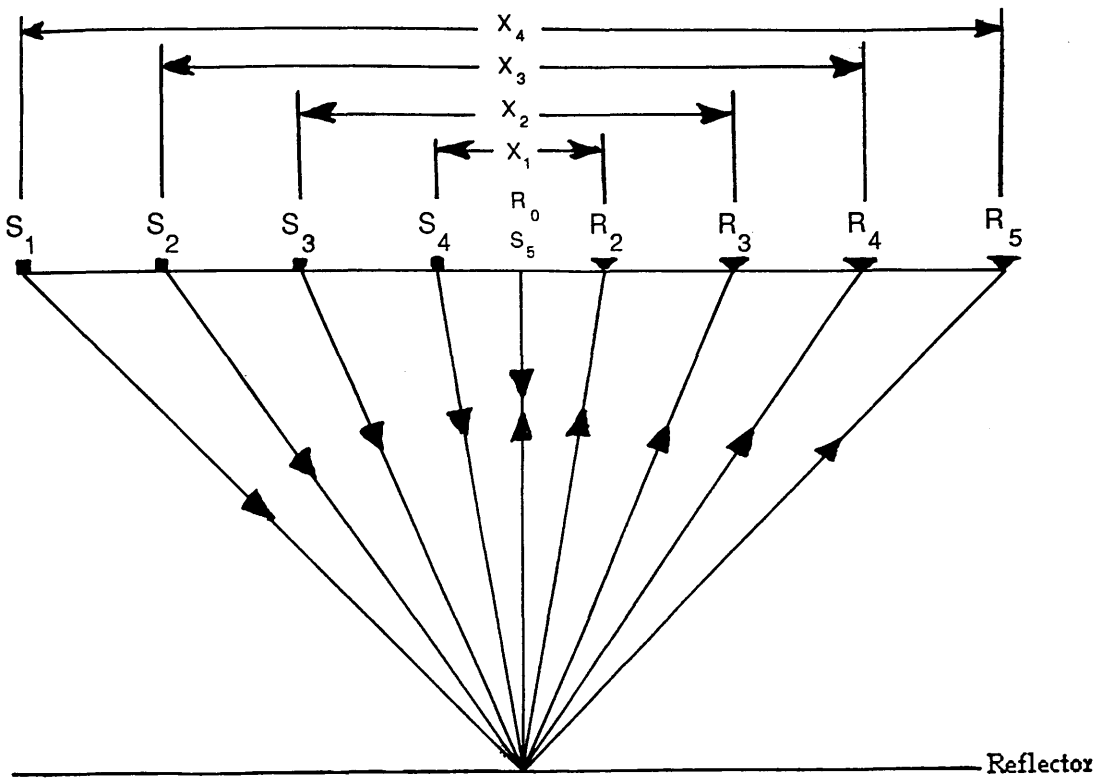


Fig 2.11a Common depth point ray paths for a horizontal layer (one layer case).

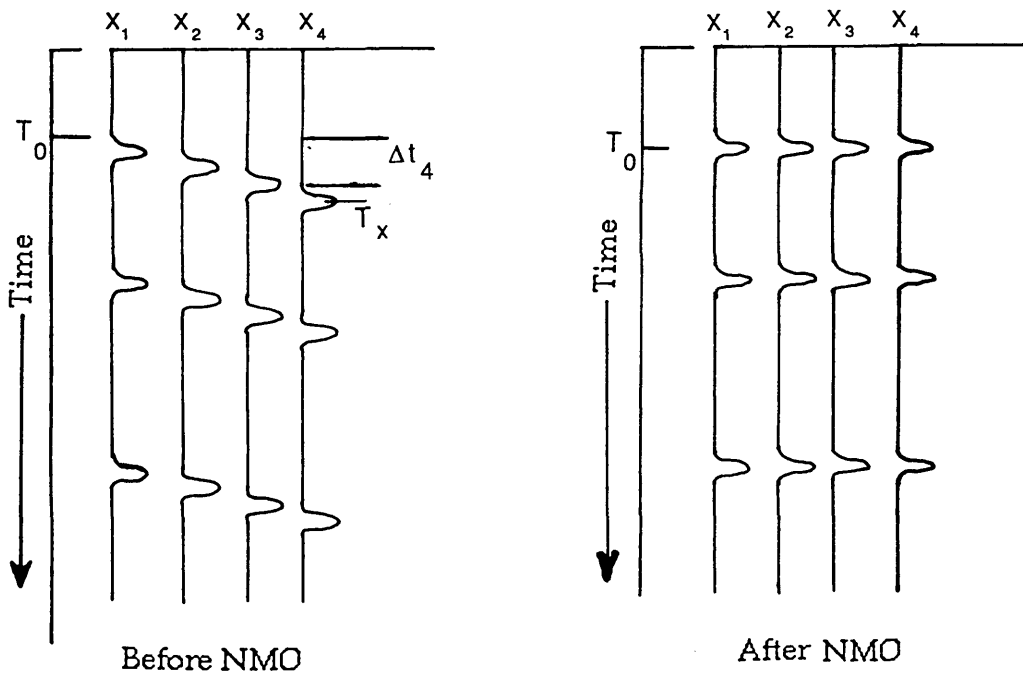


Fig 2.11b Four traces gather for 3 interfaces before and after NMO correction.

produced at an early stage (Hatton, 1986). Figure 2.12 shows a brute stack section produced using a single velocity picked from the previous processing.

2.13 VELOCITY ANALYSIS

2.13.1 Continuous velocity estimation

The velocity needed in NMO correction (V_{NMO}) is different from sonic velocity, because the sonic log measures vertical times at essentially zero offset. The seismic wave propagates over a curved path containing a wide range of interval velocities. If velocity did not change laterally, the well sonic velocity might be used to compute the velocity function needed for NMO correction (Espey 1983). The velocity function stack may be extended to evaluate velocity functions at each depth point. This is referred to as the velocity spectra or velocity scan method.

The NMO for each trace is computed and corrected, the traces are summed for each velocity value, and amplitude is observed. Amplitude and semblance versus velocity at this time level is displayed. The maximum amplitude and semblance are produced when the correct velocity is applied. The velocity spectrum not only provides the stacking velocity function, but allows one to distinguish between primary and multiple reflections. Figures 2.13a, b, c show velocity spectra for different CDPs.

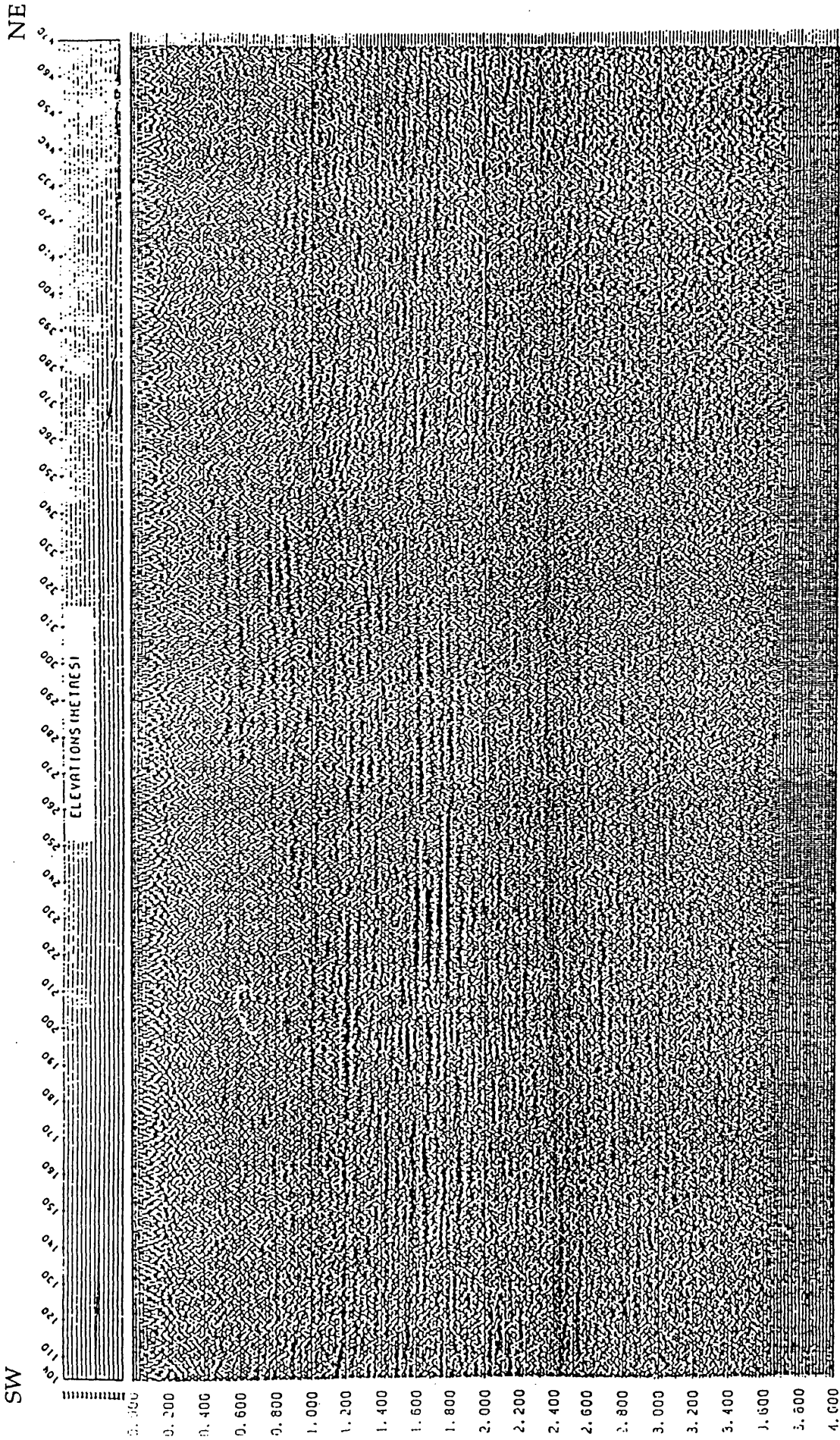
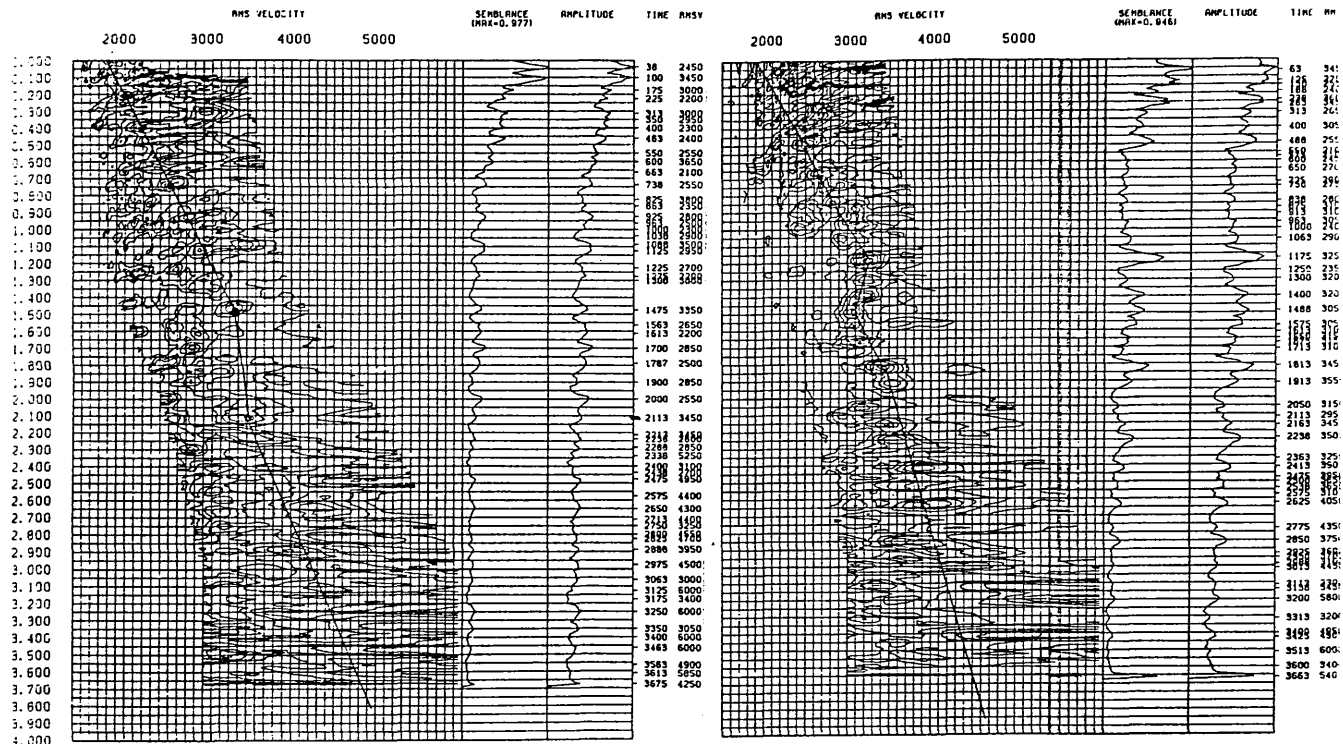


Fig 2.12 Raw stack section (stacked with one velocity picked from the previous processing).

COPS 993 TO 993

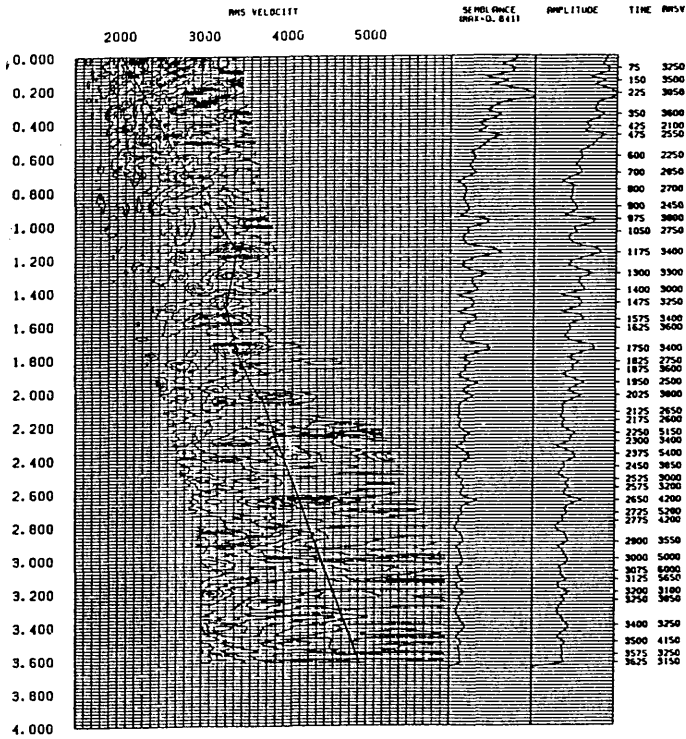
COPS 1369 TO 1369



a.

b.

COPS 1424 TO 1424



c.

Fig 2.13 (a, b, c) Velocity spectra for selected CDP gathers.

2.13.2 Velocity function stack

The velocity function stack is a variation of a constant velocity stack in which a set of velocity functions is input for NMO correction. All the velocity functions may be input, or only a central one, leaving the program to compute the surrounding ones. Many variations in algorithms and displays have been developed. One version is shown in Figure 2.14, showing a velocity function stack. A portion of the line containing 37 CDP gathers has been NMO-corrected and stacked with a range of constant velocity values. This results in a panel, where stacking velocity increases to the right (by an increment of 100m/s) and decreases to the left by the same increment around the middle point as shown in Figure 2.14. Stacking velocities are picked directly from the constant-velocity stack (CVS) panel by choosing the velocity that yields the best stack response at a selected event time (Yilmaz 1987).

2.14 RESIDUAL STATIC CORRECTION

2.14.1 Introduction

The field static correction as described earlier is not adequate to align CDP traces to produce a good S/N ratio in the stacked trace. Factors contributing to errors in the field statics include:

- 1- Incorrect assumptions as to velocity and thickness of weathering layer between measurements.
- 2- Bad uphole time or first breaks in refraction profile, which lead to wrong estimates.

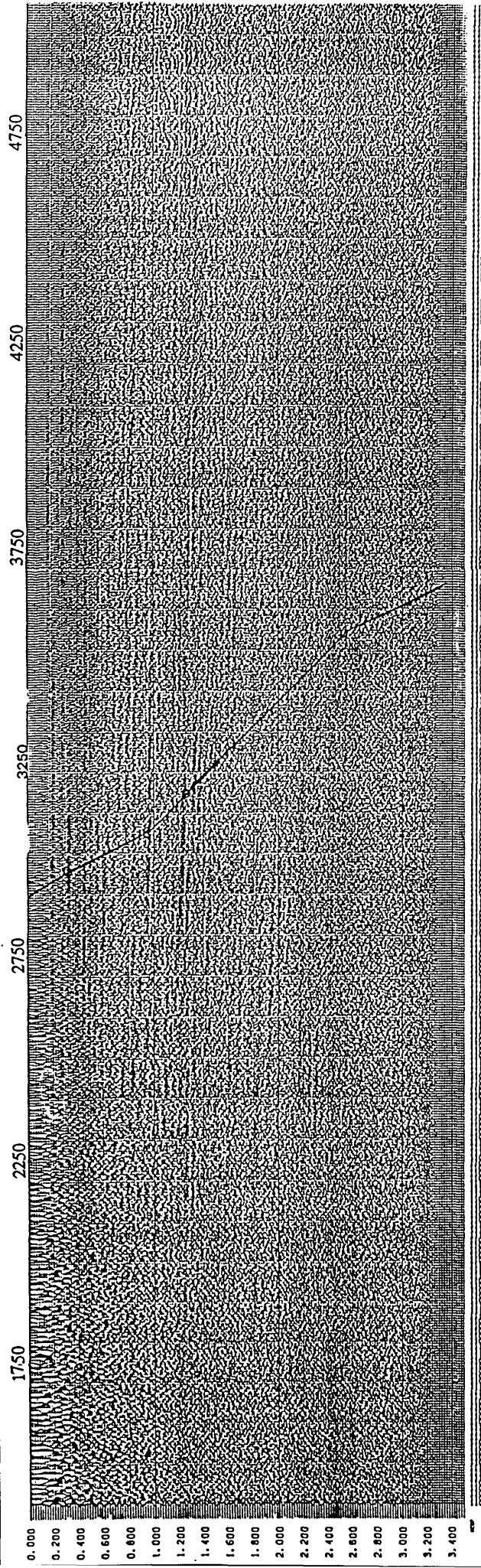


Fig 2.14 A constant velocity stack. The horizontal axis is the velocity in m/s.
Vertical axis is two way time (s).

3- Human errors in computation and/or feeding in information for field static correction.

The effect of these errors is an incomplete accounting of all trace-to-trace time anomalies. This results in a poor S/N ratio on the CDP stack. The additional time necessary to align traces to produce a better stack is called residual statics. The error in a reflection event after the field static and NMO are applied consists of the following components: dip, residual shot static, residual receiver static, and random error. All automatic correction techniques use the redundancy provided by the CDP geometry, i.e. where signals from many shot locations are recorded at the same receiver location and where signals from the same shot location are received by many receivers. This redundancy is used to compute a statistical estimate of residual static correction. The corrections are assumed to be time-invariant and surface-consistent. Surface consistent means that static shifts are time delays that solely depend on source or receiver locations at the surface, not raypaths in the subsurface (Yilmaz 1987).

After field static and NMO correction application the stacked section is inspected for residual static problems. Residual static manifests itself as unaligned or jagged reflection events. The time difference due to dip is eliminated by extracting a gate enclosing the reflection event. Residual static corrections are determined for individual CDP traces corresponding to the stacked trace. Each trace is compared with a model trace to determine the residual static. The model trace may be computed by summing all traces except the one to be corrected. The sum of the residual static errors of the traces can be assumed to be zero, so the signals on the model are at the

common shot or receiver locations and the statistical nature of the residual errors justify the above assumption. Cross correlation is used to estimate the residual static for the data being compared with the model.

The residual statics, or surface inconsistent statics, are any relative trace misalignment remaining after applying field statics and dynamic correction (NMO). These result from variation of weathering layer velocity and depth. The goal in attacking the residual static is to bring primary signals into alignment within CDP gathers while at the same time honouring the true subsurface structure and normal moveout relationship. To improve stacking quality, residual static corrections are performed in a moveout-consistent manner; that is, time shifts are dependent only on shot and receiver locations, not on the raypaths from shots to receivers. In the study area the residual statics are calculated using the SierraSEIS package following these steps.

The generation and application of surface-consistent statics involves three steps:

- 1- Generation of a stacked reference trace. A stack reference section may consist of a simple stack of the data set, or a data set consisting of a multi-pass input series of dip filtered stack traces.
- 2- Picking of non surface-consistent statics, and saving the static in a disk file.

The reference section and the CDP gathered traces that were used to construct the reference section are input to the processor for calculating non surface-consistent statics. Individual CDP gathered traces are

correlated with the reference trace that has the same CDP number. The cross-correlations output are then scanned for either the peak nearest zero lag or the maximum peak value. Control of the correlation start times, correlation end time, correlation window length, and correlation output length is provided to allow focus on, and stacking of, a particular seismic event or series of seismic events.

3- Calculating surface-consistent static and application of the statics.

The RSSAVE file created contains the non surface-consistent static picks from the RSESTIM processor and the geometry information from the following SierraSEIS common variables: KCDP (CDP number of the current trace), KRCDP (receiver CDP number of this trace), and KSCDP (sequential shot number of this shot file). This geometry information is required to establish the relationship of the CDP, source, and receiver locations. The RSCALSCS processor decomposes the RSESTIM-generated time shifts into the following components: shot static, receiver static, CDP shift, and residual normal moveout, as well as an error term. A least-squares algorithm is applied to solve the equations and to compute statics that are consistent for each source and receiver position (SierraSEIS manual 1989).

These estimated residual corrections are applied to the original CDP gathers with NMO correction as shown in the flow chart (Fig 2.15). After residual statics are applied, the velocity analysis may be repeated to improve the velocity picks. Figures 2.16 a, b, and c show velocity spectra after applying the residual static correction. The data in Figure 2.13 can be

compared with the data in Figures 2.16. The velocity spectra show a better response after application of residual static correction.

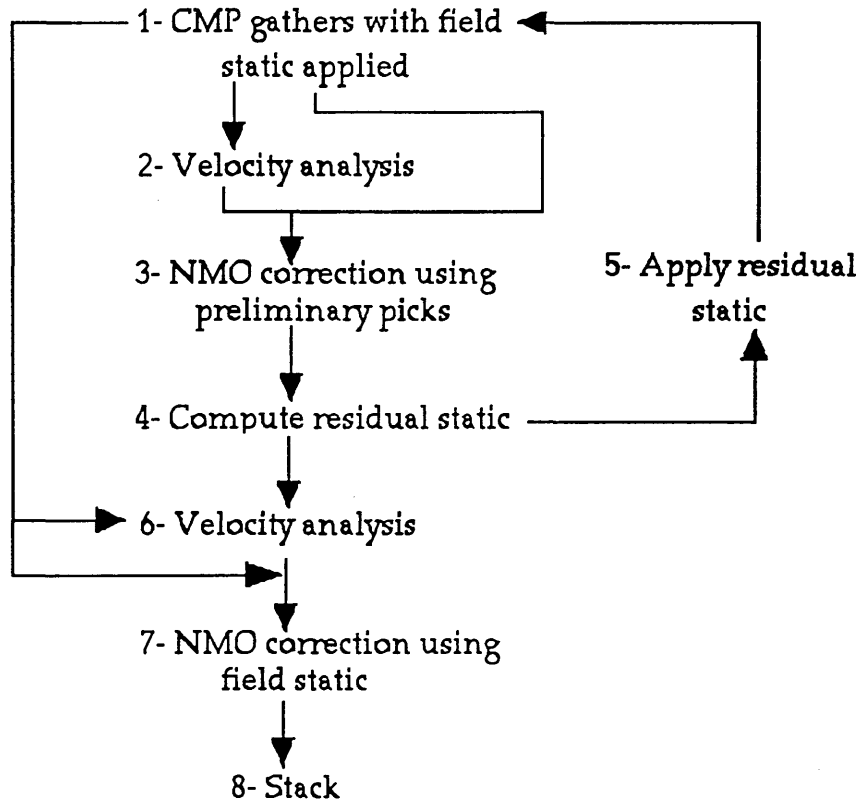
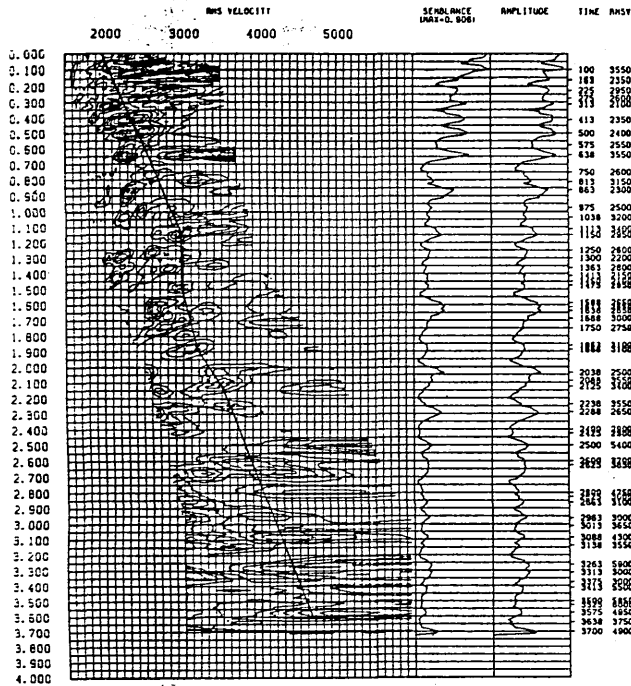


Fig 2.15 Processing flowchart with residual static correction
[After Yilmaz 1987]

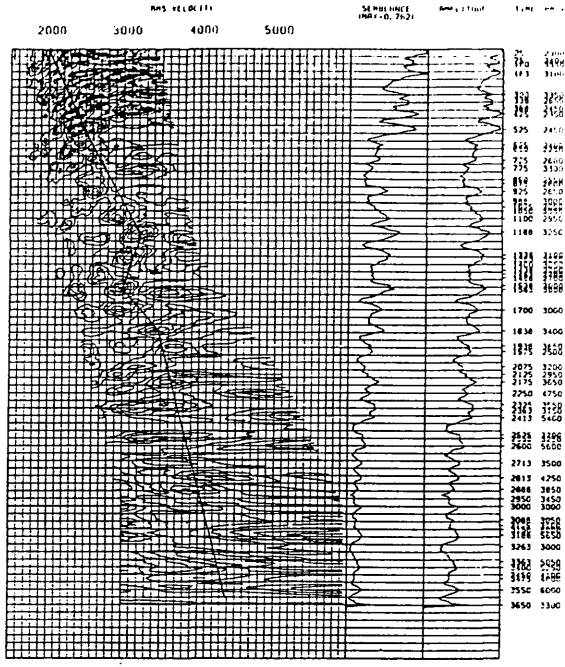
2.15 NORMAL MOVE-OUT CORRECTION

Consider the travel paths of reflected pulses when source and receiver are first coincident and then separated by distance x . The reflection boundary is flat and travel paths are completely within a constant velocity medium. The additional delay ΔT or normal move-out, for a receiver with offset X compared with one at offset zero is given by:

COPS 983 TO 983

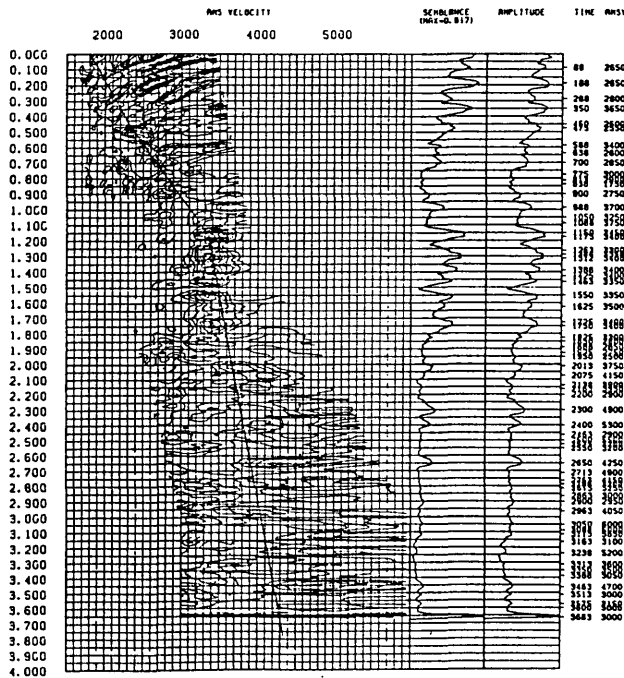


a,



b,

COPS 1424 TO 1424



c

Fig 2.16 (a, b, c) Velocity spectra for the same CDPs as shown in Figure 2.13, after applying residual static correction.

$$\Delta T = T_x - T_0 \dots\dots\dots 2.2$$

$$\Delta T = (T_0^2 + X^2 / V_{NMO}^2)^{1/2} - T_0 \dots\dots\dots 2.3$$

$$V_{NMO} = X / \sqrt{(T_x^2 - T_0^2)} \dots\dots\dots 2.4$$

Where T_0 is the time at zero offset.

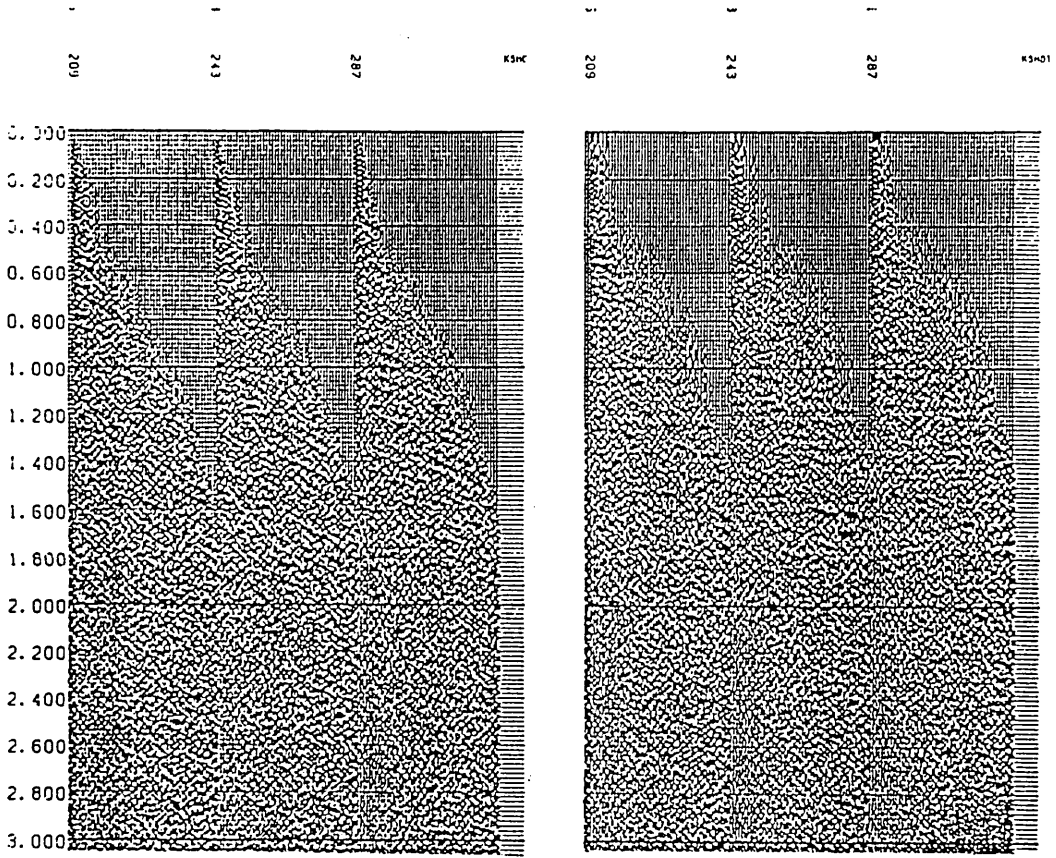
X is the offset of the trace.

V_{NMO} is the velocity at time T .

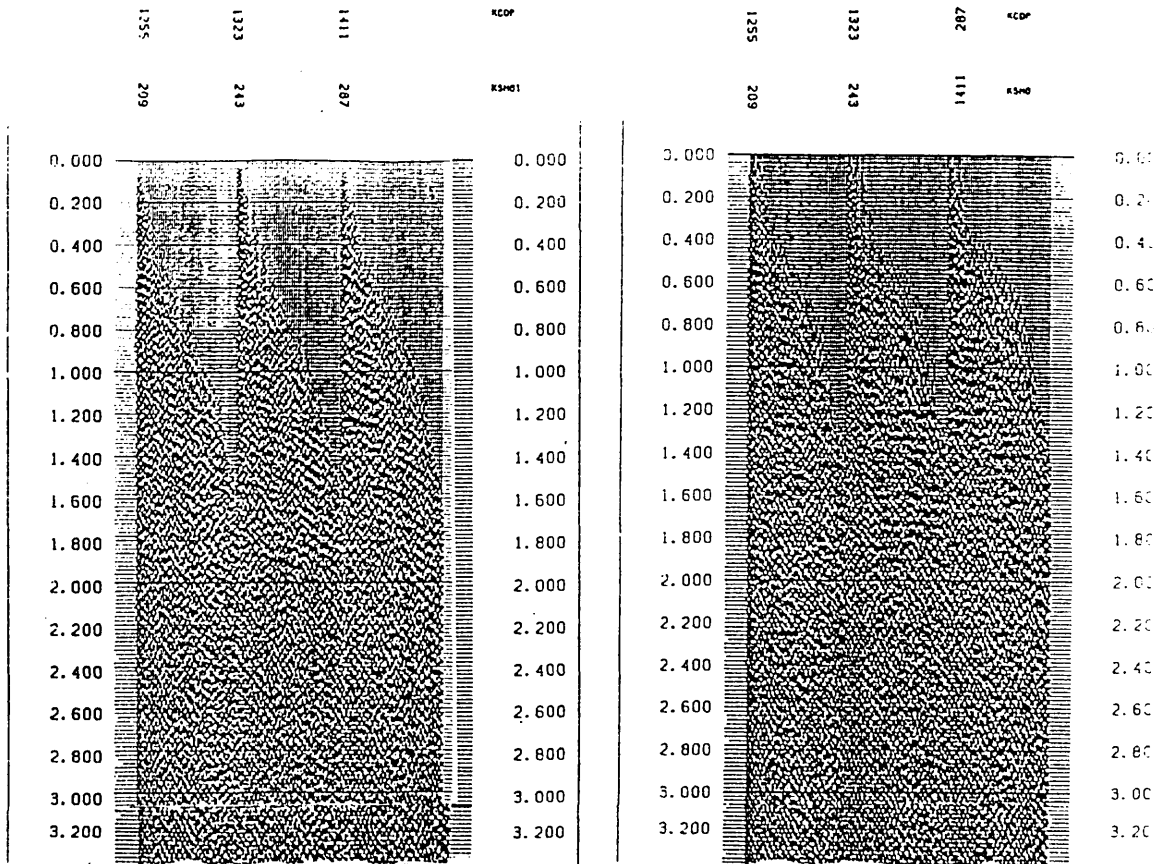
T_x is the reflection time at any offset X .

These equations are of great importance in reflection seismology and are known as the normal move-out or NMO equation. Equation 2.3 represents the hyperbolic relationship between ΔT and X and should appear as such as in a shot file display. It should be noted that when interfaces are at later time, and/or the velocity increases, the hyperbolae are flatter (Hatton, Worthington, and Makin 1986).

The purpose of the NMO correction is to flatten the reflection hyperbola to give a better stack. Some of the reflections are not flattened, but are over-corrected, which means that the velocity used is too low. If the reflections are under-corrected, the stacking velocity is too high. Figure 2.11b shows a common depth point model and a four trace gather for 3 interfaces before and after NMO correction. Figure 2.17a, b, c illustrates the result of applying NMO by using the velocity picked from velocity spectra before and after applying residual static. The data after applying the residual static correction show better alignment.



a) before residual static applied.



b) after residual static applied.

Fig 2.17 CDP gather before and after NMO correction, without (a) and with (b) application of residual static.

2.15.1 NMO Stretching

As a result of the NMO correction, a frequency distortion occurs in which events are shifted to lower frequencies, particularly for the shallow events and at large offsets. Because of the stretched waveform at large offsets, stacking the NMO-corrected CDP gather will severely distort the shallow events. This problem can be solved by muting the stretched zones in the gather. Figure 2.18 shows the stretched CDP gather after applying NMO before (a) and after (b) mute application.

2.16 STACKING

Stacking is the term indicating mixing of time functions, such as seismic traces. Mixing generally involves summing the traces to obtain the average. Stacking is one of the most useful operations in seismic data collection and processing because it improves the single-to-noise ratio. The underlying premise is that the noise N is random in phase and possibly in amplitude, while the signal is not. When n traces with these properties are mixed, the signal output is n times the signal input, while the noise tends to cancel, so the output is less than n times the noise input. When the output is scaled down by dividing by n , the S/N ratio is improved.

2.17 DECONVOLUTION AFTER STACK

The objective of deconvolution is to attenuate repetitive signals such as multiples and also to shape the propagating wavelet into a sharp high resolution pulse. Figures 2.19a, b and c show the section before, after

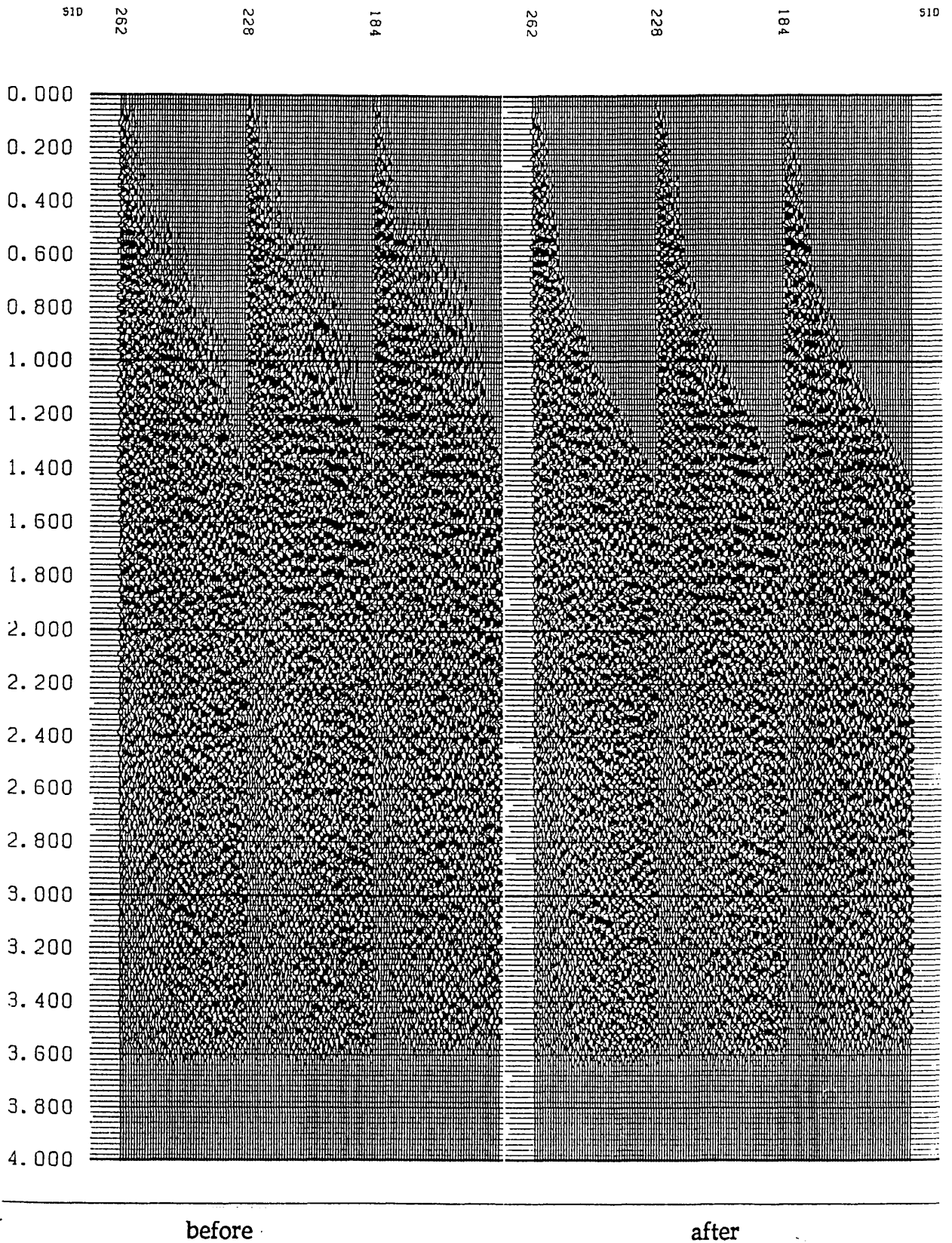


Fig 2.18 CDP gather with residual static applied before and after mute correction

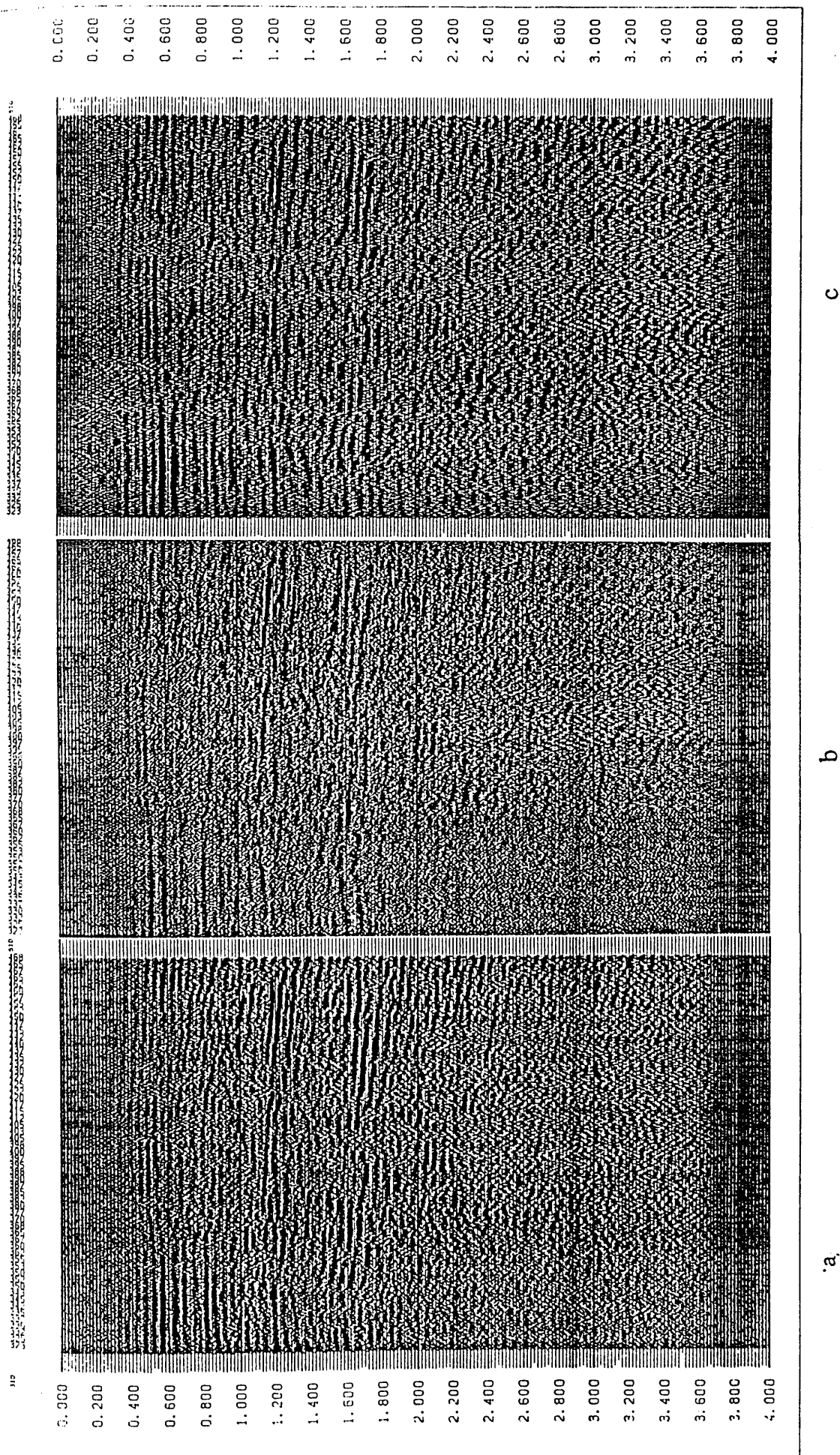


Fig 2.19 Part of stacked section
 a) Before deconvolution
 b) After deconvolution
 c) After deconvolution and band-pass filter.

applying deconvolution, and after applying deconvolution and pass-band filter respectively. After deconvolution the repetitive signal is attenuated and the reflection signals are enhanced.

2.18 FREQUENCY FILTERING AFTER STACK

Any coherent or incoherent noise event whose dominant frequency is different from that of reflected arrivals may be suppressed by frequency filtering. Since the dominant frequency of reflected arrivals reduces with increasing length of travel path, due to the more rapid absorption of the higher frequencies, the characteristics of frequency filters are normally varied as a function of reflection time.

A frequency analysis made on the stacked traces shows that the dominant frequency is in the range 10-45 Hz. Using the stacked section, two different portions on the seismic section were filtered with a series of mostly 10 Hz wide band-pass filters to test sections of the profile. Figures 2.20 and 2.21 illustrate the result of applying these different band-pass filters to test section of the profile. Figure 2.22 shows part of the stacked section filtered with different filters, to compare the effectiveness of filters on different parts of the seismic section. Two filters are applied to the final stacked section: The data between 0-1400 ms are filtered with 10-20Hz, and from 1500 ms to longer times the filter is 5-20 Hz. These frequencies are low, but seem to give good results with this kind of data.

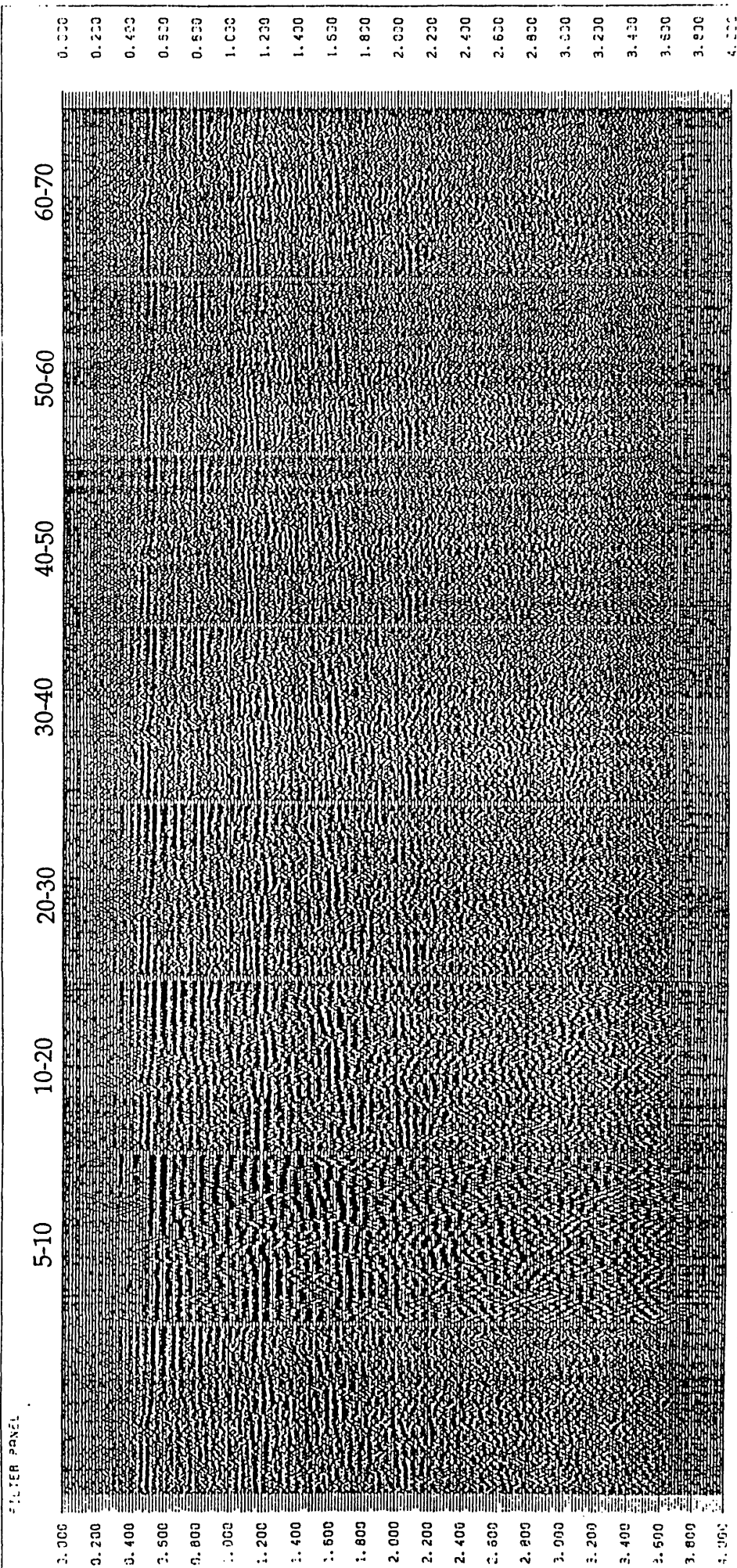


Fig 2.20 (shot points 339 to 405) Stacked data (left panel) with various band-pass filtered versions.

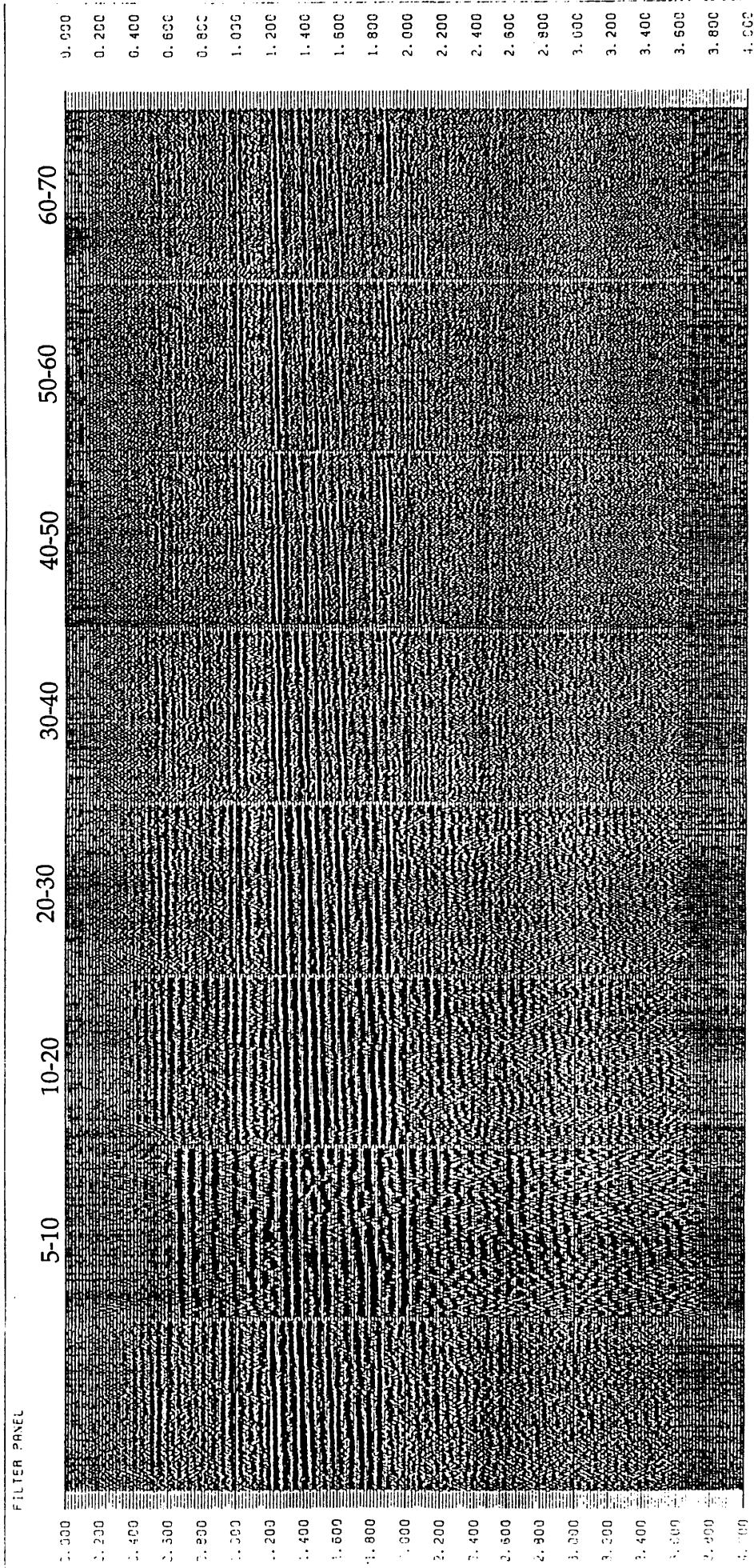


Fig 2.21 (shot points 181 to 240) Stacked data (left panel) with various band-pass filtered versions.

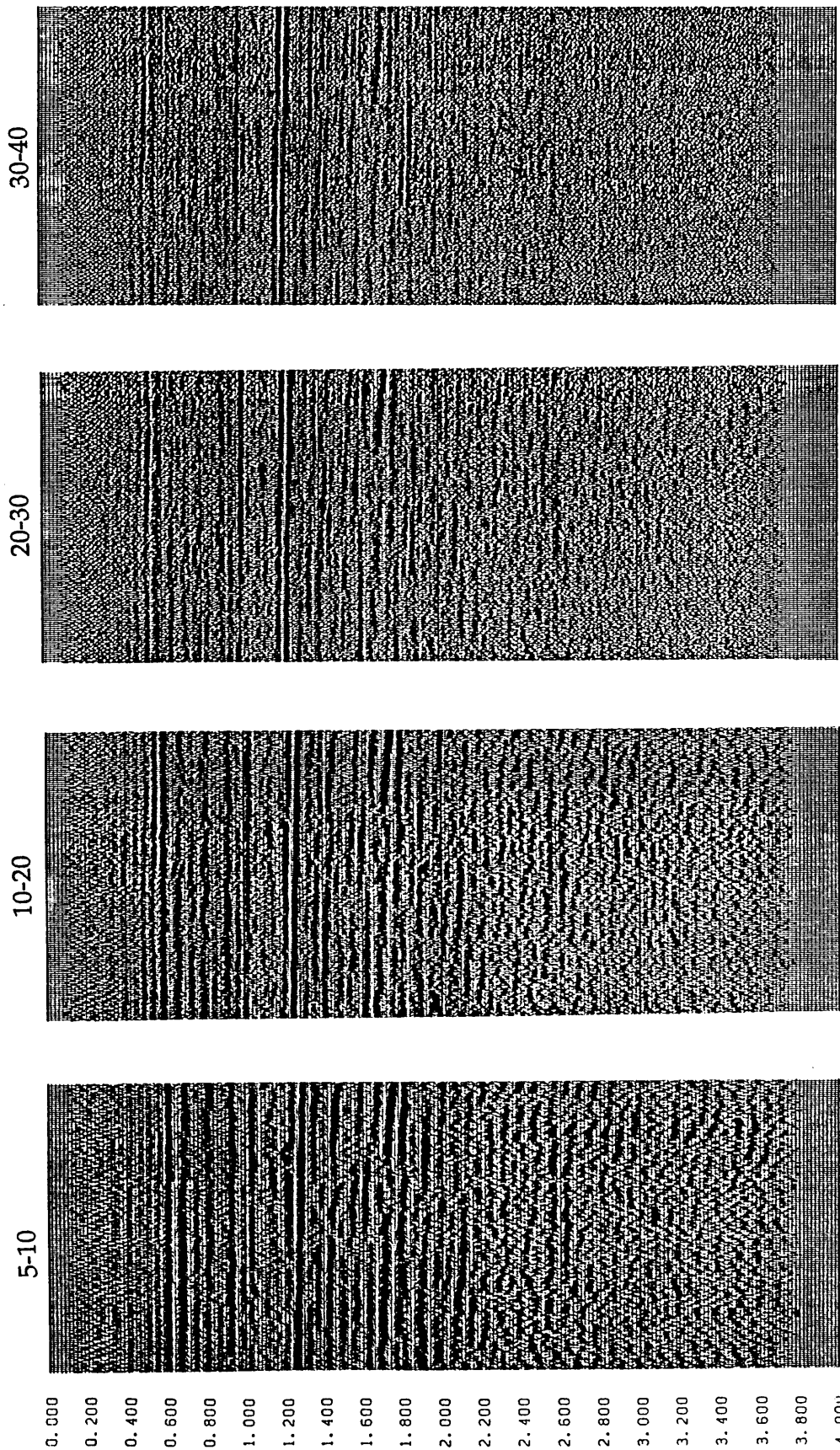


Fig 2.22 (shot 160 to 230) Part of stacked section with different filters applied.

2.19 FINAL STACK SECTION

Three final stack sections have been produced using the SierraSEIS package with uphole statics applied.

- a) Figure 2.23 shows a final section stacked using velocity spectrum in which no deconvolution has been applied after stack.
- b) Figure 2.24 shows a final section stacked using velocity spectrum, with deconvolution and filtering is applied after stack.
- c) Figure 2.25 shows a final section stacked using the velocity function, with deconvolution and filtering applied after stack.

2.20 MIGRATION

2.20.1 Introduction

On a processed, stacked seismic section, each event appears to be directly below the receiver. The reflection surface picked by the interpreter will show the true configuration of the lithological surface only if the surface is flat. In a dipping geological setting and in the presence of folding and faulting, the reflector subsurface position deviates considerably from the true geological position. Migration is the process of making the reflection surface coincide with the geological surface by moving, or migrating, each reflection point to its proper position in the subsurface.

The ability of seismic waves to bend around corners is known as diffraction, which occurs at sharp edges such as the edge of a fault. The diffraction patterns need to be collapsed to the diffracting point by the process

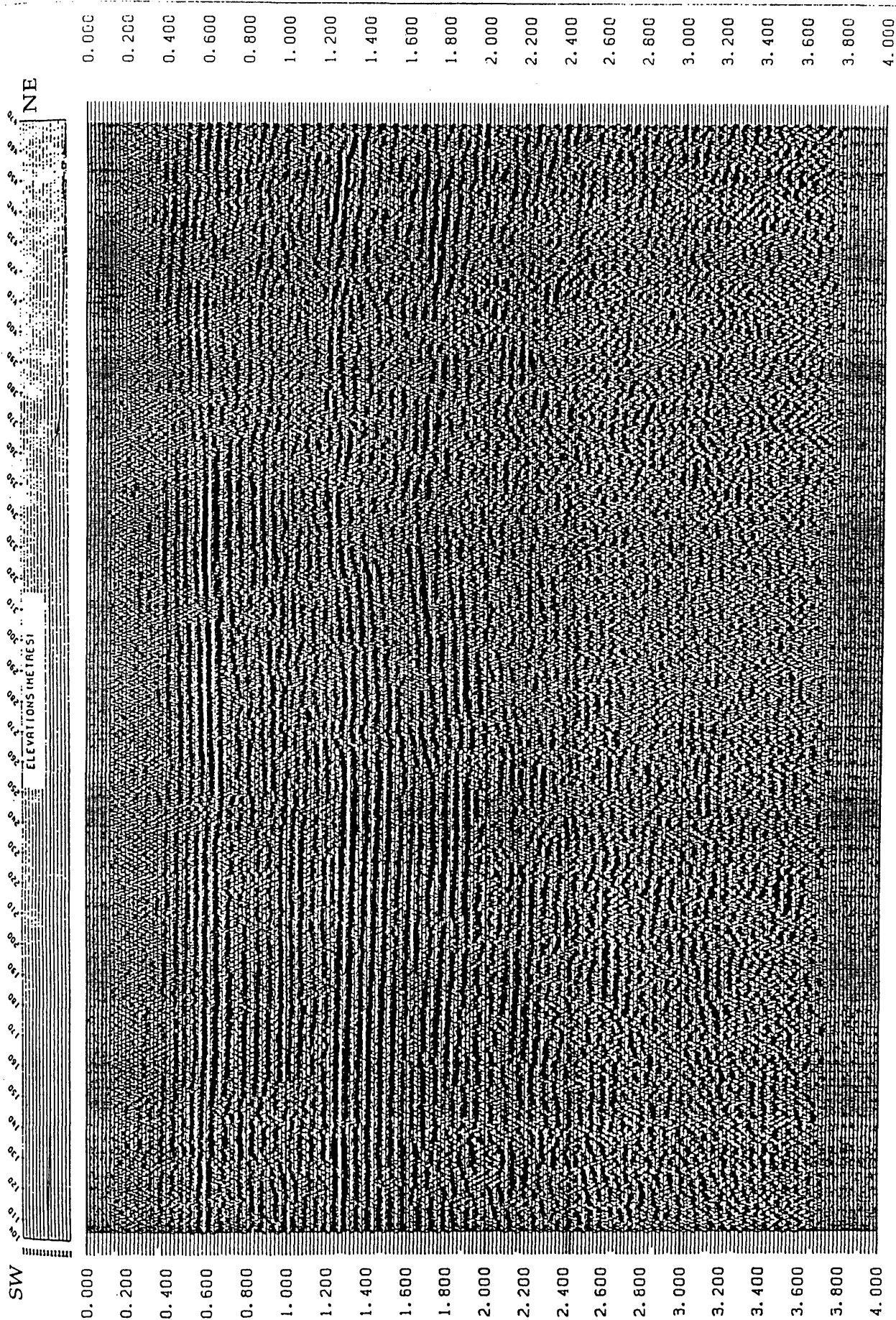


Fig 2.23 Final stack section (no deconvolution applied after stack).

Horizontal scale 0 2km

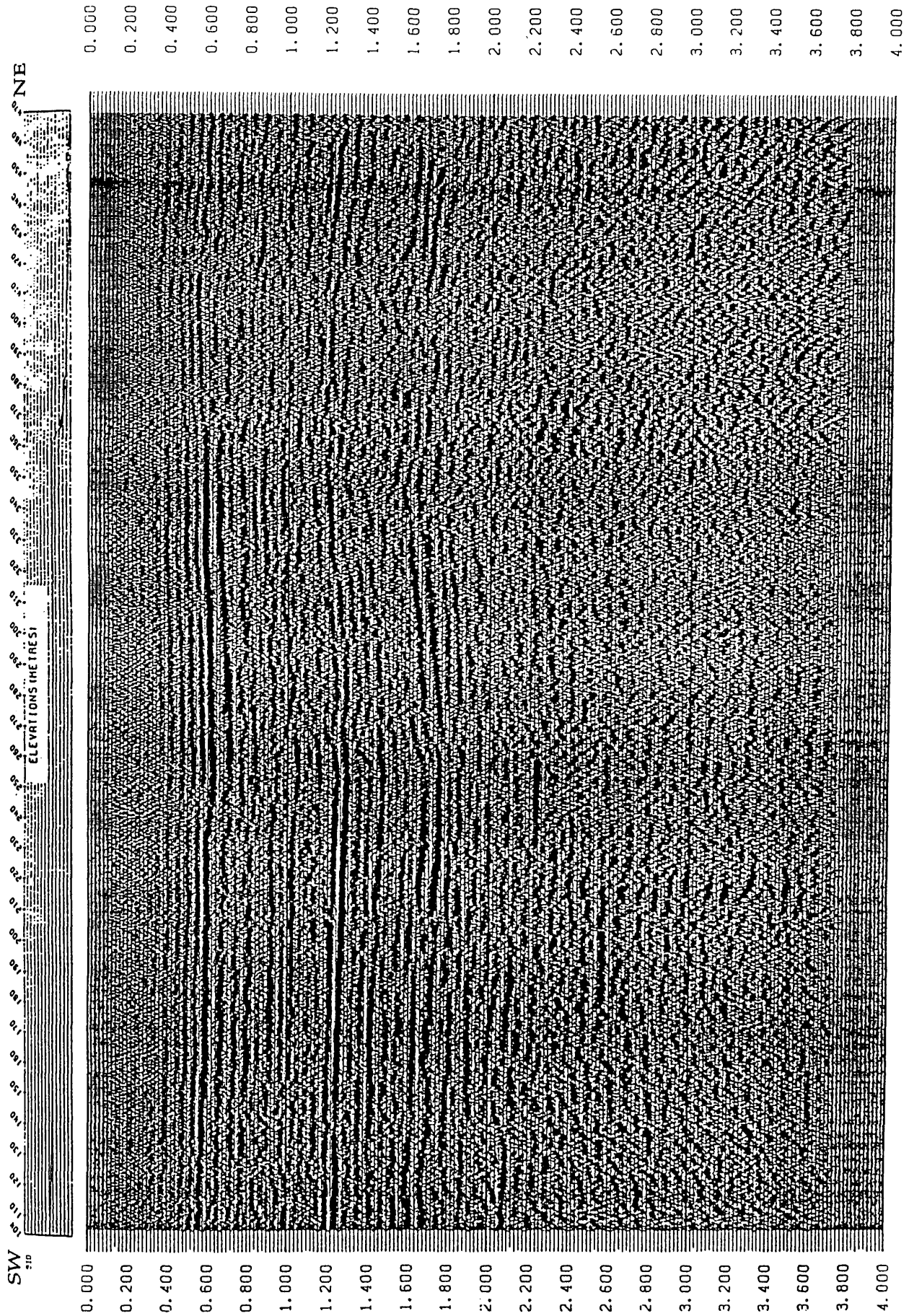


Fig 2.24 Final stack section (with deconvolution applied).

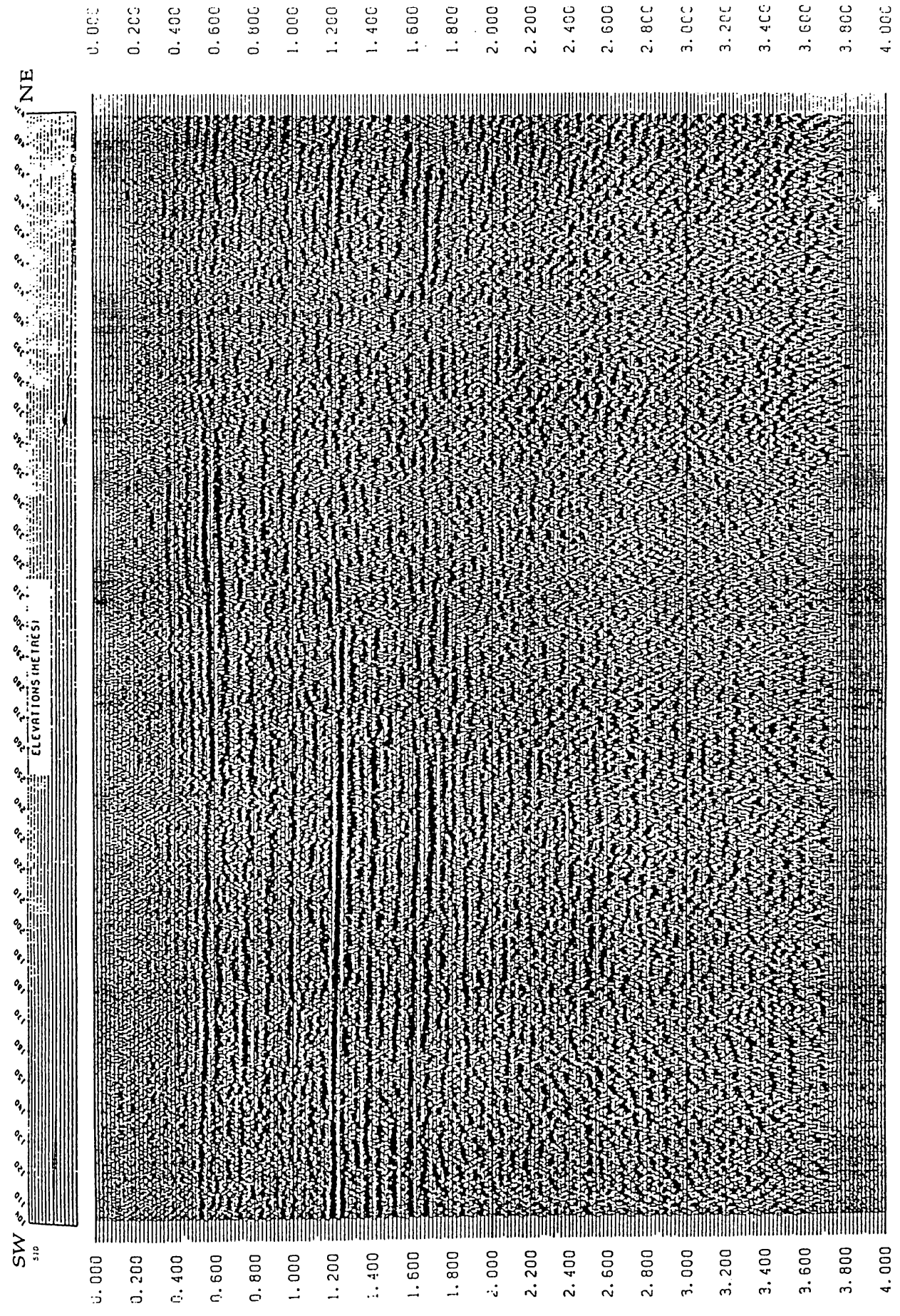


Fig 2.25 Final stack section (stacked with velocity picked using velocity function). Horizontal scale 0 2km

of migration. Another phenomenon which migration can handle is the "bow-tie" reflection pattern. This pattern results from synclinal features when the radius of curvature of the syncline is less than that of the wave front; the result is a blurred focus. This effect is shown in Figure 2.26, where more than one reflection point is recorded at the same reflection location. For example, at surface location N, there are three possible paths to sample the syncline, the two paths labeled N1, N2 and the vertical path (not shown).

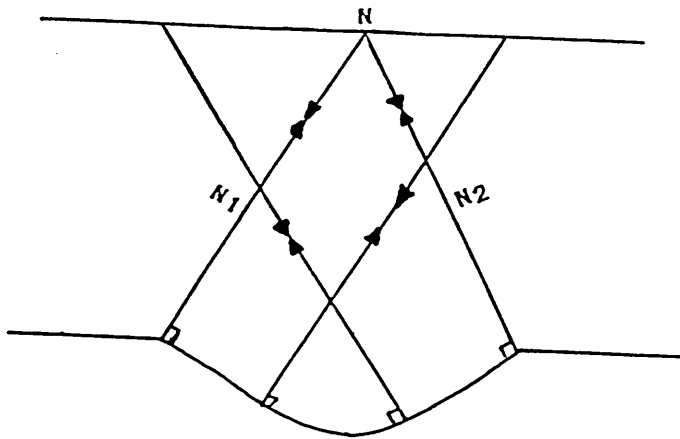


Fig 2.26 Seismic response from a syncline.
Zero-offset ray paths are shown

In some cases, events on both sides and at the bottom of the bow-tie pattern interfere and give the appearance of anticline, which results in ambiguous if not misleading interpretation. Migration strives to recover the shape of the syncline from its reflection pattern (Morgan 1985).

Migration moves dipping reflectors into their true subsurface positions and collapses diffractions, thereby delineating detailed subsurface features such as fault planes (Yilmaz 1987). The goal of the migration

process is to make the stacked section appear similar to the geological cross section along the seismic line. The migrated section is commonly displayed in time (Yilmaz 1987). The estimated velocity based on seismic and other data always is limited in accuracy, therefore depth conversion is not completely accurate. The effectiveness of migration is dependent on the use of accurate velocity control. A velocity that is too low will not migrate events far enough, while too high a velocity will over-migrate the data.

In the study area FK migration is used to migrate the stacking section. FK migration assumes a constant velocity and therefore is less accurate for lines that exhibit larger lateral velocity variation. In the study area line V07-85 is migrated using one velocity. Part of the seismic section shown in Figure 2.24 has been migrated using different velocities, as shown in figure 2.27a, b, and c. Figure 2.27a is migrated using the stacking velocity, whereas (b) and (c) are migrated using a velocity 10% higher and lower respectively than stacking velocity.

The increase and decrease in velocity does not appear to affect the data. From these tests the stacking velocities are used for migrating the seismic section. Figure 2.28 shows the migrated section.

Deconvolution after stack has been applied to the final section shown in Figure 2.24 before migration. The section shows less signal repetition, or ringiness, compared with stack section of Figure 2.23.

The final stack section fig 2.28, when compared with the version produced by Western Geophysical (Fig 3.4), shows these differences:

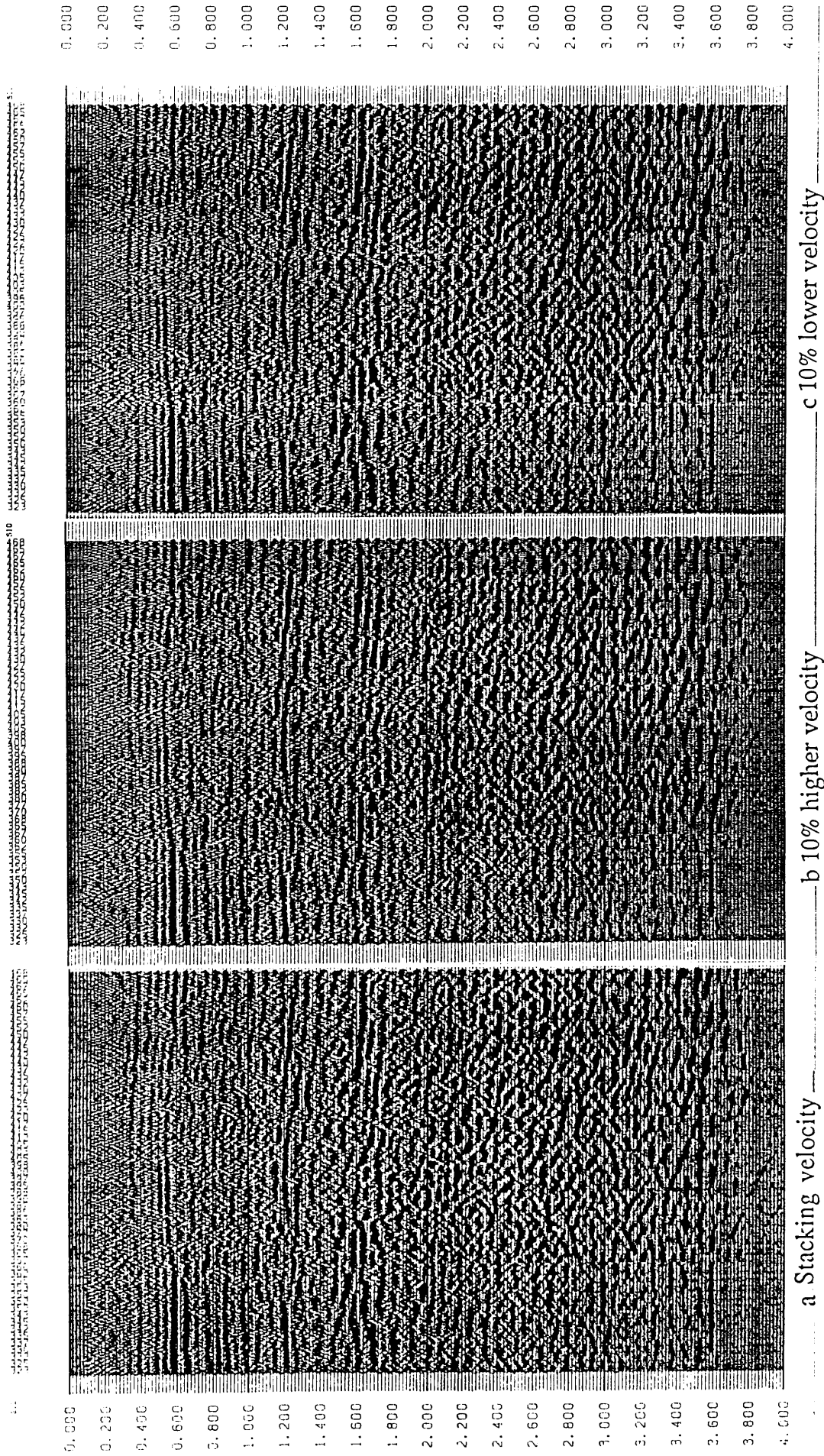


Fig 2.27 FK migrated section with different migration velocities applied.

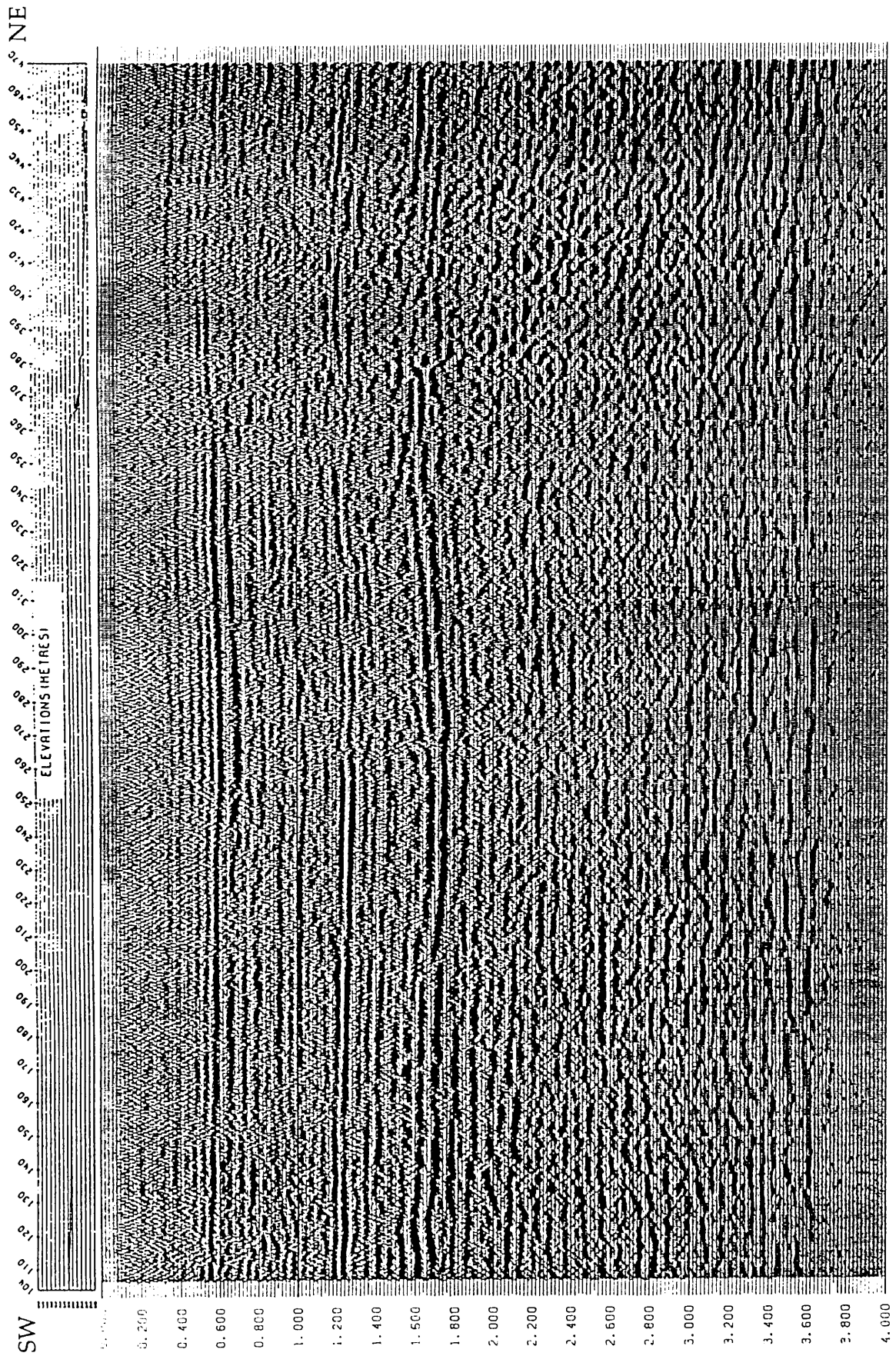


Fig 2.28 Migrated final stack section.

- a) The section processed using SierraSEIS shows less ringing.
- b) The static problem between shot points 360 and 398, where the elevation changed from "off Jabel" to "on Jabel" has been solved by using the uphole static correction method see fig 2.28 and fig 3.4.

Figure 2.29a, b and c show a comparison of the original Western Geophysical section with the unmigrated and migrated SierraSEIS sections.

The SierraSEIS processing sequences is shown in Fig 2.30 and the Western Geophysical processing sequence is shown in Fig 2.31. The differences are mainly:-

- 1) In the field statics applied. Uphole statics have been used on the reprocessed section, whereas the Sabkha formula has been used on the section processed by Western Geophysical.
- 2) Differences in velocity analyses. In the reprocessed section the velocity analyses were computed after static correction were applied to the CDP gather, whereas in the Western Geophysical section the computation of velocity analysis was done before applying the static correction (i.e. the velocity was calculated from the surface).
- 3) Differences in deconvolution application after stack. No deconvolution after stack was applied to the Western section but deconvolution after stack has been applied to the the reprocessed section.

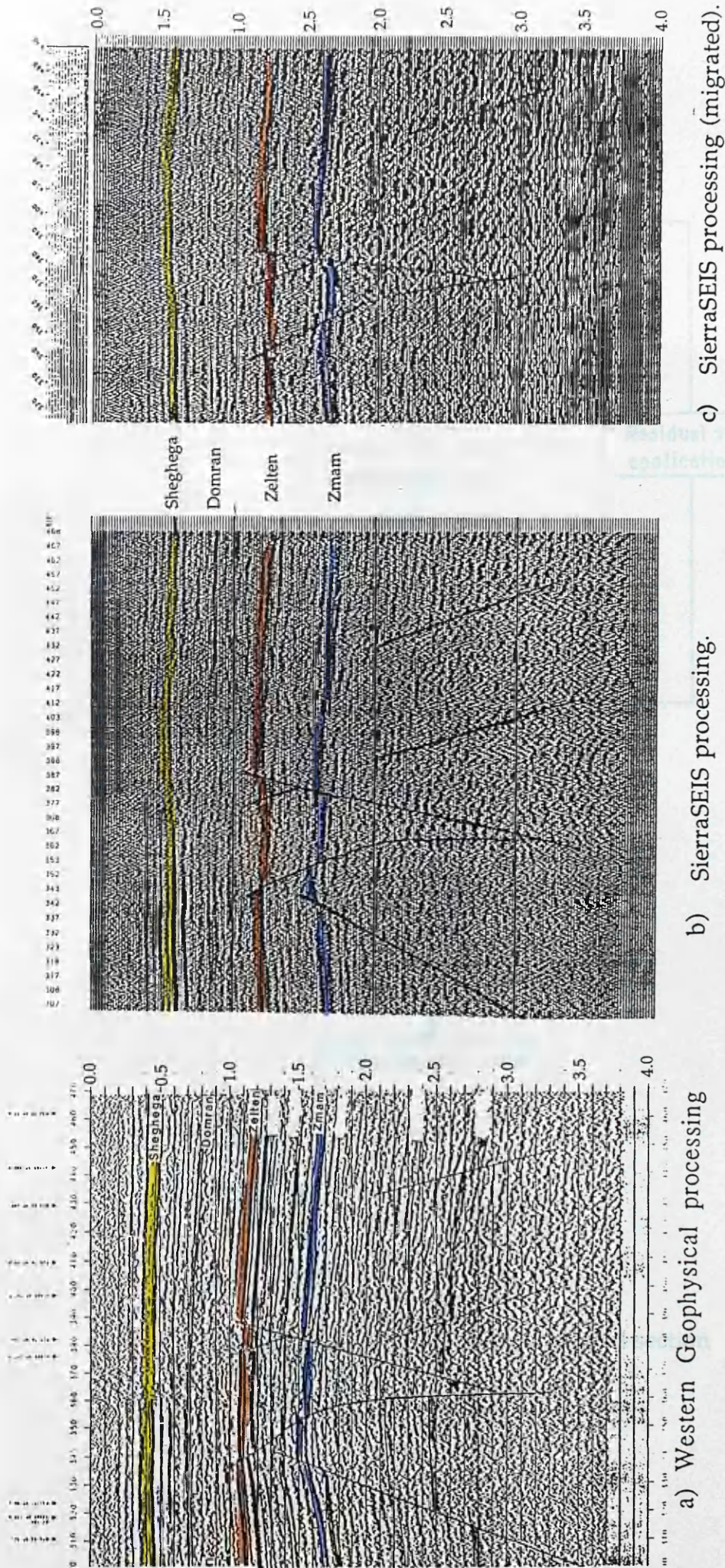


Fig 2.229a, b and c Interpreted seismic sections showing the difference between Western Geophysical section and SierraSEIS section.

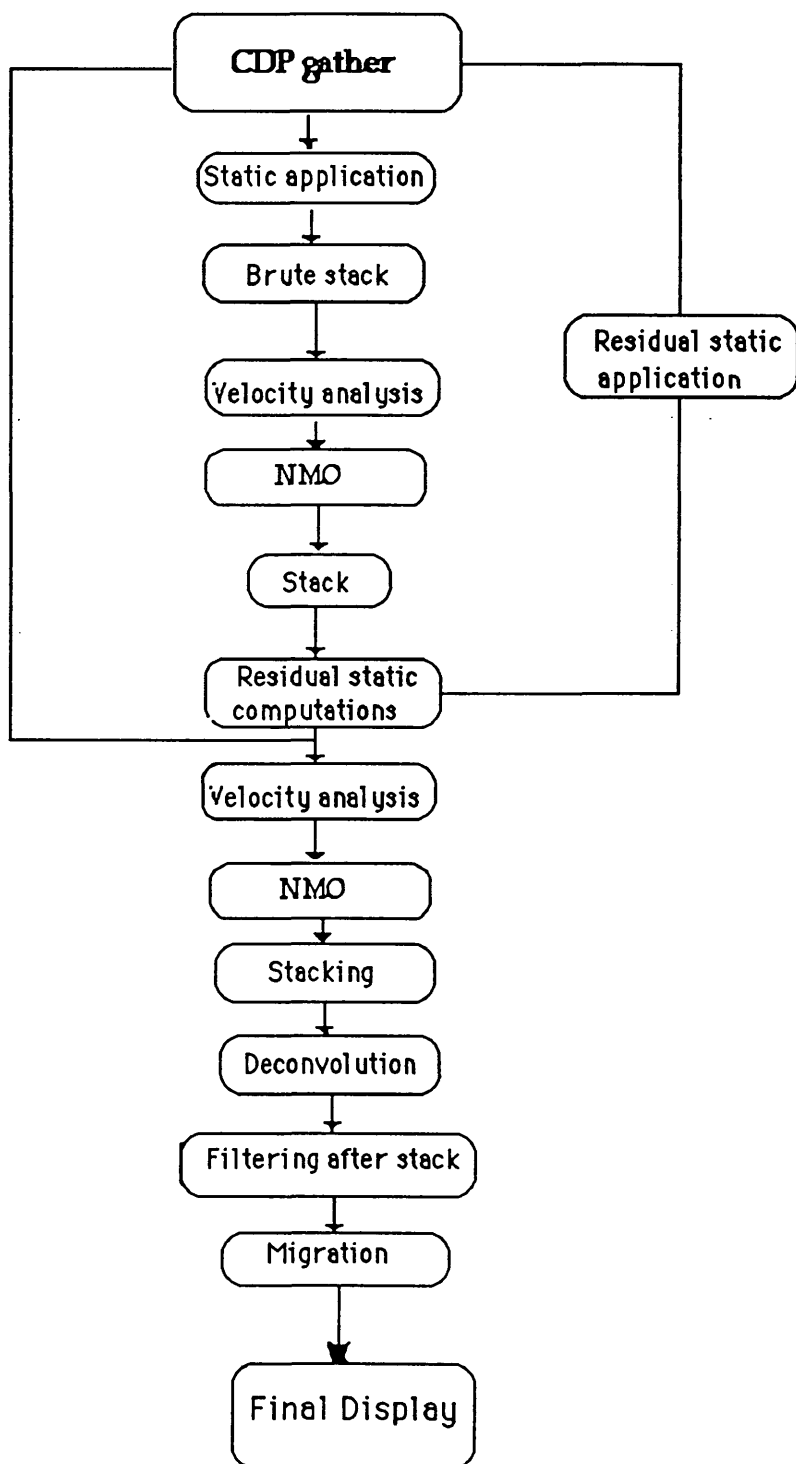

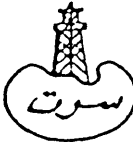



Fig 2.30 Processing flow chart of the reprocessed section

 SIRTE	شركة سرت للنفط SIRTE OIL COMPANY	 سرت
 WESTERN GEOPHYSICAL Litton		
AREA S.P.L.A.J. CONCESSION 149		W.G.C. CONTRACT..... 103 SHOT BY..... RCO PARTY 9 DATE SHOT..... MAY 1984 PROCESSED IN LOC..... DECEMBER 1985 REEL NUMBER..... 134869

PROCESSING SEQUENCE

DEMULT-VIBCORR

OUTPUT - 4 SECONDS
DESKEW CORRECTION APPLIED

PREPROCESSOR-DECONVOLUTION

A) GEOMETRIC SPREADING GAIN APPLIED
 B) INSERT STATICS INTO TRACE HEADER
 C) DECONVOLUTION-WIN PHASE INV FLIR
 1 WINDOW:

	ACORR	DECON
NEAR TR	0.4-2.5	0.4-4.0 SEC
FAR TR	1.2-2.5	0.8-4.0 SEC
MIN PREDICTIVE LAG (GAP)	.12 MS	
ACTIVE OPERATOR LENGTH	.250 MS	
WHITE NOISE	.0.1 2	

B) COMMON DEPTH POINT GATHER
 C) TRACE BALANCE

AUTOMATIC RESIDUAL STATICS

WISER®

WINDOW..... 300-2400 MSEC
 SHIFT..... 32 MSEC
 MODEL COMPUTATION OVER 7 COF'S

VELOCITY ANALYSIS

EXPANDED VELANS
 1 EVERY 2 RMS
 UNLESS SHOWN BY VELOCITIES LOCATION
 ON HEADER

AUTOMATIC RESIDUAL STATICS

WISER® ON COP 1-370

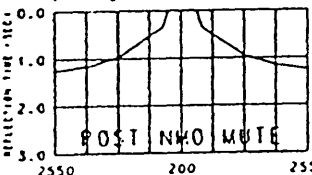
WINDOW..... 300-1400 MSEC
 SHIFT..... 32 MSEC
 MODEL COMPUTATION OVER 10COF'S

APPLY STATICS-NWO-MUTE

1352 STRETCH MUTE

OFFSET TRACE NUMBER

1	24	48	72	96
---	----	----	----	----



REFLECTION TIME (SEC)

2550 200 2550
OFFSET DISTANCE (M)

48 FOLD STACK

GAIN AFTER STACK

REFLECTION STRENGTH GAIN 1.1

BAND PASS FILTER

L.C. #17/DB/OC1 IN. C.
 10 / 18 40 / 36

PLAYBACK

GAIN..... 12 DB
 BIAS..... 6

SCALES

HORIZONTAL 1:75,000 1:50,000
 VERTICAL 40CMS/SEC 30CMS/SEC

0 10 20 30 40 50 60 70 80 90 100

Fig 2.31 Label of seismic line V07-85 summarizing the processing sequence carried out by Western Geophysical in 1985.

Chapter 3

Seismic interpretation

- 3.1 Seismic interpretation
- 3.2 Interpretation steps
- 3.3 Problem in interpretation of the data
- 3.4 Time structure maps
- 3.5 Isochron maps
- 3.6 Types of trap
- 3.7 Hydrocarbon entrapment
- 3.8 Back-stripping

3.1 SEISMIC INTERPRETATION

3.1.1 Introduction

The interpretation of seismic data in geological terms is the objective and end product of seismic work. The main objectives of hydrocarbon seismic interpretation are to produce time and depth structure maps, isochron and isopach maps, to locate the structure and to determine the kind of traps that exist.

3.1.2 Definition

Interpretation may be defined as the graphical and written description of the subsurface, based on the combination of the physical measurements, geological facts and understanding of earth physics.

The reflection coefficient is defined by:

$$\text{Reflection coefficient} = (\underline{V}_2 * \underline{d}_2 - \underline{V}_1 * \underline{d}_1) / (\underline{V}_2 * \underline{d}_2 + \underline{V}_1 * \underline{d}_1) \dots\dots\dots 3.1$$

where \underline{d}_1 and \underline{d}_2 are the densities on the near (incident) side and far side of the boundary respectively, and \underline{V}_1 and \underline{V}_2 are the corresponding velocities for the two sides.

The sign of the reflection coefficient and its amplitude depend on the contrast in acoustic impedance across the reflecting interface. Any lateral change in the velocity or density of one or both of the materials separated

by the interface will cause the amplitude of the reflection from this boundary to vary laterally. Its value varies from -1 to +1.

The geometry and character of reflections, their amplitudes, and the formation velocities are used to determine the stratigraphic setting, depositional history, lithology and hydrocarbon presence in the area of seismic interpretation.

3.2 INTERPRETATION STEPS

3.2.1 Well tie

Seismic interpretation is begun by tying wells to the seismic data. Tying well data and seismic data is an essential step in an interpretation, and begins with an analysis of the data collected in the well.

Before tying well data and seismic data relevant information needs to be collected (well tops in metres or in feet and the equivalent time in milliseconds). This information requires wire logs to be available such as compilation, sonic or calibrated velocity log relating depth to time. No compilation, sonic or velocity logs were available for this study. Tying well data to seismic data is done in this study by using the check shot data which are available for five wells (D6, D7, D8, D9, and K1-149):

a) The locations of the wells are checked on the base map. Table 3.1 shows the relation between the seismic lines and well locations.

Table 3.1

Well name	Seismic line	Shot point	Location of the well on the seismic line
D6-149	V16-85	650	On line
D7-149	V14-85 88-112	260 1315	Projected (600m off) Projected (400m off)
D8-149	V11-85	310	Projected (400m off)
D9-149	V16-85	710	On line
K1-149	V35-85	310	On line

Table 3.1 Link between wells with check shot survey and seismic data.

- b) All the check shot data are corrected for angularity.
- c) The check shot data are corrected to the datum by stripping the static correction applied to the seismic section near to or passing through the well.
- d) All the formation tops in the area are corrected to the sea level datum by subtracting the kelly bushing (KB) elevation above sea level to get subsea depth.
- e) The check shot data in the study area are used to help define the acoustic impedance and predict the seismic response. The anticipated seismic response depends on the seismic display polarity.

The SEG standard for polarity is as follows:

A compressional event (marine data) or upward motion of the geophone case (land data) is recorded as negative numbers on tape and displayed as a trough (white) on the wiggle/VAR seismic section. Thus a reflection from an interface with a positive reflection coefficient (e.g. shale and limestone contact) will be displayed as shown in Fig 3.1.

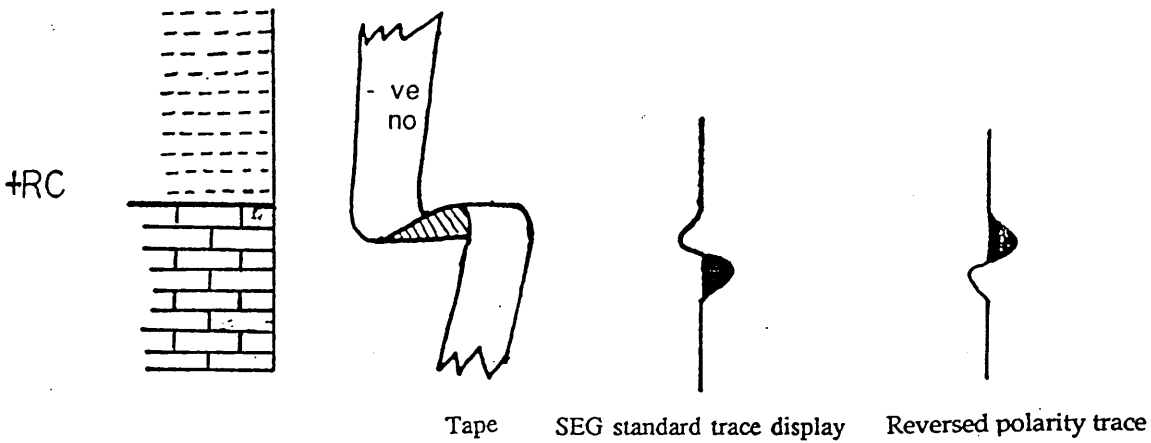


Fig 3.1 Example of normal and reversed polarity minimum phase wavelet.

In the study area the data display polarities, as shown in the seismic section side-labels of the surveys used, are shown in Table 3.2.

Table 3.2

Type of data and year of acquisition	Display polarity	Deconvolution
Dinoseis 1970-1971	Not known	Minimum phase
Dynamite 1983	Not known	Minimum phase
Vibroseis 1985	"Reverse polarity to tie with existing data"	Minimum phase
Vibroseis 1988	Sirte standard (SEG)	Minimum phase

Table 3.2 Type of data and the year of acquisition, display polarity and deconvolution.

Determining the seismic pulse can be difficult. In the first instance we can read the seismic section side-label and see what type of seismic pulse should have been generated by the processing sequence. For example, minimum phase deconvolution should produce minimum phase seismic pulses. Often we have a mix of operators in the processing, for example, minimum phase deconvolution followed by a zero phase time variant filter. The result should be a slightly mixed phase response with the underlying minimum phase data being dominant in this situation. Visual inspection of the data to determine the pulse shape is a rather crude method, and interference effects can modify this wavelet and produce an incorrect pulse shape (Badley 1989). In the study area neither the filter polarity nor the display polarity of the seismic sections are known.

Table 3.3 shows the well name, subsea depth in metres, corresponding one way time in milliseconds and anticipated seismic response calculated from the well velocity data. The one way travel times shown in Table 3.3 are doubled and tied to the seismic section. Comparing the two-way times observed in the wells (time as picked from check shot data) with those in the seismic sections passing through or close to the wells reveals mis-ties as shown in Table 3.4.

The geological boundary is a marker between beds where the lithology has changed, and can be determined by the lithological logging or rock chippings and cores obtained from borehole. The geophysical boundary is an interface where the reflections occur, and its depend on the physical properties of the rock (change in velocity and density to produce acoustic impedance). Reflectors usually correspond with the boundary between rocks of markedly different lithology. Such a boundary does not

Table 3.3

Well name	Seismic line	Formation top	Depth in metres	Time in millisecond	anticipated seismic response
D6-149	V16-85	Sheghega	-438	191.4	+ve
		Domran	-956	331.0	+ve
		Zelten	-1519	522.0	-ve
		Heira	-1870	561.0	-ve
		Zmam	-2467	744.0	+ve
		Socna	-2552	761.0	+ve
		Nubian	-2903	867.0	+ve
		Gargaf	-3471	989.0	+ve
D7-149	V14-85	Sheghega	-458	229.4	+ve
		Domran	-981	368.0	+ve
		Zelten	-1777	571.0	+ve
		Heira	-1915	600.9	-ve
		Zmam	-2538	797.0	+ve
		Socna	-2733	837.0	-ve
		Nubian	-3282	1019.0	+ve
		Gargaf	-3760	1088.0	+ve
D8-149	V11-85	Sheghega	-441	224.0	+ve
		Domran	-953	361.0	+ve
		Zelten	-1731	559.6	+ve
		Heira	-1882	592.0	-ve
		Zmam	-2483	779.5	+ve
		Socna	-2674	821.0	-ve
		Nubian	-3235	986.6	+ve
		Gargaf	-3370	1009.0	+ve
D9-149	V16-85	Sheghega	-443	235.0	+ve
		Domran	-965	375.0	+ve
		Zelten	-1451	573.0	+ve
		Heira	-1903	601.0	-ve
		Zmam	-2430	766.0	+ve
		Socna	-2620	810.0	-ve
		Nubian	-3581	1108.0	+ve
		Gargaf	NP	-	-
K1-149	V35-85	Sheghega	-448	228.0	+ve
		Domran	-971	368.5	+ve
		Zelten	-1761	561.0	+ve
		Heira	-1893	590.0	-ve
		Zmam	-2429	754.0	+ve
		Socna	-2626	795.8	-ve
		Nubian	-3400	1033.3	+ve
		Gargaf	-3965	1139.0	+ve

Table 3.3 Well name, seismic line passing through the well, depth in metres and equivalent (one-way) time in milliseconds.
NP: formation is not penetrated by the well.

Table 3.4

Well name	Seismic line	Formation top	Depth in metres	Well TWT (ms)	Seismic TWT (ms)	Difference in millisecond
D6-149	V16-85	Sheghega	-438	382.0	430	-52
		Domran	-956	662.0	715	-47
		Zelten	-1519	1044.0	1060	-16
		Heira	-1870	1122.0	1140	-18
		Zmam	-2467	1488.0	1530	+58
		Socna	-2552	1522.0	1600	+78
		Nubian	-2903	1734.0	1750	+16
		Gargaf	-3471	1978.0	1925	-53
D7-149	V14-85	Sheghega	-458	458.0	445	-13
		Domran	-981	736.0	740	+4
		Zelten	-1777	1142.0	1140	-2
		Heira	-1915	1202.0	1210	+8
		Zmam	-2538	1594.0	1570	-24
		Socna	-2733	1684.0	1685	+1
		Nubian	-3282	2038.0	2020	-18
		Gargaf	-3760	2176.0	2184	+8
D8-149	V11-85	Sheghega	-441	448.0	440	-8
		Domran	-953	722.0	730	+8
		Zelten	-1731	1119.0	1100	-19
		Heira	-1882	1184.0	1165	-19
		Zmam	-2483	1559.0	1530	-29
		Socna	-2674	1542.0	1600	+18
		Nubian	-3282	1973.0	1970	-3
		Gargaf	-3370	2018.0	2018	0
D9-149	V16-85	Sheghega	-443	470.0	450	-20
		Domran	-965	750.0	740	-10
		Zelten	-1451	1146.0	1120	-26
		Heira	-1903	1202.0	1205	+3
		Zmam	-2430	1532.0	1535	+3
		Socna	-2620	1620.0	1625	+5
		Nubian	-3581	2216.0	2270	+54
		Gargaf	NP	-	-	-
K1-149	V35-85	Sheghega	-448	456.0	440	-16
		Domran	-971	737.0	735	-2
		Zelten	-1761	1122.0	1120	-2
		Heira	-1893	1180.0	1170	-10
		Zmam	-2429	1508.0	1515	+7
		Socna	-2626	1592.0	1600	+8
		Nubian	-3400	2067.0	2070	+3
		Gargaf	-3965	2278.0	2270	-8

Table 3.4 Formation tops, two-way time in the wells and seismic with the mis-ties.

NP: formation is not penetrated by the well.

always occur exactly at the geological horizon of major chronostratigraphic importance, such as the base or top of a system or series, but may be simply a seismic reflector which occurs close to that boundary.

3.2.2 Closing loops

The line intersections of the entire survey should be tied together, making sure that all line intersections are consistent, but some problems often occur, such as mis-ties between the different surveys, and even within the same survey due to static problems. The mis-ties between the different surveys are due to:

- (a) Reversal of polarity between seismic sections from different surveys. Particularly with older data, it is often difficult to know whether a polarity reversal is present or not.
- (b) Difference in processing parameters, such as stacking velocities, deconvolution parameters and filter settings.
- (c) The difference in the type of sources that have been used for gathering the data in the field.

3.2.3 Picking and posting the data

1) Taking into consideration all the points mentioned above, the picking of the horizons was consistent for all the data sets. Fig 3.2 shows examples of seismic sections for the four kinds of survey, and the seismic events which were picked for the different formations. The check shot survey data from wells D6, D7, D8, D9 and K1-149 have been used to identify the reflections. The lithological or stratigraphical boundaries in the wells

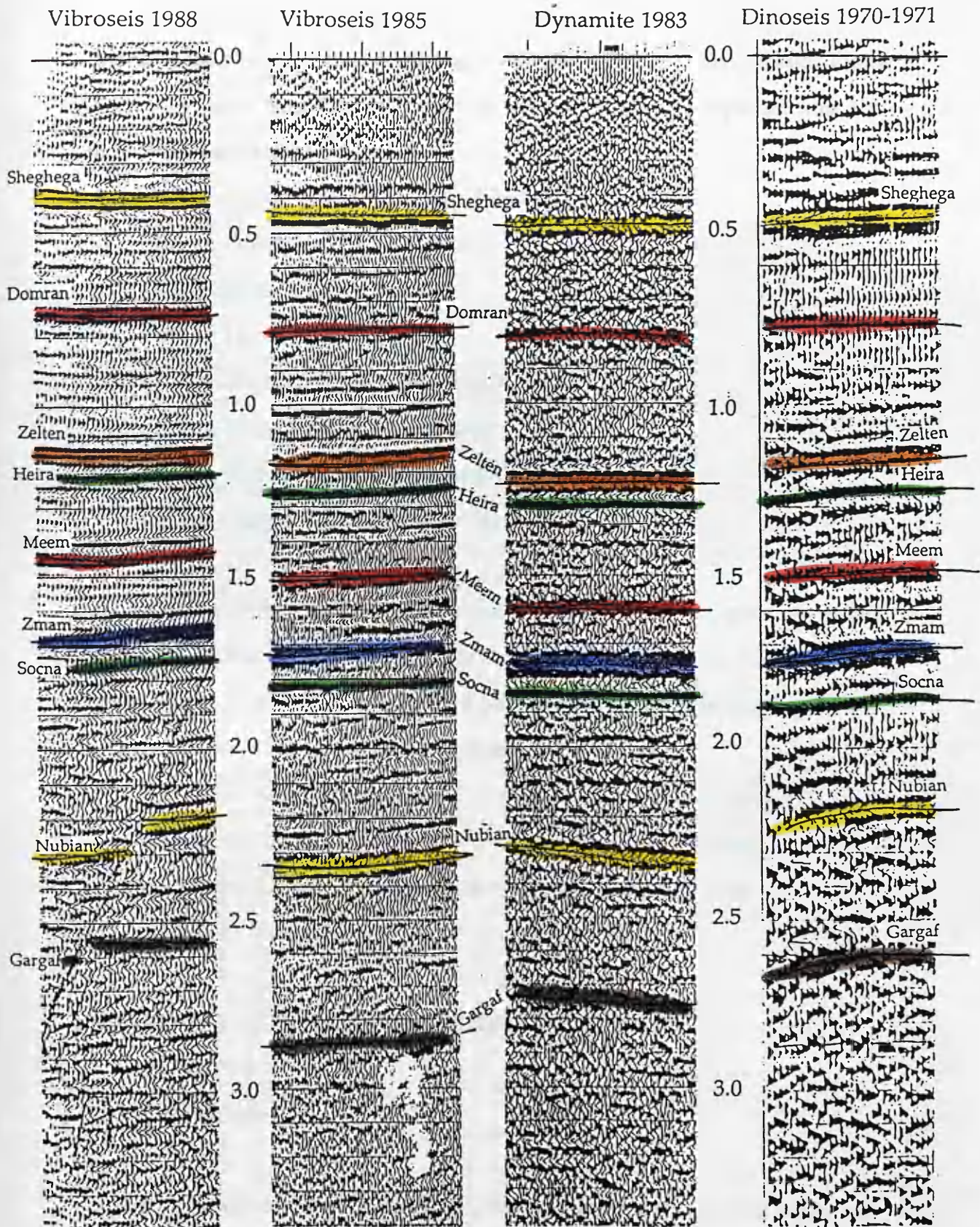


Fig 3.2 Examples of the seismic data for different surveys and the events picked for every formation mapped.

which would be expected to produce seismic reflections are picked. Eight reflectors have been marked on the seismic sections, representing the following formations:

- (1) Top Sheghega (Middle Eocene).
- (2) Top Domran (Lower Eocene).
- (3) Top Zelten (Lower Eocene).
- (4) Top Heira (Palaeocene).
- (5) Top Zmam (Upper Cretaceous).
- (6) Top Socna (Upper Cretaceous).
- (7) Top Nubian (Lower Cretaceous).
- (8) Top Gargaf (Cambro-Ordovician).

2) The interpreted seismic sections are then timed, i.e. two-way times are read off the sections. Times picked from four horizons (Gargaf, Nubian, Zmam and Zelten) are posted on the shot point base map and four time structure maps are contoured. These are:

- (1) Gargaf (Cambro-Ordovician) time structure contour map.
- (2) Nubian (Lower Cretaceous) time structure contour map.
- (3) Zmam (Upper Cretaceous) time structure contour map.
- (4) Zelten (Lower Eocene) time structure contour map.

3.3 PROBLEMS IN INTERPRETATION OF THE DATA

3.3.1 Basin style

A tectonic sequence forming a graben, if allowed to evolve fully, can result in two or possibly three dissimilar sedimentary basin styles (Fig 3.3):

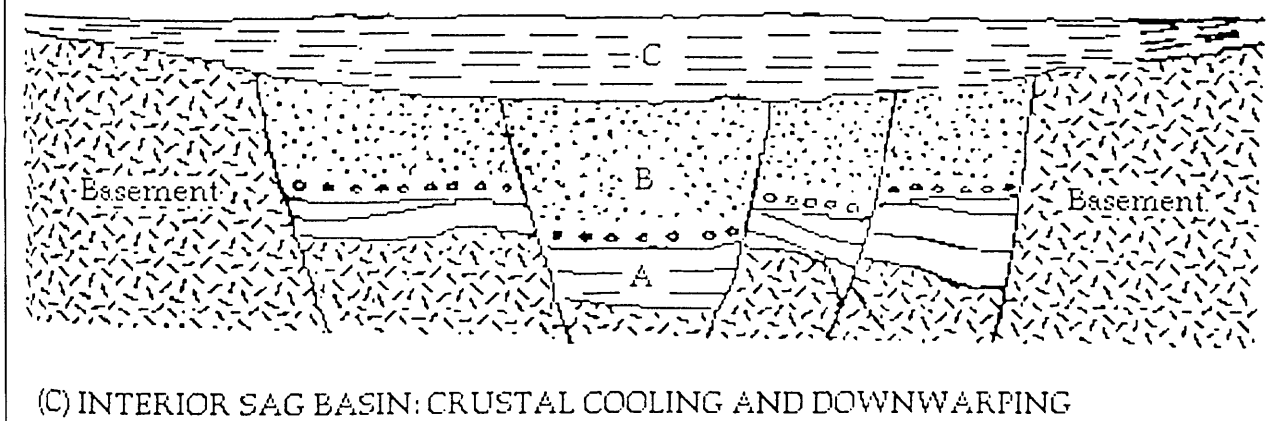
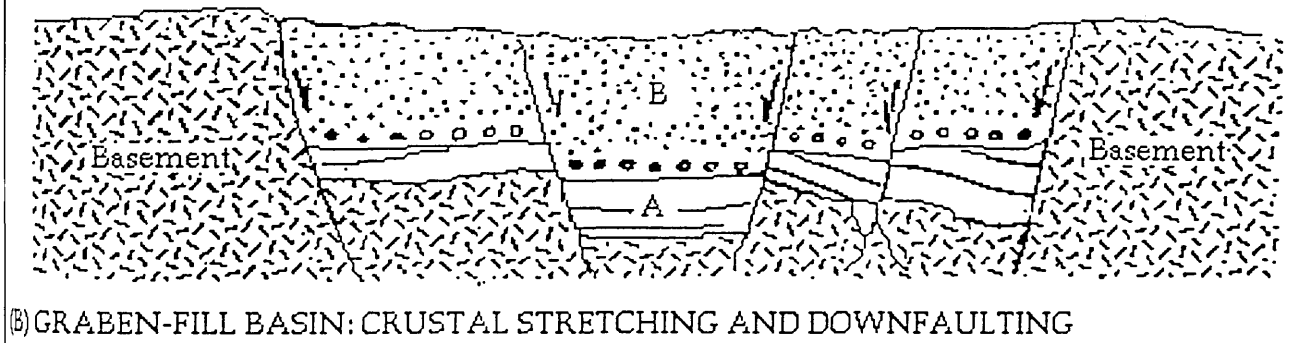
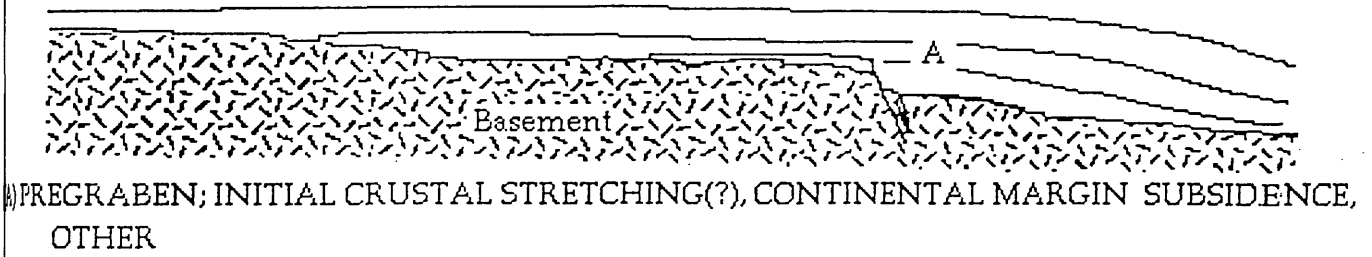


Fig 3.3 Sequence of sedimentary basins containing major hydrocarbon accumulations in graben setting and their dominant subsidence mechanisms (After Harding 1984).

- (a) Pregraben sedimentary cover deposited prior to graben formation.
- (b) Graben-fill basin deposited during faulting.
- (c) Interior-sag basin deposited after faulting.

In the Sirte Basin, all three potential sedimentary cycles (pregraben, graben fill, and interior sag) are present and productive. These cycles are found in three broad graben arms, Sirte Basin deep and Hagfa Trough, the Tumayn Sub-basin, and the Sarir-Hameimat Trough, which define a large triple junction within the continental crust of the African plate (Harding 1984); see Fig 1.2. The post interior sag is essentially a syncline that forms in the final thermal subsidence phase of the graben tectonics. In the area of study these three cycles are present. Line V07-85 (Fig 3.4) demonstrates all three styles.

3.3.2 Faulting

As an indication of a fault in a seismic section, reflection events terminate sharply as the point of reflection reaches the fault plane, then they resume again in displaced positions on the other side of the fault. The reflection sequence on either side has a sufficiently individual character that the two portions on the opposite sides of the fault can be recognized, and the fault throw determined. In practice, diffractions usually prolong events laterally, so that the locations of fault planes are not clearly evident, although occasionally it is possible to observe sharp terminations. Time migration of the stacked section helps to reposition diffracted energy at the reflector termination.

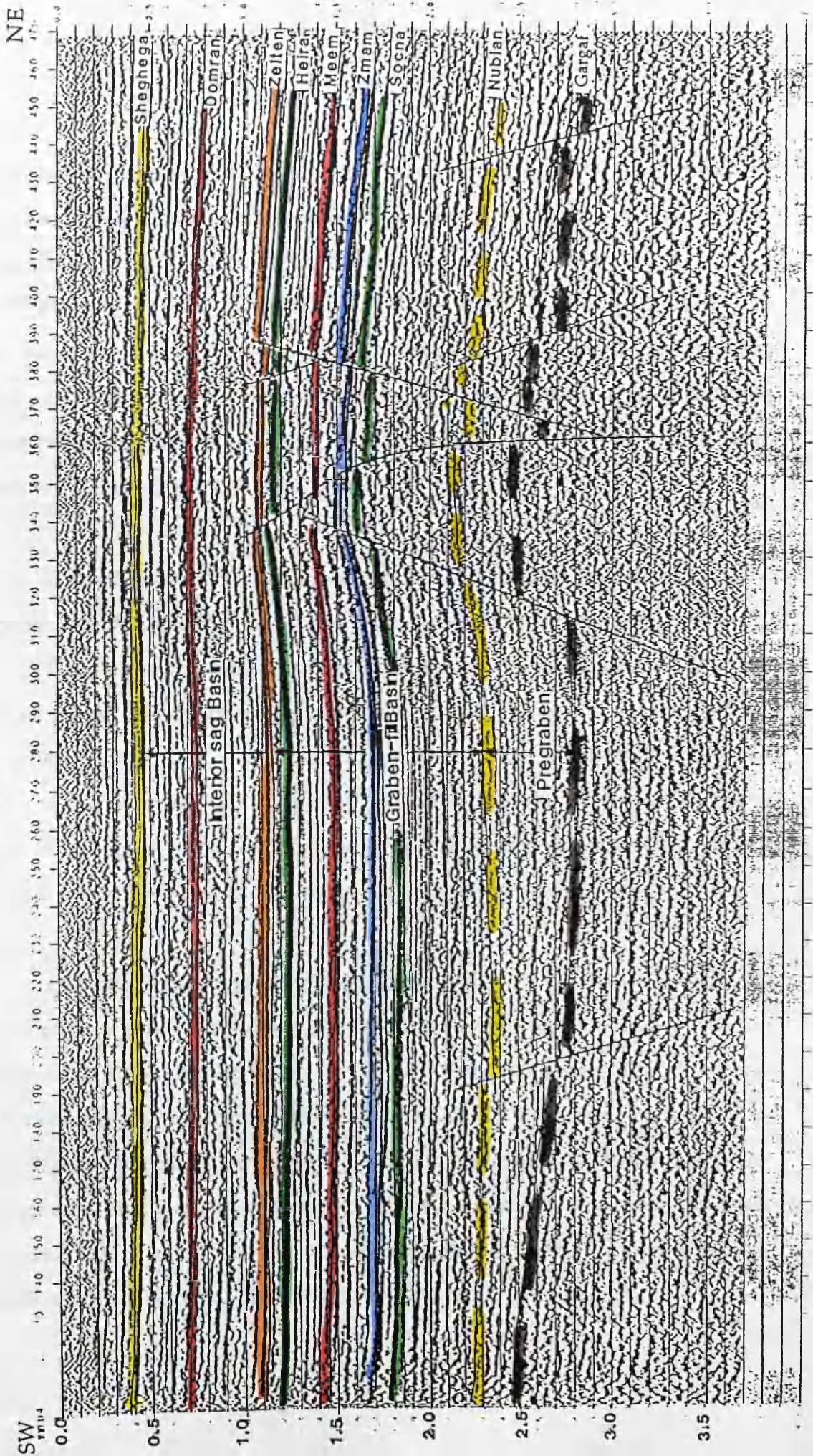


Fig 3.4 Line V07-85

Faults are produced by unbalanced stresses which exceed the strength of rocks. The type of fault depends largely on whether the vertical or horizontal stresses are the larger. Normal faults result when the maximum compressive stress (σ_1) is vertical and the minimum (σ_3) is horizontal. In the study area a normal faulted style of horsts, grabens and half grabens formed the structure in the Wadi field. The fault pattern in the Wadi field has been determined using the seismic sections and the information from the wells drilled to date in the area.

Growth faulting is usually closely associated with tectonic instability, being found commonly in such environments as deltas (subsiding rapidly under an increasing sediment load) and in areas in which basinal salt rock has become plastically mobile. There is good evidence that the form of the growth fault surface is not planar, but tends to be spoon-shaped like the slip plane of many major landslide features. Thus the plan view of many growth faults is a curved fault trace that is concave towards the downthrown side (Jenyon and Goudswaard 1989).

Growth faults frequently occur in series, with the downthrown side or hanging wall of one fault being the upthrown side or footwall of the next fault down to the basin. In deltaic areas, rapid subsidence of great thicknesses of sediments frequently results in the formation of overpressured shales in the depositional pile, and growth faults are often associated with negative seismic velocity anomalies produced by such shales. The development of large growth faults is often highly complex, and is not characterized by continuous or regular movement.

In the area of study, line V35-85 (Fig 3.5) shows a possible growth fault around shot points 155-180. This fault is characterized by thick Socna shale (Upper Cretaceous), which reaches a thickness of more than 1524 m, and by the evaporitic salt which appears around shot point 160 at a time of 2.15 s. Growth faults are often associated with the negative seismic velocity anomalies produced by such shale.

The Wadi field is located in a horst structure basement high. The horst lies in the Hagfa Trough, bounded by two major faults, on the west by the Zelten Hagfa fault and on the east by the Hagfa-Beda fault. Seismic line V13-85 (Fig 3.6) shows the horst and Figures 1.1 and 1.2 show its location.

The Wadi field structure is defined on the basis of well data and the time structure maps for the tops of the Gargaf, Nubian, Zmam, and Zelten Formations. Twelve wells have been drilled within the Wadi field. Eight of these wells penetrated the Gargaf Formation (see Table 3.4 and cross section 1, Fig 3.18). At the crest of the structure in the field, where most of the wells have been drilled, it is difficult to seismically identify and correlate the top of the deeper horizons (Gargaf and Nubian), due to the poor signal to noise ratio and due to the diffractions from the faults. However, the shallower horizons Zmam (Upper Cretaceous), and Zelten (Lower Eocene) are easily recognized strong reflectors, relatively unaffected by faulting.

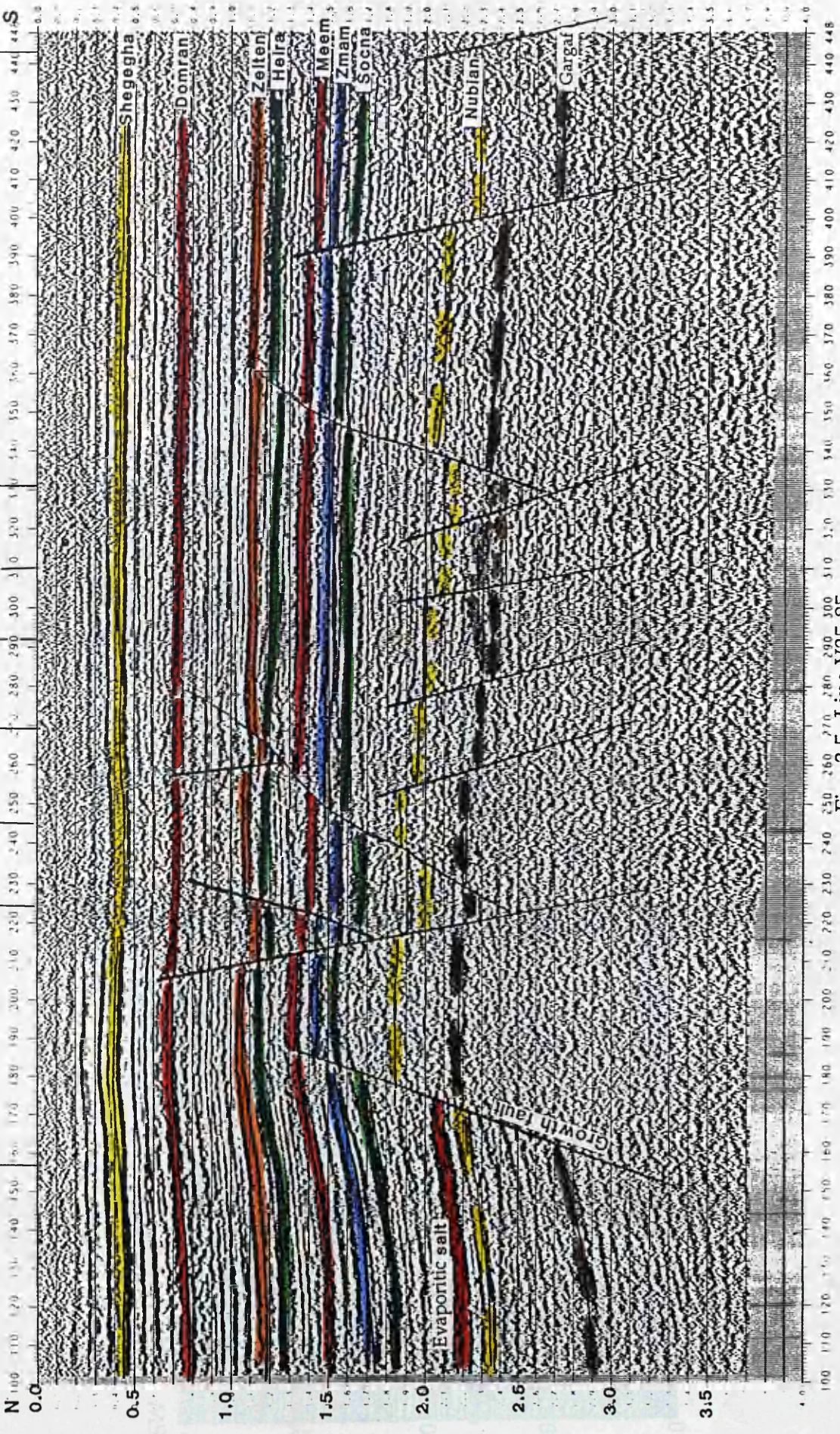


Fig 3.5 Line V35-85

D3-104

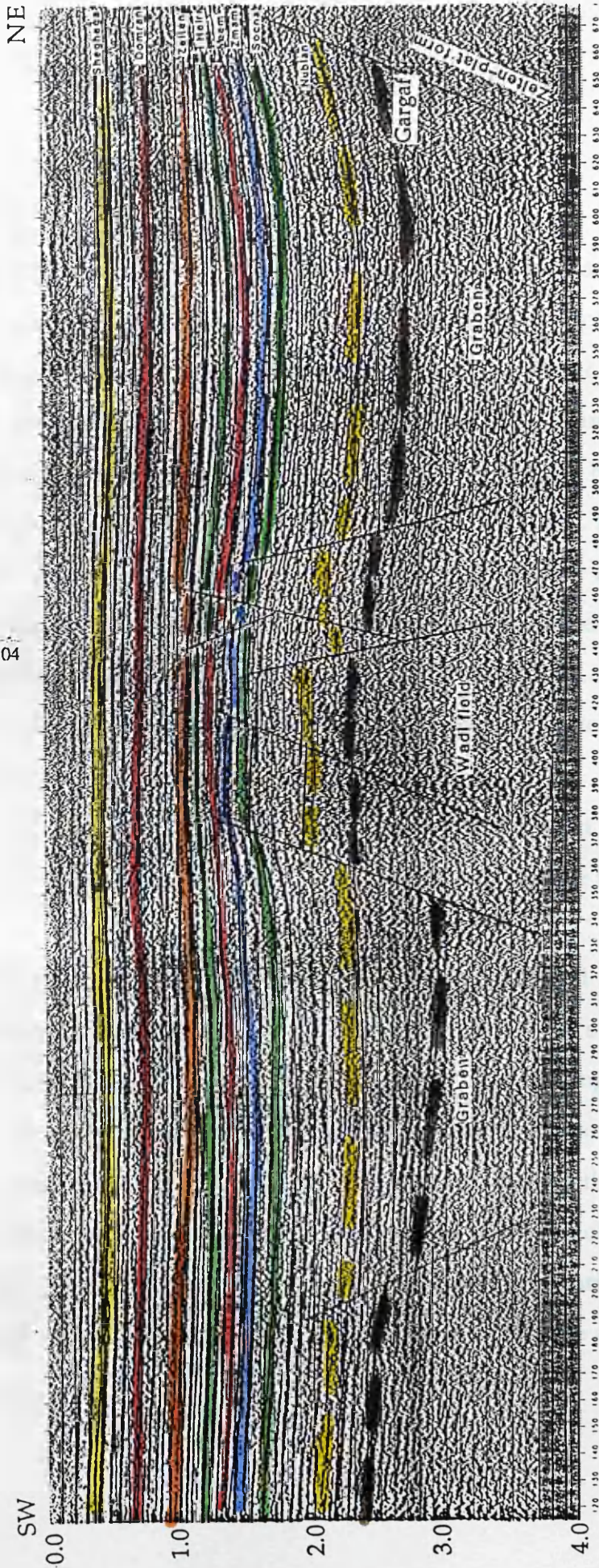


Fig 3.6 Line V13-85

3.4 TIME STRUCTURE MAPS

Time structure maps for the top Gargaf and Nubian Formations have been produced at a scale of 1: 50,000 and contour interval of 50 ms. Time structure maps for the top Zmam and Zelten have a contour interval of 20 ms. They show that the structure is subdivided into a number of inter-linked grabens and half-grabens, separated by structurally high horsts or footwall highs bounded by two grabens on the east and west. Reduced-scale versions of these maps are shown in Figures 3.7, 3.8, 3.9, and 3.10. The structural highs are coloured red and the lows are coloured blue. Several factors affect the accuracy of the maps in the study area, such as:

- a) Mis-ties between the sections, due to the factors mentioned earlier in the chapter.
- b) mis-ties between the different data due to the different static applied (e.g. Sabkha formula, "onJabel-off Jabel" formula and uphole static).

Although all mis-ties problems have been considered and shift has been added or subtracted from the picked values, some errors still affect the accuracy of the maps. These will be due to the error in picking the two way time. For the maps representing the shallow reflectors (Zmam, Meem, and Zelten), where the seismic data is reliable, the accuracy of these maps are within the contoure interval, and are subject to a correction of no more than 20 ms. The mis-ties are much higher for the deeper horizons (Nubian and Gargaf) where the S/N is poor, and they may be require a correction of up to 70 ms.

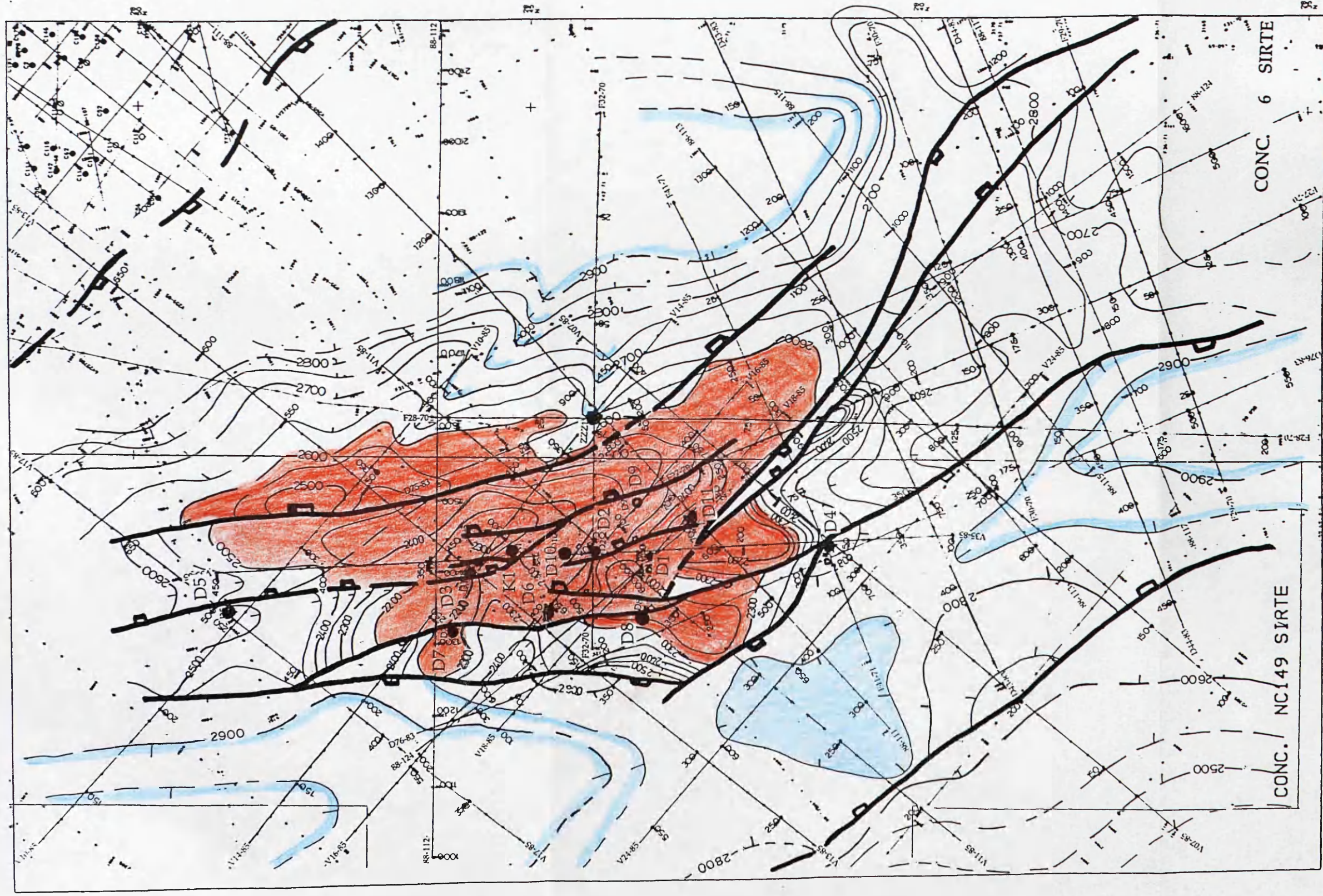


Fig 3.7 Time structure map top Gargaf (Cambro-Ordovician)

Contour interval 50 ms.

Datum Sea level.

Red colour indicates high structure.

Blue colour indicates low structure

SCALE



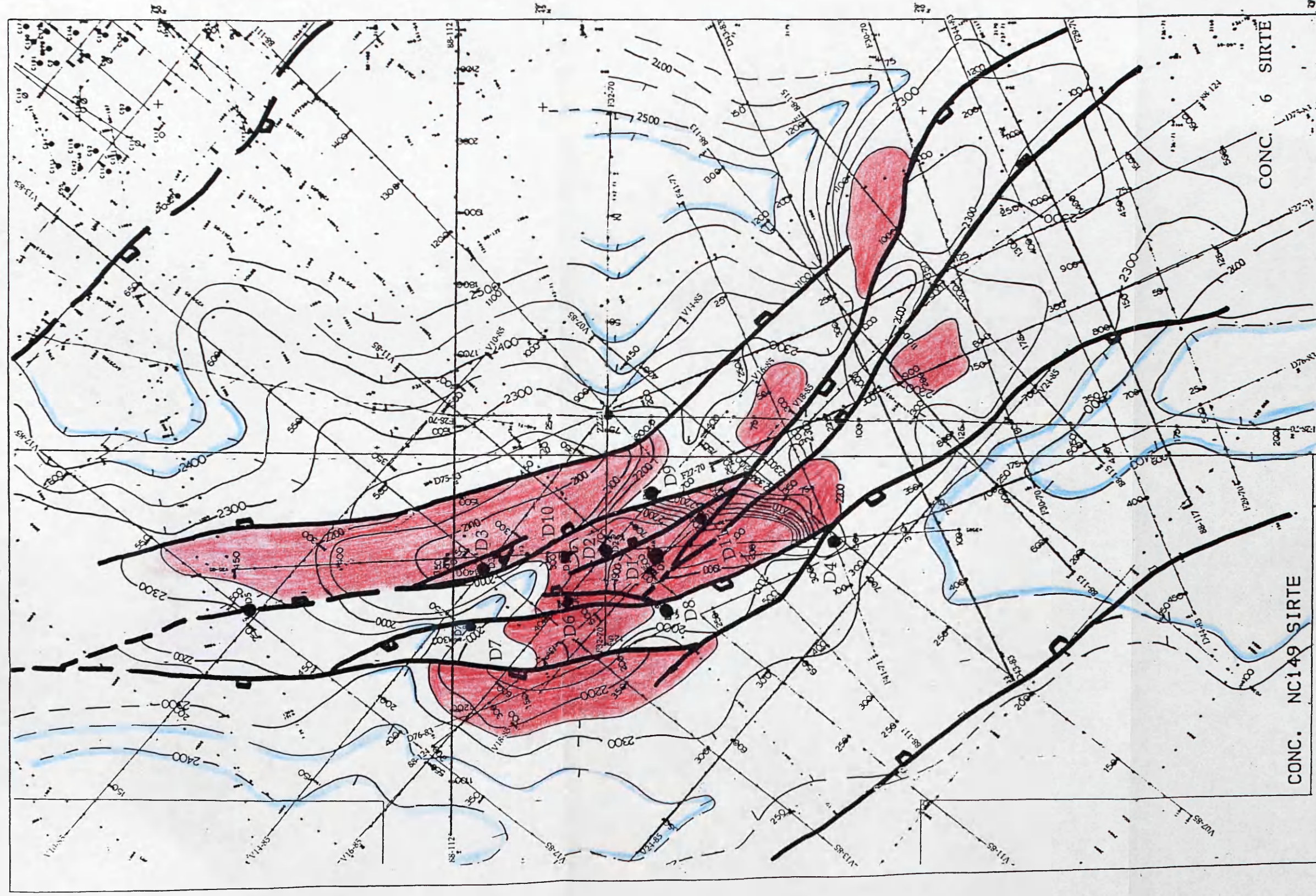


Fig 3.8 Time structure map top Nubian (Lower Cretaceous).

Contour interval 50 ms.

Datum Sea level.

Red colour indicates high structure. Blue colour indicates low structure.

SCALE



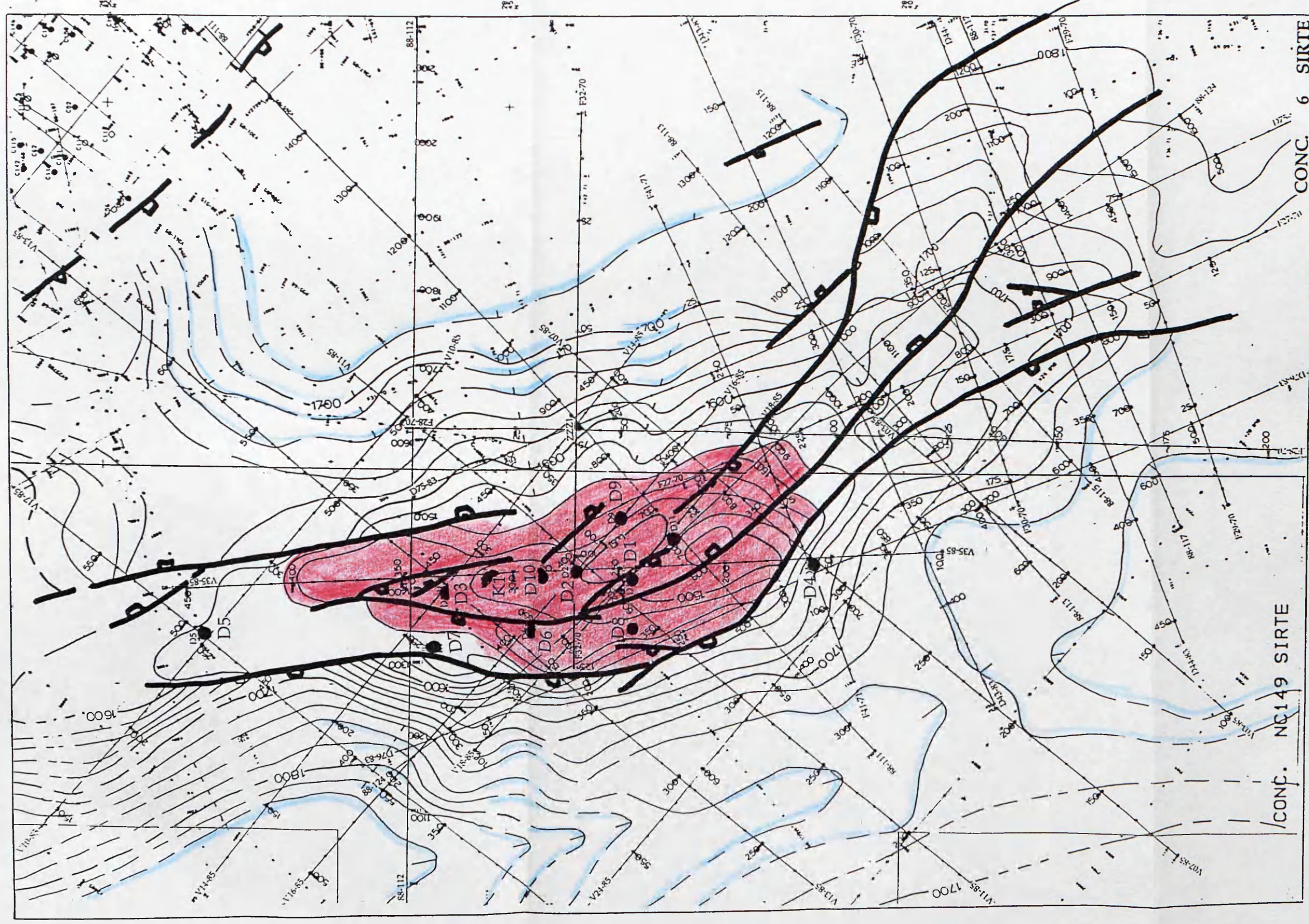
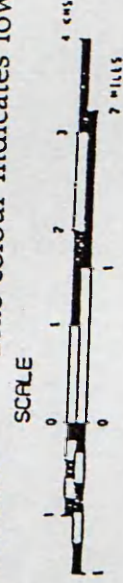


Fig 3.9 Time structure map top Znam (Upper Cretaceous).
 Contour interval 20 ms. Datum Sea level.
 Red colour indicates high structure. Blue colour indicates low structure.



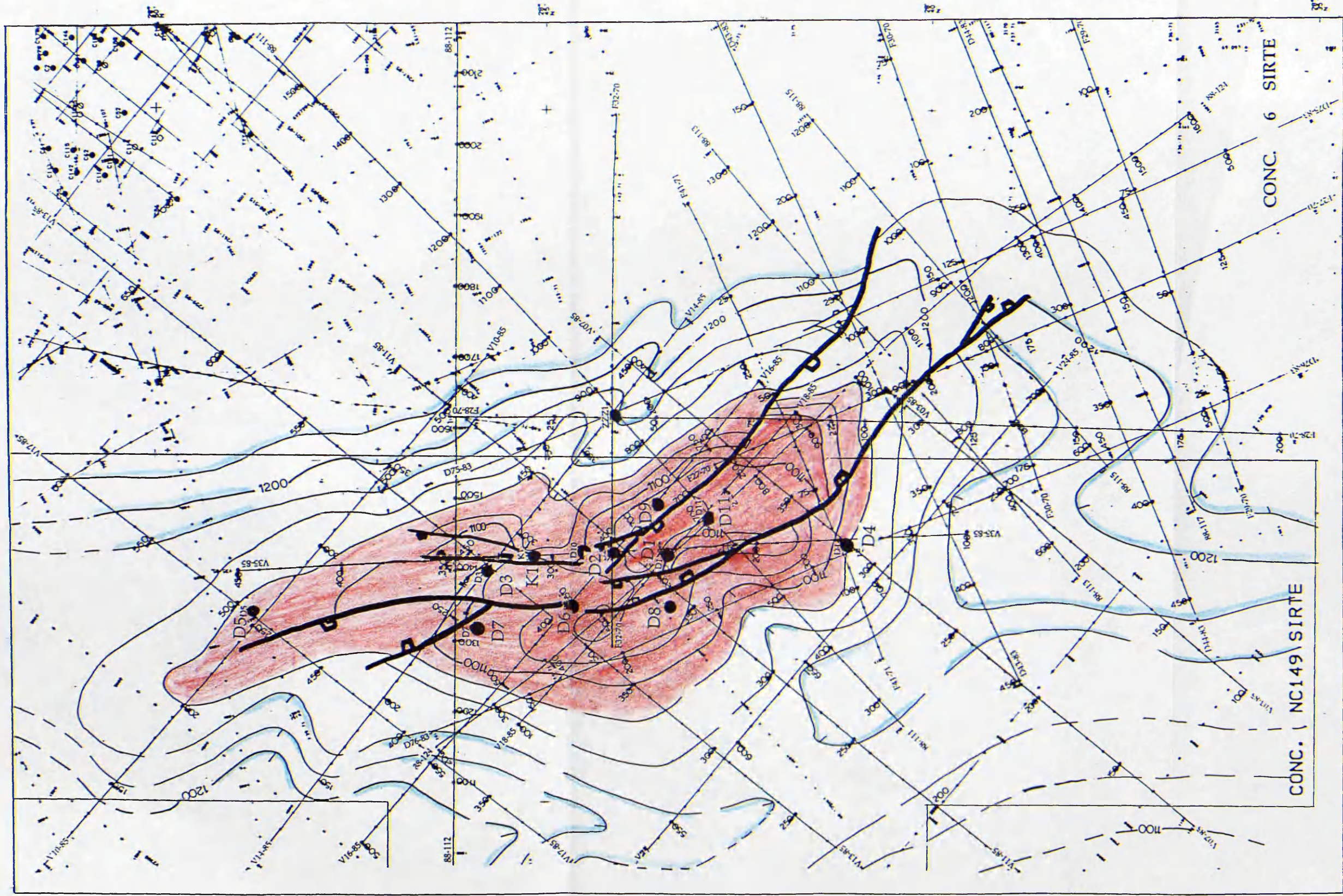


Fig 3.10 Time structure map top Zeltén (Lower Eocene).
 Contour interval 20 ms. Datum Sea level.
 Red colour indicates high structure. Blue colour indicates low structure.

3.4.1 Grabens

Three grabens exist in the area between the Zelten platform and the Beda platform. Two of these are the major grabens which form the Hagfa Trough (see seismic line V13-85; Fig 3.6). The third one is a small localized graben which can be traced in the Gargaf Formation (Cambrian or Cambro-Ordovician) up to the Ruaga Formation (Upper Eocene). Within this graben there are two small grabens formed at Zelten Formation level (Lower Eocene), which formed by antithetic faults (see seismic line V07-85, Fig 3.4).

The faults are normal faults trending NW-SE. All faults die out upward at the Socna shale (Upper Cretaceous), at the Heira shale (Palaeocene), or at the Domran (Lower Eocene). The existence of localized grabens has been proved by wells D1-104 and D2-104 (see cross section 1 Fig 3.18, and line V35-85; Fig 3.5).

3.4.2 Compaction synclines

Compaction synclines form in the following way. When sediment is deposited, it has a high initial fluid content. When compaction occurs in a thick sequence within the hanging wall of a normal fault, the differential compaction against the more rigid footwall gives rise to the hanging wall syncline (Badley 1989). Line V11-85, Fig 3.11 shows this phenomenon.

The vertical throws of the faults at the Zmam level are in range of 15 to 50 ms. This suggests that the main reservoir faults existed prior to

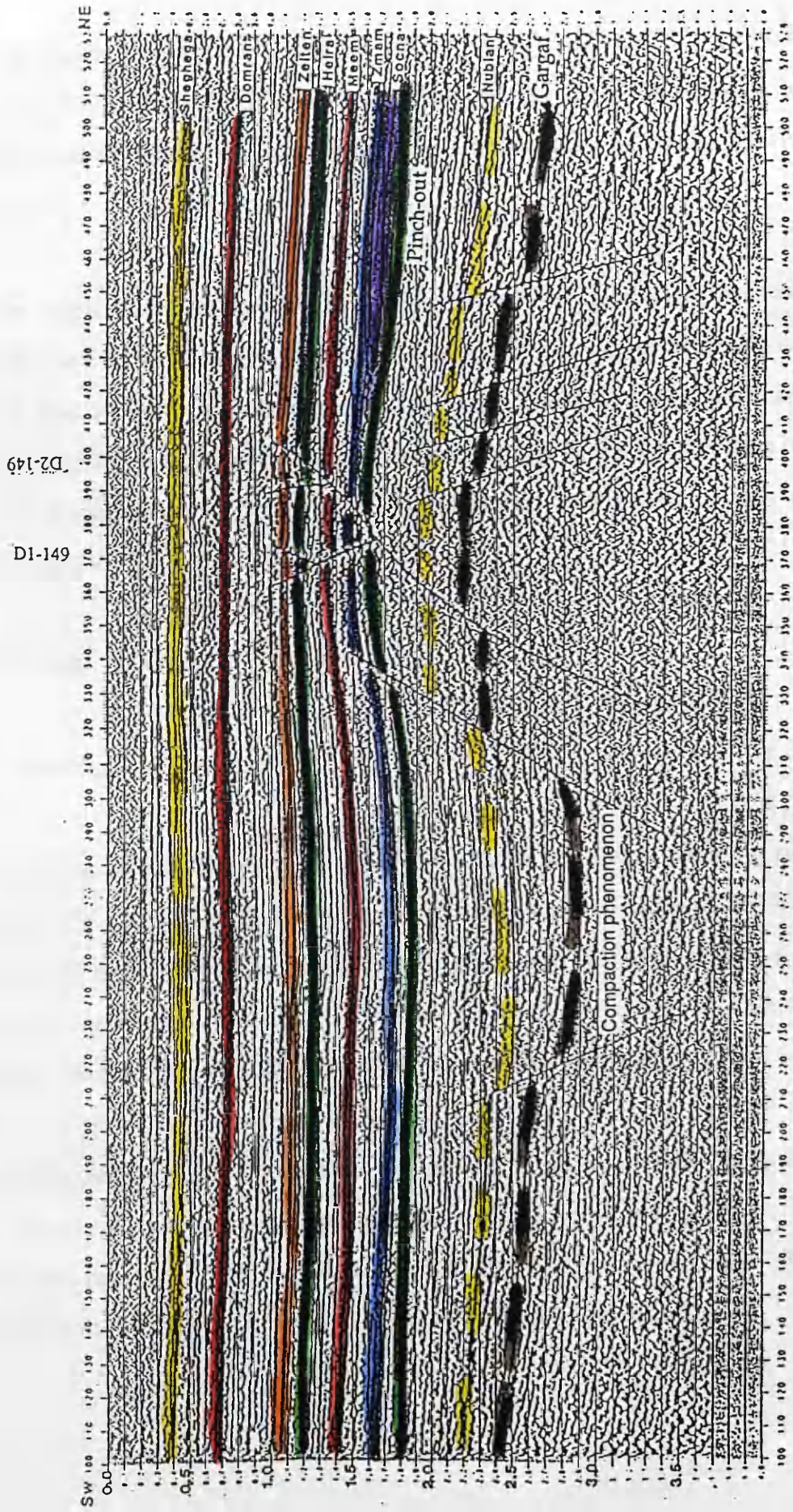


Fig 3.11 Line V11-85

Zmam deposition. Also the presence of the thick Socna section, which ranges from 610 m at well D1-149 to more than 1345 m at D4-104, appears to have absorbed the throw of most of the faults before they reach the Zmam level above.

The west bounding major fault penetrates the shallower section above the Meem member. Apparently this fault was active throughout most of the tectonic adjustment of the Sirte Basin, or at least until Palaeocene time. The syn-depositional nature of these faults can be seen by the great thickness of the Socna shales, which reach more than 1345 m to the south of D4-104.

3.5 ISOCHRON MAPS

3.5.1 Introduction

Isochron maps, showing the thickness of the sediments between two horizons, are useful in studying palaeostructure and structural growth. The interval between the horizons is often measured in terms of two-way traveltime rather than thickness in metres or feet, assuming that velocity variation effects are minor compared to the thickness variations.

In the area of study the thickness in terms of time in milliseconds has been calculated using a program called Isochron, and indicated on the maps with the same accuracy mentioned in the time structure maps. The program and the results of line V07-85 are shown in Appendix 2.

Three maps have been contoured.

- (1) Isochron map between top Gargaf and top Nubian reflectors.
- (2) Isochron map between top Nubian and top Zmam reflectors.
- (3) Isochron map between top Zmam and top Zelten reflectors.

The isochron maps all show thinning of the sediment on the crest of the structure, and thickening on the flanks of the structure towards the grabens (see Figs 3.12, 3.13, and 3.14). Table 3.5 shows the thickness of the sediment of the different formations in metres as shown in the wells.

3.5.2 The structure

There is a thinning of the sediment over the crest of the structure and an increase in thickness away from the crest. This indicates that the deposition was contemporaneous with the growth of the structure.

On the sides of the structure in the Wadi field the contours show a trend towards increased thickness in the direction of the major faults. This suggests that the region was tilted downward in that direction during the time of deposition. In contrast, the sediments above the Heira Formation (Palaeocene) show a uniform thickness, which indicates that the horst structure beneath formed before their deposition.

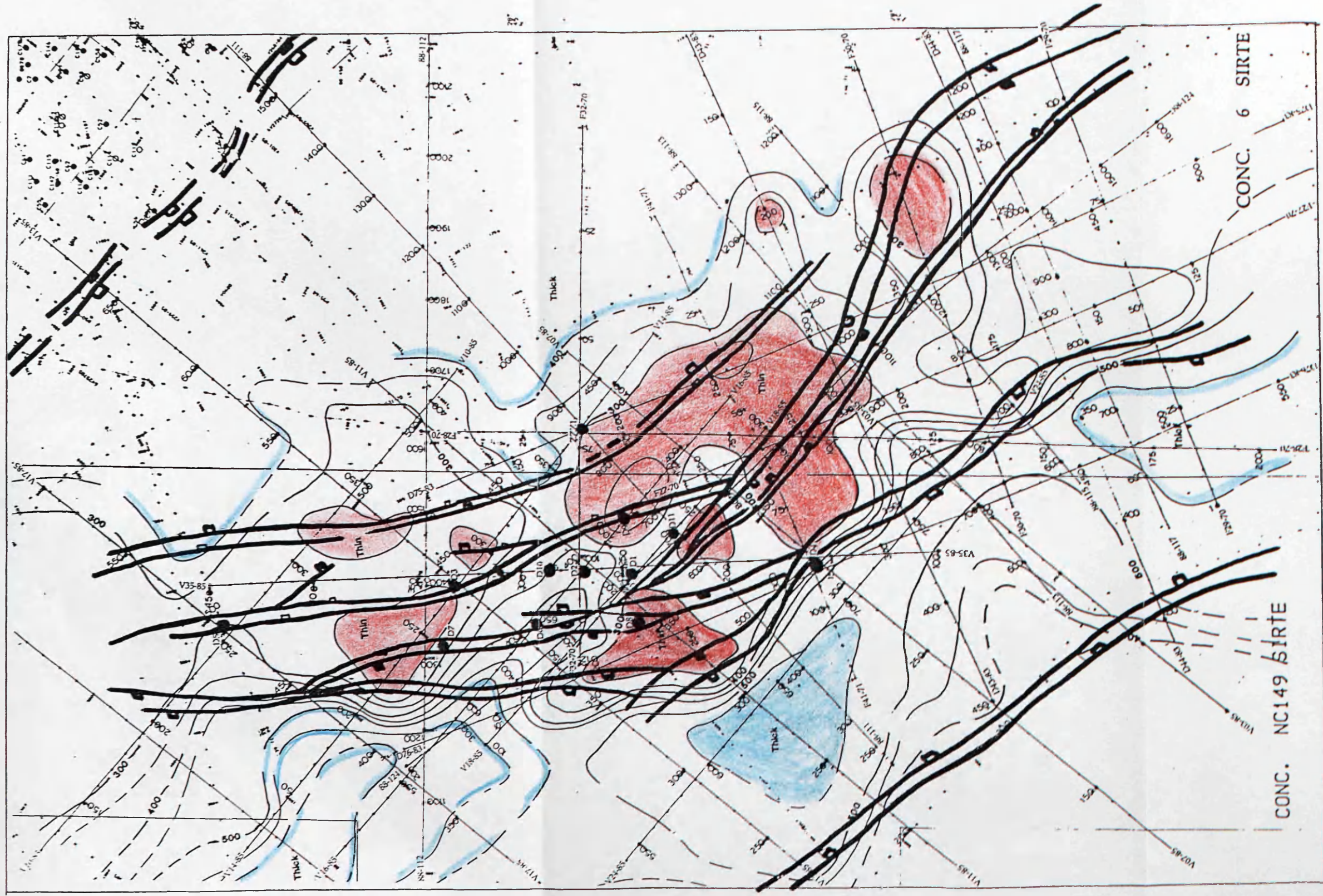


Fig 3.12 Isochron map between Nubian (Lower-Cretaceous) and Gargaf (Cambro-Ordovician).
 Contour interval 50 ms. Datum Sea level.
 Red colour indicates thin structure. Blue colour indicates thick structure.

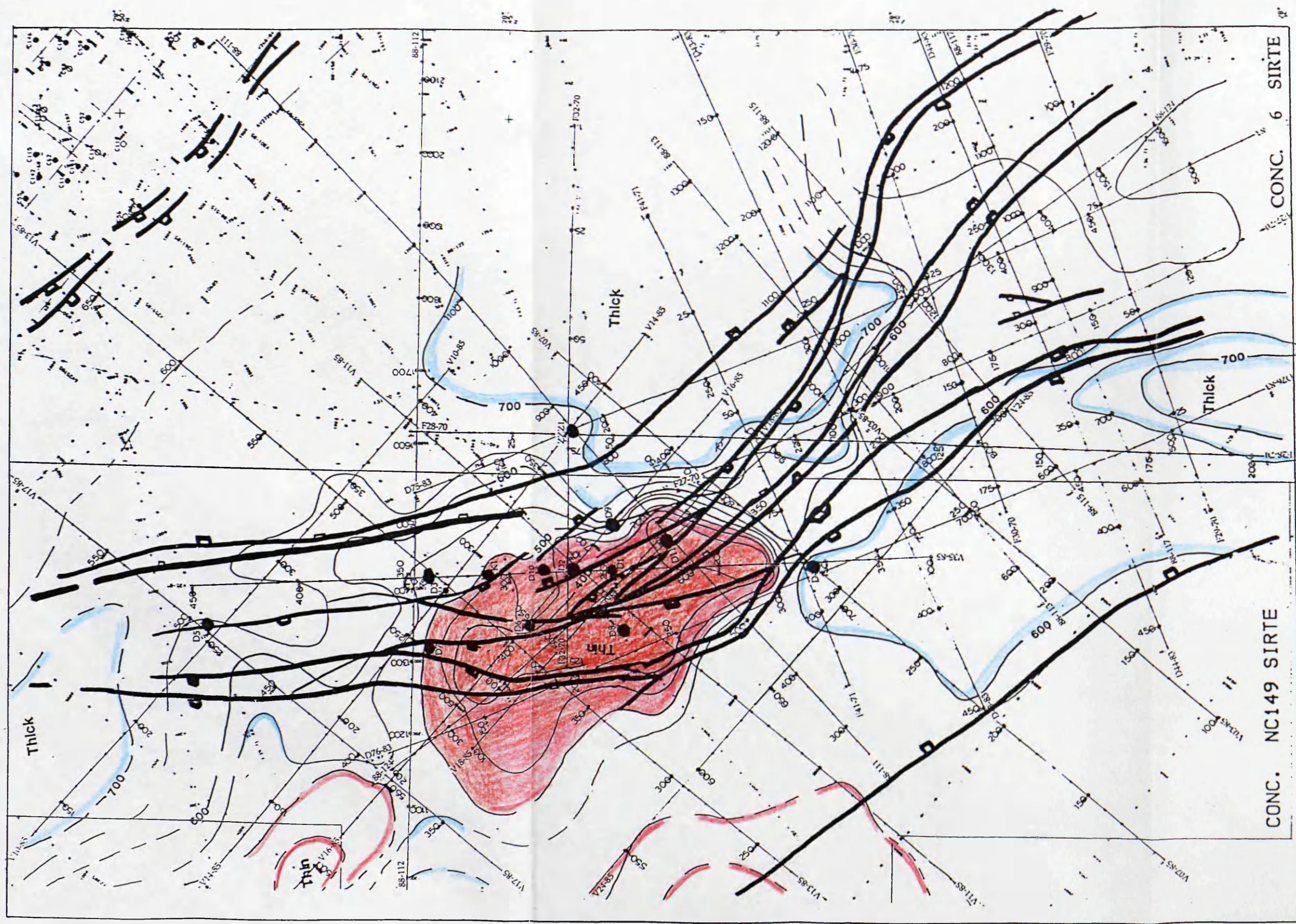


Fig 3.13 Isochron map between Znam (Upper-Cretaceous) and Nubian (Lower Cretaceous).
 Contour interval 50 ms. Datum Sea level.
 Red colour indicates thin structure. Blue colour indicates thick structure.

Formation name	D1-149 Thickness in metres	D2-149 Thickness in metres	D3-149 Thickness in metres	D4-149 Thickness in metres	D5-149 Thickness in metres	D6-149 Thickness in metres	D7-149 Thickness in metres	D8-149 Thickness in metres	D9-149 Thickness in metres	D10-149 Thickness in metres	D11-149 Thickness in metres	K1-149 Thickness in metres
Sheghega	306	523	526	513	539	518	523	511	522	524	505	530
Domran	564	623	596	602	581	547	570	558	593	617	574	606
Zelten	105	104	107	119	111	103	108	105	101	93	112	107
Heira	559	515	525	688	700	597	617	601	527	545	492	537
Mecm	11	12	12	12	11	12	12	14	9	12	F	12
Zmam	114	180	185	289	232	84	193	191	189	181	188	197
Socna	+476	617	793	+1345	873	319	527	535	948	667	627	772
Nubian	537	498	+352	NIP	F	568	502	+135	+386	568	F	565

Table 3.5 Well names and the formation thicknesses in the Wadi field.

Np: Formation is not penetrated by the well.

F: Well cutting the fault at the formation.

+: Not the total thickness of the formation

3.6 HYDROCARBON RESERVOIRS

3.6.1 Structural traps

The essential characteristic of a trap is a porous permeable bed overlain by an impermeable bed which prevents fluid from escaping. Oil and gas can collect in the reservoir of an anticline until the anticline is filled to the spill point. The spill point is the highest point at which oil or gas can escape from the anticline. The contour through the spill point is the closing contour, and the vertical distance between the spill point and the highest point in the anticline is the amount of closure. Fault traps occur, in which permeable beds overlain by impermeable beds, are faulted against impermeable beds. If the fault seals, a trap can exist if there is closure in the direction parallel to the fault. In the study area all the oil entrapment is due to structural traps when the Nubian sandstone is overlain by impermeable bed Socna shale, and is faulted against the Nubian sandstone.

3.6.2 Stratigraphic traps

A permeable bed can grade into an impermeable bed, as might result where a sand grades into a shale. Sometimes permeable beds gradually thin and eventually pinch out to form pinchout traps. In the study area one of the possible mechanisms of oil entrapment within the Meem member is the pinching against the down thrown side of a fault or structural high.

3.6.4 Reservoir rocks

There are two reservoirs in the Wadi field, the Nubian equivalent sandstone and Meem member carbonate (a member within the Heira shale).

3.6.5 Nubian

The term Nubian sandstone, originally defined in upper Egypt (Russeger, 1837, as cited by Gumati and Kanes, 1985), is used informally in Libya to cover a broad group of poorly dated detrital sediments. Local sandstones such as the Srir and Faregh sandstones fall within the general term Nubian sandstone. Nubian is a useful term here, and can be retained until more detailed mapping has been done and more precise stratigraphy has been established (Gumati and Kanes, 1985). The reservoir consists of a homogeneous quartzitic sandstone of the Cretaceous Nubian equivalent. The reservoir is divided into two main units separated by a well defined shale break. Because the age of the reservoir has not been determined, the two units were labelled temporarily as the A-reservoir for the upper unit and the B-reservoir for the lower unit. They are assumed to be of Nubian equivalent age (El-jard, 1988).

3.6.6 Meem Member

The Meem Member of the Heira shale is considered as a viable reservoir (which tested oil in the Wadi field). This member thins out over

most of the Zelten platform but thickens towards the west. It averages 17 m in thickness (see cross section 1; Fig 3.18).

3.7 HYDROCARBON ENTRAPMENT

The Wadi field is defined on the west and the south by major bounding faults that caused the northwest early tilting of the Wadi reservoir. The tilting is responsible for the entrapment of the oil in the reservoir against the Socna shale.

In the Meem member reservoir the oil entrapment is dependent upon a seal against the downthrown fault block or local grabens (as in wells D1-149 and D4-104), or it is a combination of the two. The other interpretation could be the oil entrapment is due to the pinching-out against the downthrown side of the fault or structure high as shown in Figure 3.15. But due to the lack of information in well D4-104, this interpretation needs more well information to be verified. Line F41-71 (Fig 3.15) demonstrates the quality of the Dinoseis data and shows a pinch-out within the Heira shale at shot point 95 at 1.55 seconds. Line V11-85 and line V14-85 (Fig 3.16) show pinch-out within the Socna Formation.

3.7.1 Source rock and oil migration

Generation of hydrocarbon is directly related to the degree of the source rock maturation. General, the greater the maturation the lighter the hydrocarbon formed (Dow et al., 1978 as cited by El-Jard 1988). In the Sirte Basin area the most likely source rocks are the overpressured Socna shale

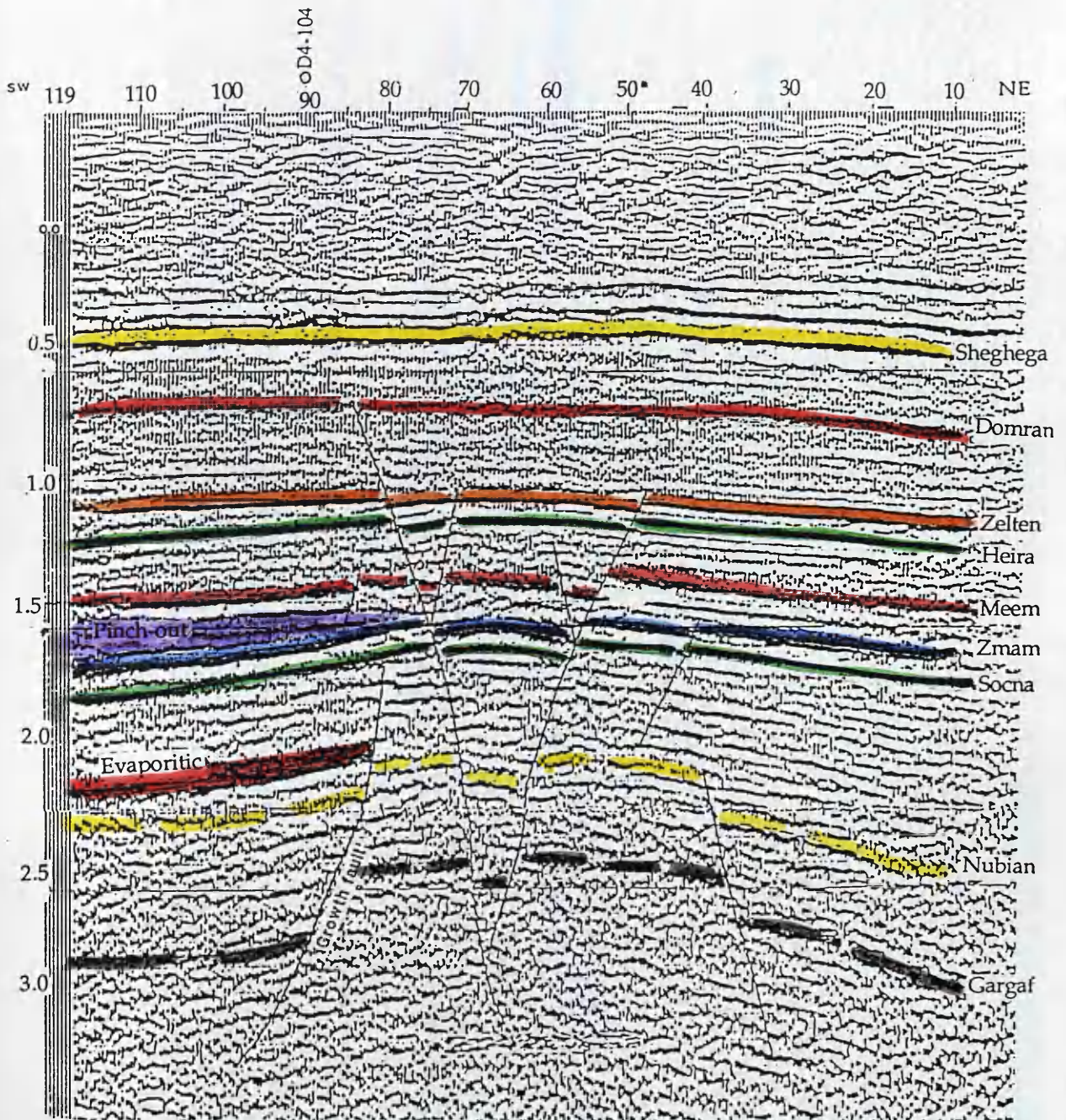


Fig 3.15 Line F41-71

D3-104

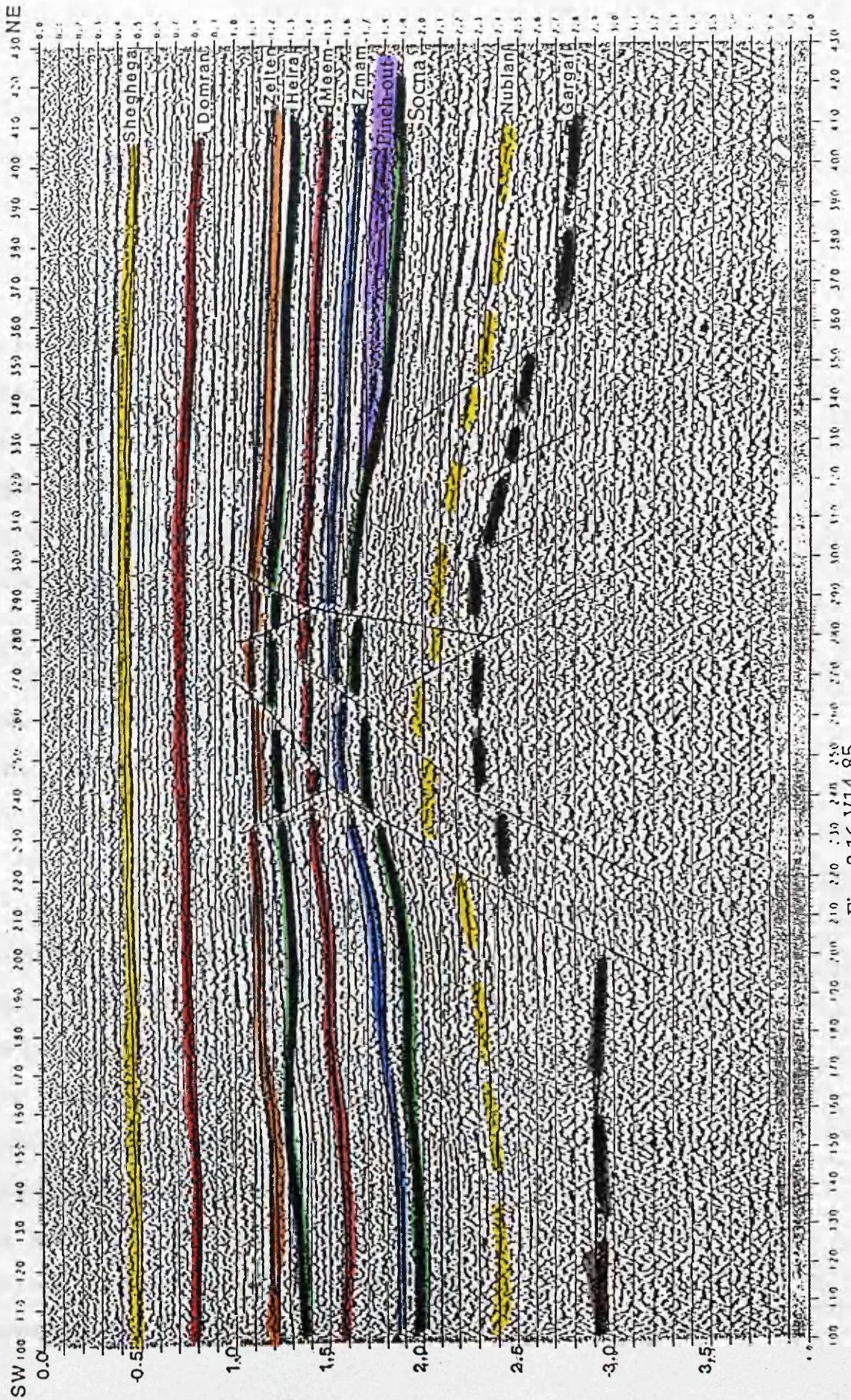


Fig 3.16 V14-85

and less pressured Heira shales. Both of these source rocks generated oil in troughs in earlier times, in larger amounts than were generated in the horsts.

The Upper Cretaceous Socna shales are accepted to be the main source rock for the hydrocarbon accumulations in the Sirte Basin, and the source of the hydrocarbons in the Nubian (equivalent) Formation in the Wadi field. Since the Socna shales were the dominant oil generator in the troughs, the closure on the traps in this area must have been initiated prior to, or about the same time as, the Socna reached its maturity, or Middle Eocene time.

The early initiation of the Wadi field structure took place during the Upper Cretaceous time. The structure reached its final setting and stability during Paleocene time during which the final movement of the western major Wadi bounding fault ended in the Heira just after breaking through the Meem member. Accordingly the migration of the hydrocarbons from the Socna to the Wadi field reservoir could have happened gradually since Middle Miocene time when the Socna was exposed to maximum compaction and thermal maturity. Most hydrocarbons were believed to be sourced from the Socna, but vertical downward migration to the reservoir is also possible due to the differential pressures and the reservoir is also possible due to the differential pressures and the reservoir's open fractures. In the Paleocene Meem member reservoir hydrocarbons migration paths were most likely forced by the impermeable Heira around the thin carbonate reservoir and direct input of oil was not introduced to this reservoir until Oligocene time.

3.8 BACK-STRIPPING

The back-stripping technique (with decompaction ignored) has been used to help clarify the timing of faulting in the study area, and is not used to calculate the throws of the faults or the formation thicknesses.

The tops of different formations (at certain times) are used successively as datum, and the thickness of each of these formations is subtracted successively back in time. Fig 3.17 shows the steps which have been used to evaluate the structural framework.

In the Lower Cretaceous (Nubian Formation) the thickness of the Nubian Formation does not change much, but D2-104 shows less sediment thickness than the other wells. This indicates that well D2-104 was high at the time of deposition.

In Upper Cretaceous time the thickness of the Socna Formation shows a change in the sediment thickness from one well to another, with D1-149 showing least sediment. This suggests that the deposition was controlled by the faulting, and that the faults were formed at the beginning of the deposition of the Socna Formation shale in the Cenomanian. During the Upper Cretaceous time (Zmam Formation) some of the faults have been attenuated by the thick Socna shale, whereas other faults continued through the Zmam Formation.

In Palaeocene time the two major faults on the south and north have been attenuated in the Heira shale, but the faults forming the local graben

N

S

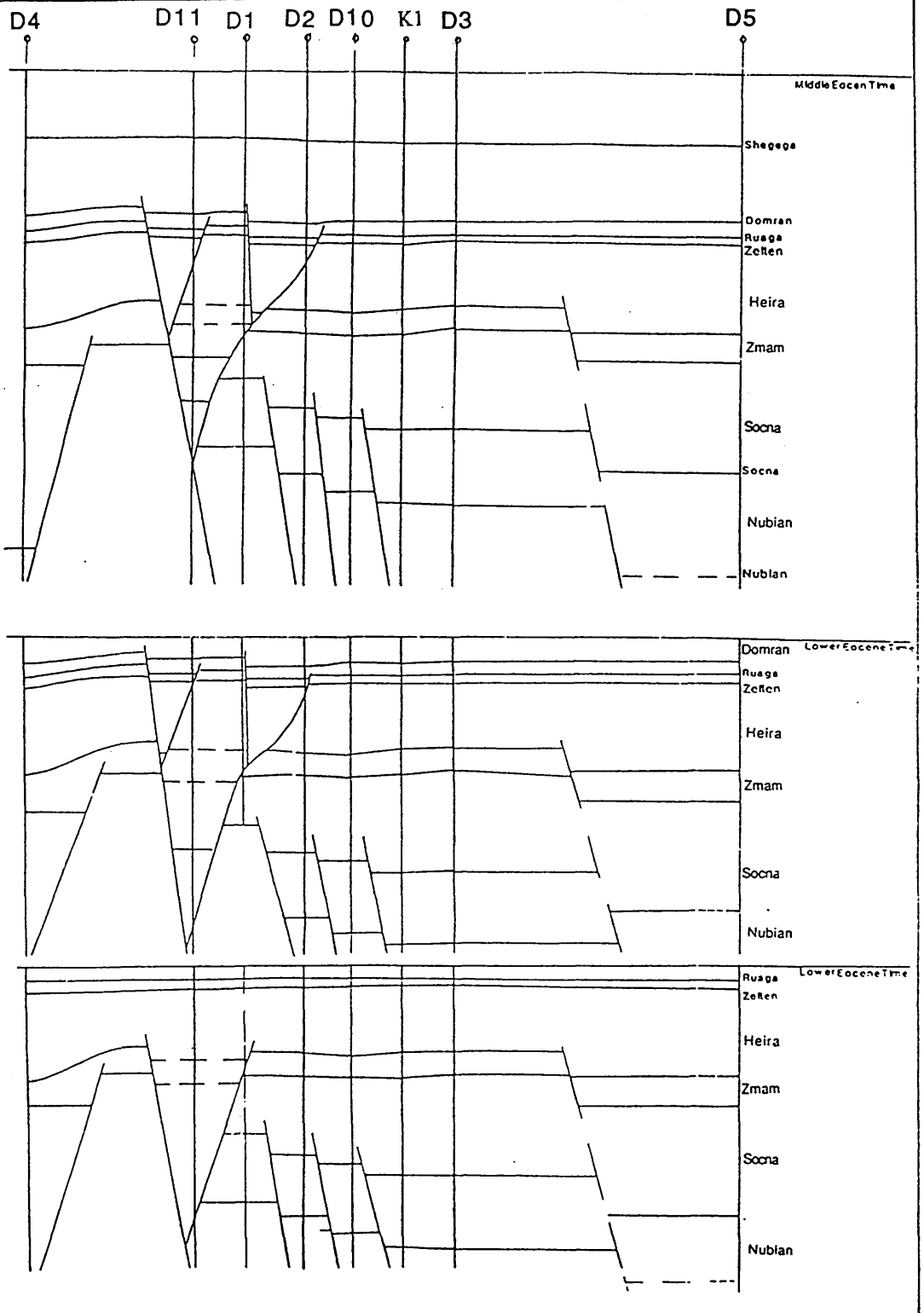


Fig 3.17 Palinspastic reconstructions across the Wadi Field (upper part of the section)

N

S

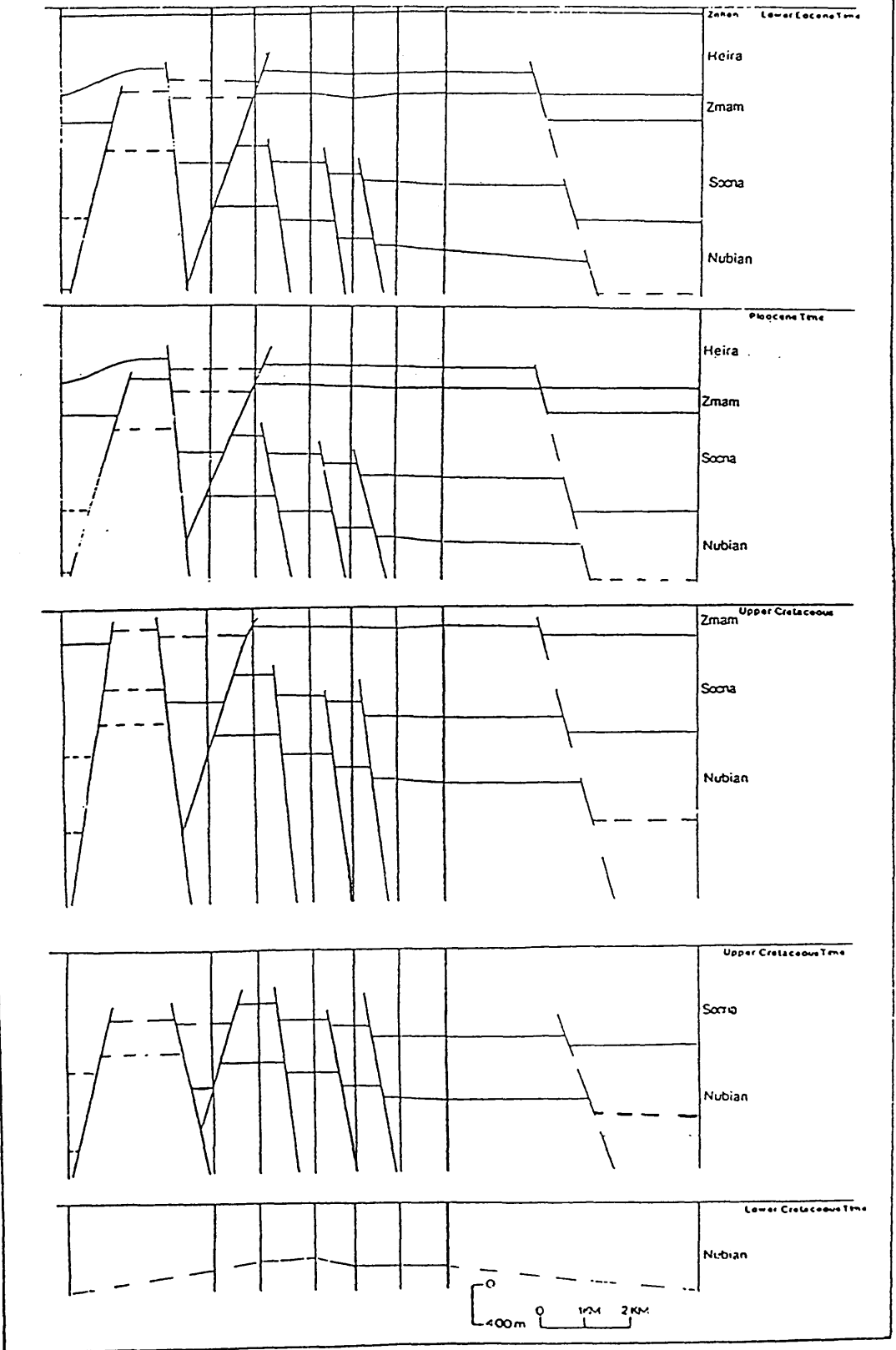


Fig 3.17 (continued). Palinspastic reconstructions across the Wadi Field (lower part of the section)

were still active. The faults were not active during the Lower Eocene time (Zelten Formation). In Lower Eocene time the faults forming the localized graben were reactivated, and another two small grabens were formed on both sides of the graben by antithetic faults. During the Middle Eocene time (Sheghega Formation) there is no activation of the faults.

In summary, the cross section no. 1 (Fig 3.18) represents how the structure looks today. It shows a small graben around D3-104 between K1-149 and D5-104. This graben was formed in Eocene time, and this suggests that the faulting in the Wadi field was active until the Upper Eocene.

Figure 3.19 represents the relationship between the seismic data (represented by line V35-85) and well depths for the wells lying on this line. The correlation has been made on the basis of the seismic data. The unscaled subsea depths in metres are plotted on the top of the formations on the seismic section, to compare the dip of the strata in terms of milliseconds and depth in metres.

The seismic line in Fig 3.19, when compared with the cross section between the wells (Fig 3.18), shows that structures of 40 m or less in amplitude are not noticeable on the seismic section, and that small elevation changes at the reflector of less than 30 m cannot be determined from the seismic section.

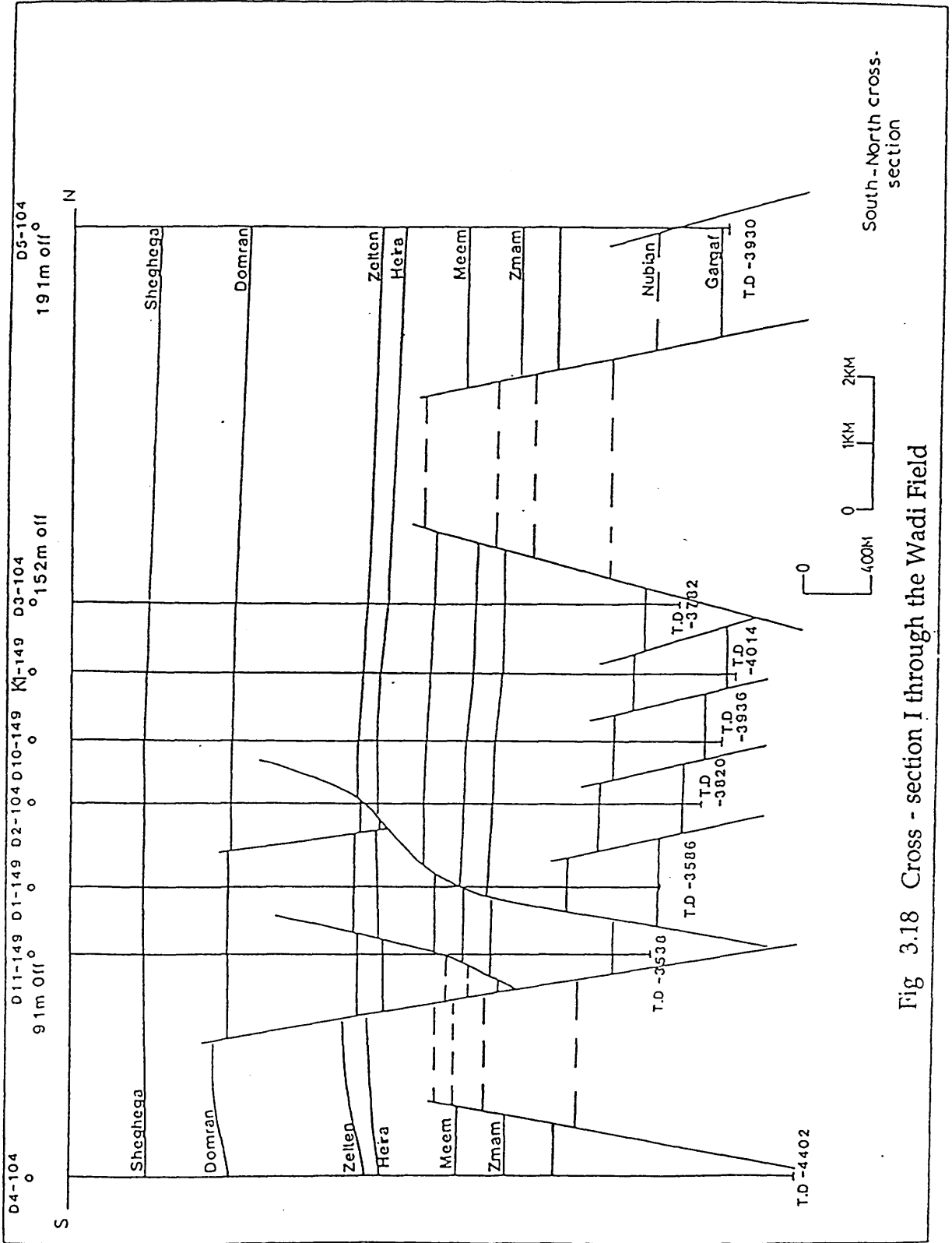


Fig 3.18 Cross - section I through the Wadi Field

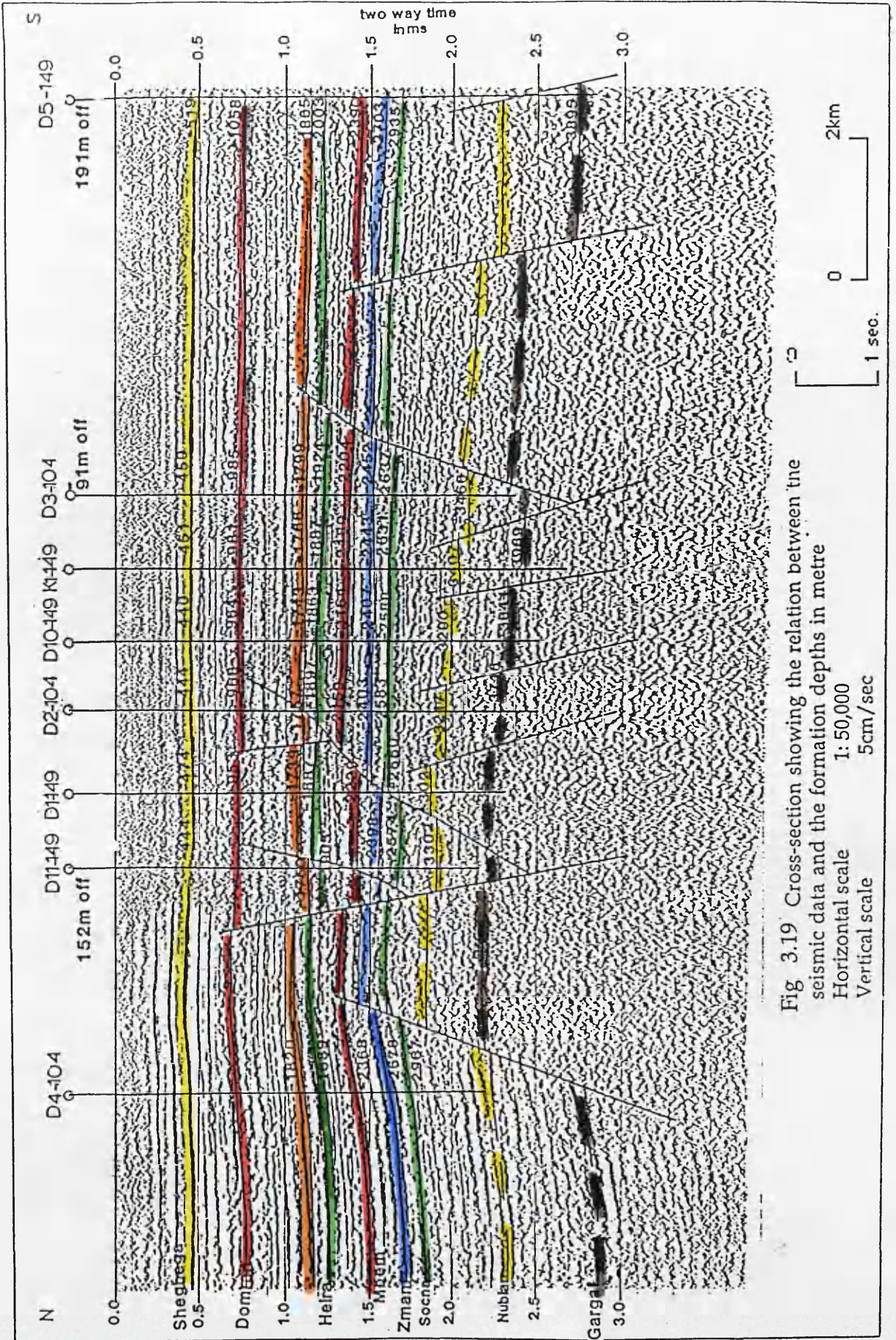


Fig 3.19 Cross-section showing the relation between the seismic data and the formation depths in metre

Horizontal scale 1:50,000

Vertical scale 5cm/sec

Chapter 4

Velocity and depth conversion

- 4.1 Introduction
- 4.2 Check shot survey or well shooting
- 4.3 Seismic velocities
- 4.4 Factors affecting velocity
- 4.5 Interpretation of velocity data
- 4.6 Depth conversion
- 4.7 Depth maps

4.1 INTRODUCTION

The key parameter in seismic processing and interpretation is seismic velocity, the speed of seismic waves in different geological strata. It is employed for normal move-out correction, static correction, and in converting the time section to the more meaningful depth section. To determine velocity in a deep borehole, two type of well surveys are used, the conventional method of shooting and sonic logging (or continuous velocity shooting). An airgun in a mud pit (or in the water for marine wells) can also be used as an energy source.

A sonic log (continuous velocity log) shows the interval velocity near the borehole of the formations penetrated by the wells as function of depth. The accuracy of sonic logs is often poor. Sonic logs can suffer from inadequate penetration, hole caving.

4.2 CHECK SHOT SURVEY OR WELL SHOOTING

Well shooting has two objectives:

- a) To obtain accurate seismic velocity information about the sub-surface.
- b) To calibrate the continuous velocity log.

Measurement of the Earth's velocity function is obtained by a charge detonated near the surface. A Vibroseis unit can be operated alongside a deep borehole, or an airgun may be employed as a sound source (Fig 4.1). Shots are fired at one or more points near the well-head, and the geophone

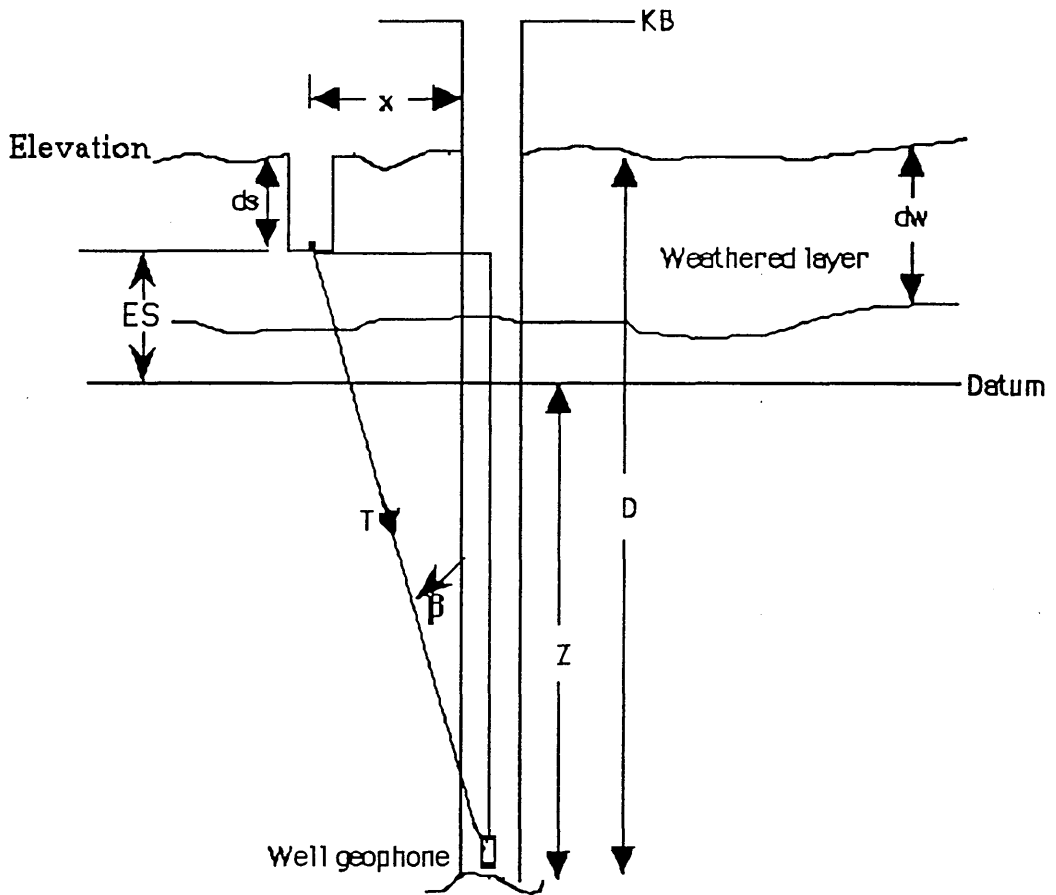


Fig 4.1 Well shooting

KB = Kelly bushing

D = Depth of well geophone below KB

Z = Depth of geophone below datum

ES = Elevation of the shot above datum

ds = Depth of shot

dw = Depth of weathering

X = Horizontal distance from well to the shot

β = Incident angle at well geophone levels

T = Observed travel-time from charge to well geophone

is moved between the shots, so that the results are a set of travel times from the surface down to various depths. The geophone positions are chosen to include the most important geological markers such as tops of the formations, unconformities and also intermediate locations so that the travel time between successive measurements is small. To ensure accuracy the reading is taken twice at the same level, with the geophone first going down the well, and then going up the well.

In the study area Check shot surveys are available for five wells D6, D7, D8, D9, and K1-149; see well location map (Fig 1.3). The relations between the time depth curve, average, interval, and rms velocities for these wells are shown in Figures 4.2-4.6. A program called Velocity is used to calculate the average, interval and rms velocities using equations 4.1 to 4.4. The program and the results of calculation are shown in Appendix 3.

4.3.1 SEISMIC VELOCITIES

4.3.1 Interval velocity

The interval velocity (V_{int}) for the i 'th layer is obtained by taking the difference in arrival times at the two depths after the arrival times have been corrected for angularity of the wave path:

$$V_{int} = (D_i - D_{i-1}) / (T_i - T_{i-1}) \dots\dots\dots 4.1$$

Where: V_{int} Interval velocity (metres/second)
 D_i The lower reflector depth in metres

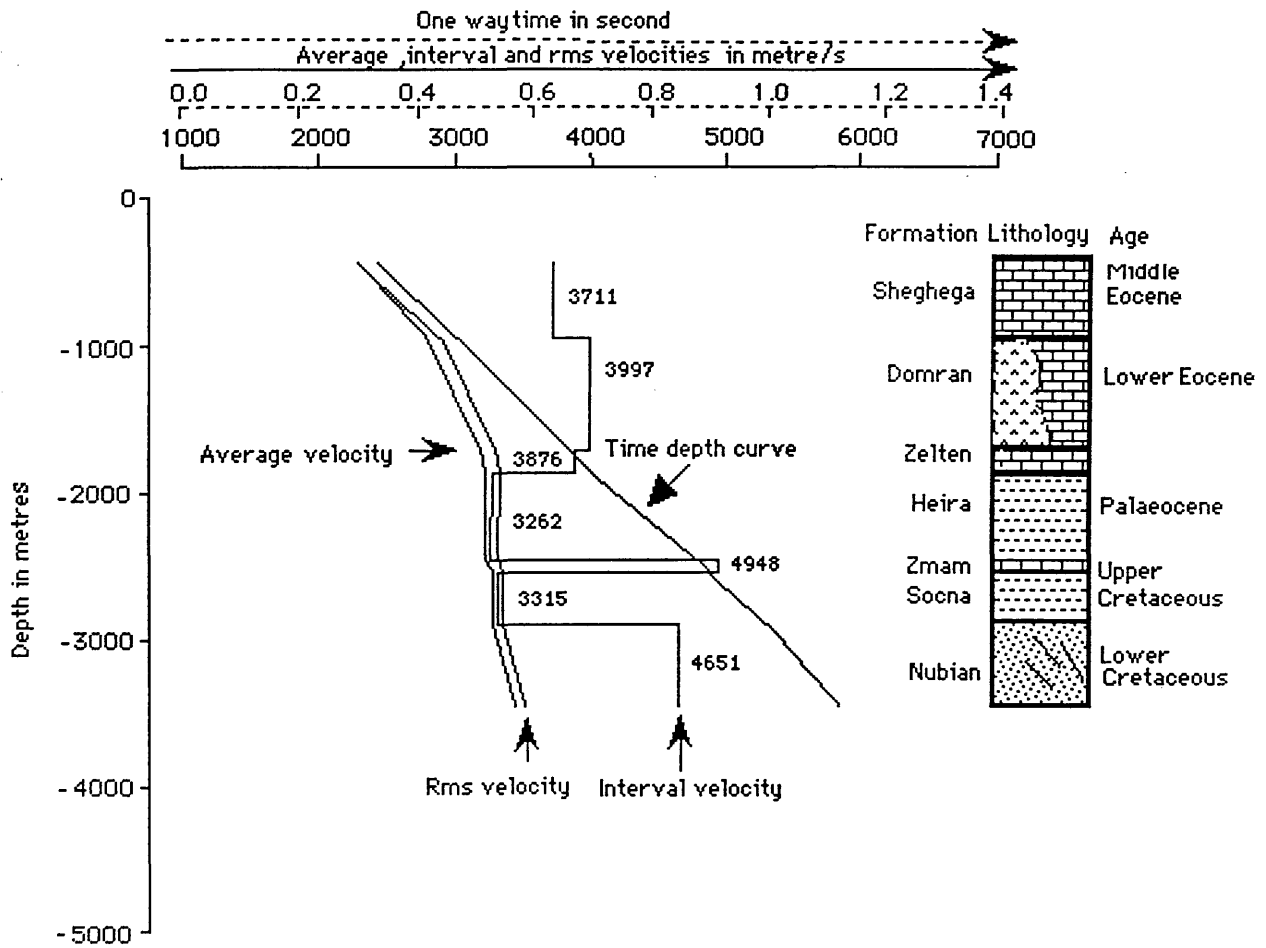


Fig 4.2 (D6-149) The relation between time depth curve and Average, Interval, RMS velocities from datum

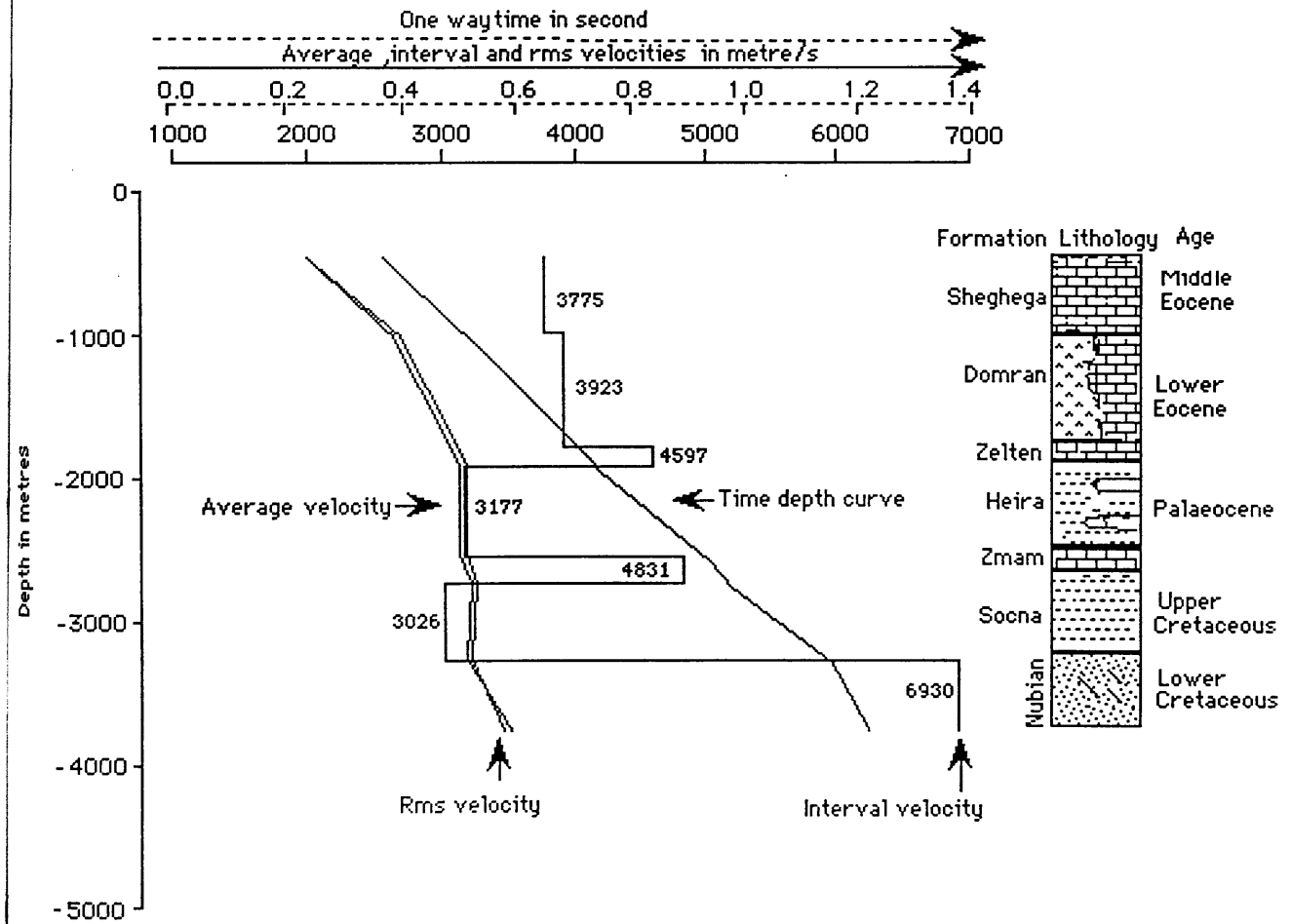


Fig 4.3 (D7-149) The relation between time depth curve and Average, Interval, RMS velocities from datum

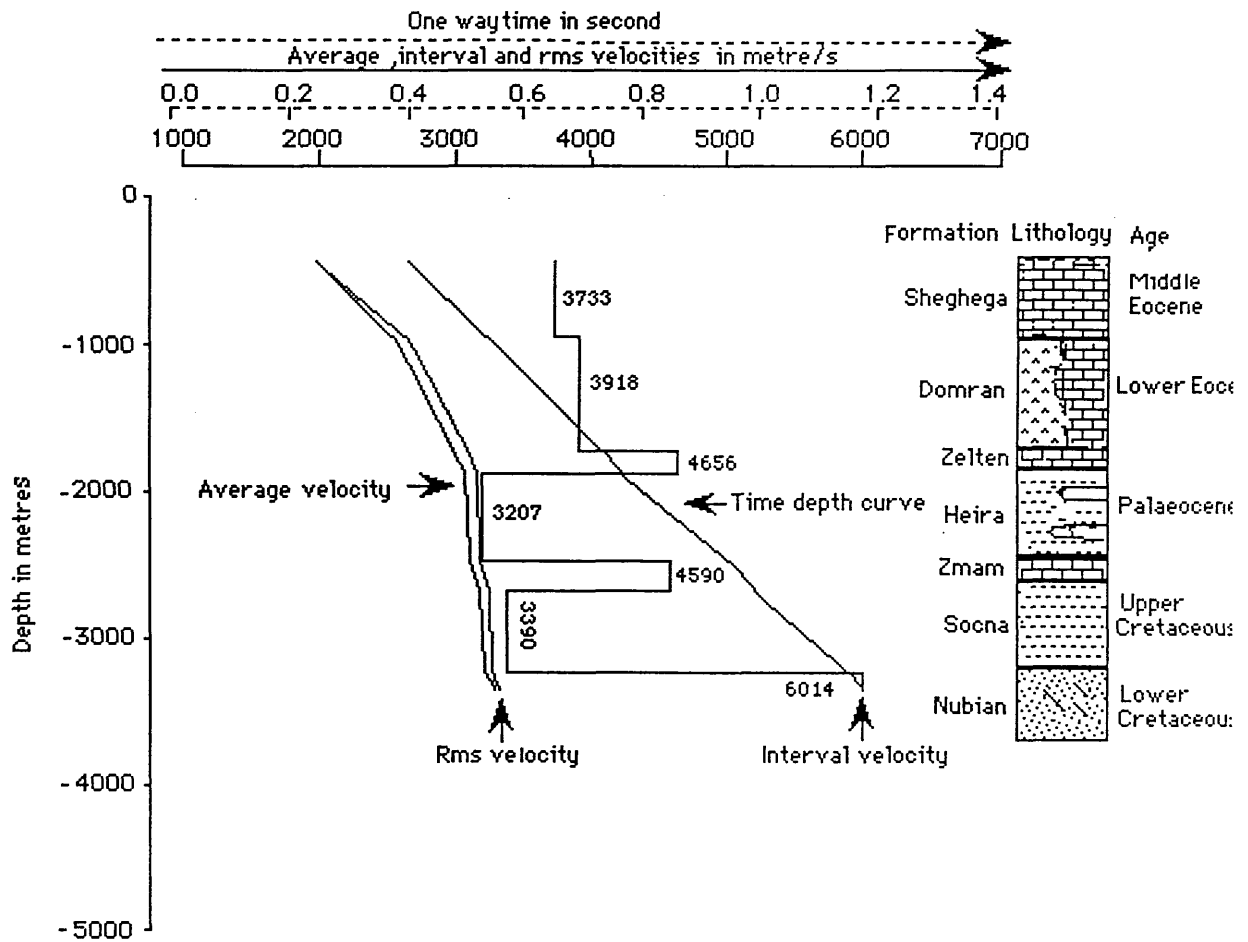


Fig 4.4 (D8-149) The relation between time depth curve and Average, Interval, RMS velocities from datum

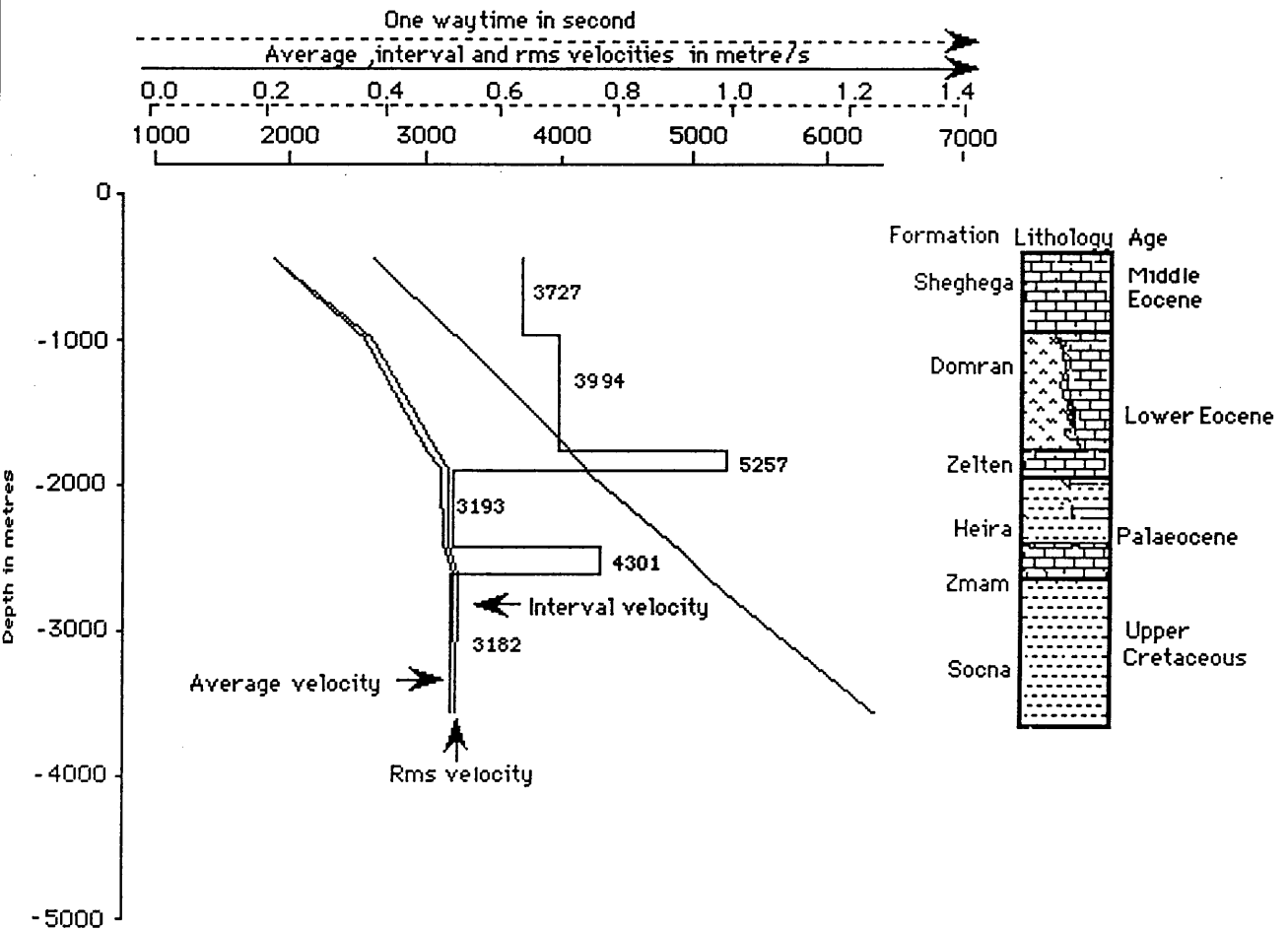


Fig 4.5 (D9-149) The relation between time depth curve and Average, Interval, RMS velocities from datum

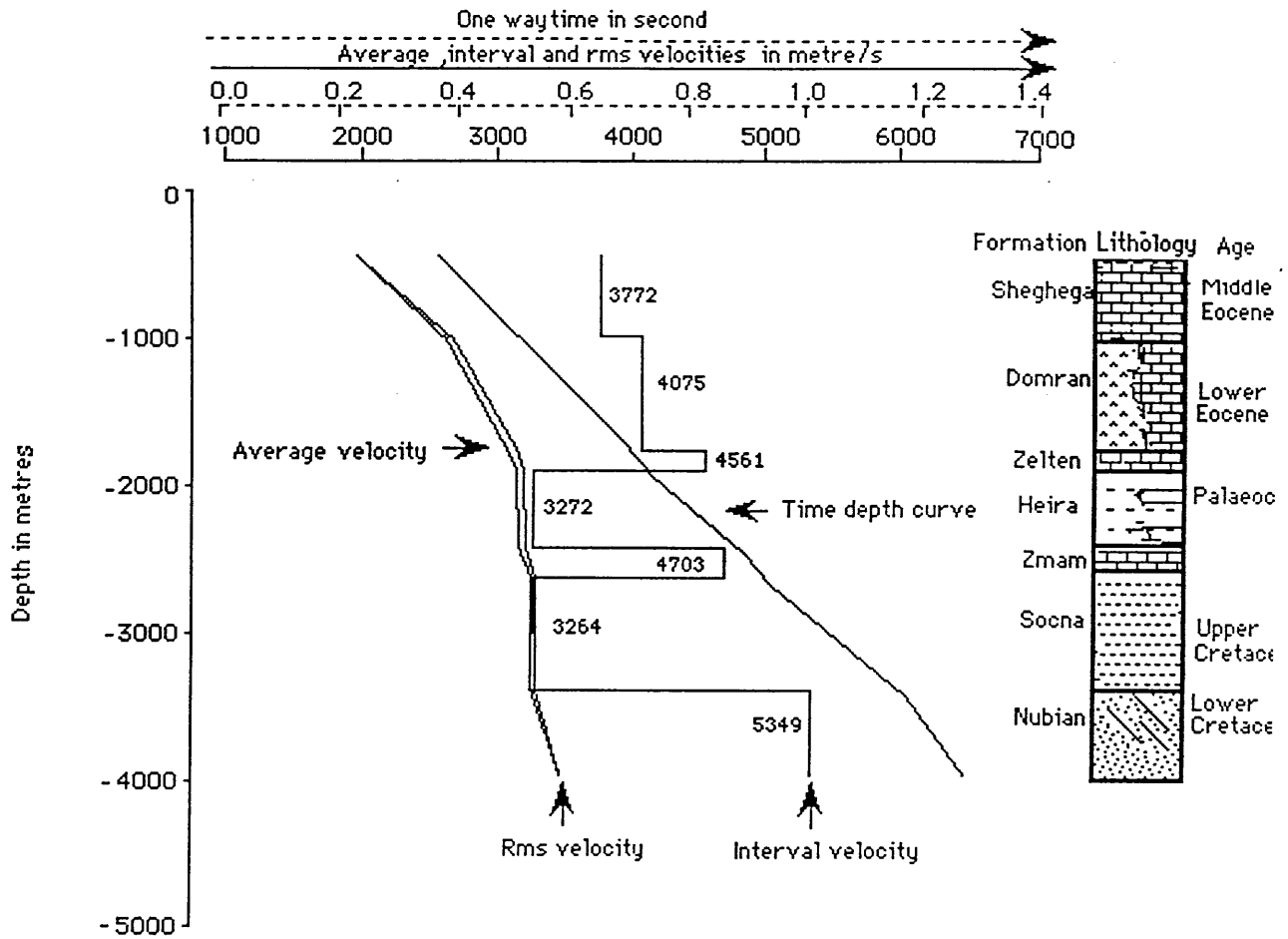


Fig 4.6 (K1-149) The relation between time depth curve and Average, Interval, RMS velocities from datum

D_{i-1} The upper reflector depth in metres

T_i The vertical datum corrected travel time in seconds to the lower reflector

T_{i-1} The vertical datum corrected travel time in seconds to the upper reflector

4.3.2 Average velocity

The average velocity is either the actual distance from source to receiver divided by the observed time, or the vertical component of distance divided by the appropriately corrected time:

$$V_a = D / T \quad \dots\dots\dots 4.2$$

where the D is the subsea depth in metres and T is the vertical travel time in seconds.

4.3.3 RMS velocity

The rms velocity is calculated using the relation between rms and interval velocity, where rms velocity is the weighted root mean square of layer interval velocities, the weight being determined by the time interval of the layer:

$$V_{rms} = \left(\sum_{i=1}^n (V_i)^2 * t_i / \sum_{i=1}^n t_i \right)^{1/2} \dots\dots\dots 4.3$$

where V_i is the interval velocity in m/s in layer i

t_i is the time in seconds.

4.4 FACTORS AFFECTING VELOCITY

An understanding of the factors affecting velocity helps us to foresee the kind of velocity variations to be expected in an area, and hence the velocity distributions to expect in the seismic data.

4.4.1 Lithology

Lithology is the most obvious factor affecting velocity. High velocities for sedimentary rocks generally indicate carbonates, and low velocities indicate sand or shale, but an intermediate velocity can indicate either. The chart in Figure 4.7 shows overlapping of velocity value for different lithologies, which suggests that velocity is not a good criterion for determining lithology. The density of the rock depends directly upon the densities of the minerals making up the rock, and high density generally corresponds to high velocities; for example shale and sand have low density and correspondingly a relatively low velocity. Dolomite has a high density, which corresponds to a high velocity.

4.4.2 Porosity

Most igneous and metamorphic rocks have little or no porosity, and the velocities of seismic waves depend mainly on the elastic properties of minerals making up the rock material itself. This is also the case with massive limestones, dolomite and evaporites. Sandstone, shale, and

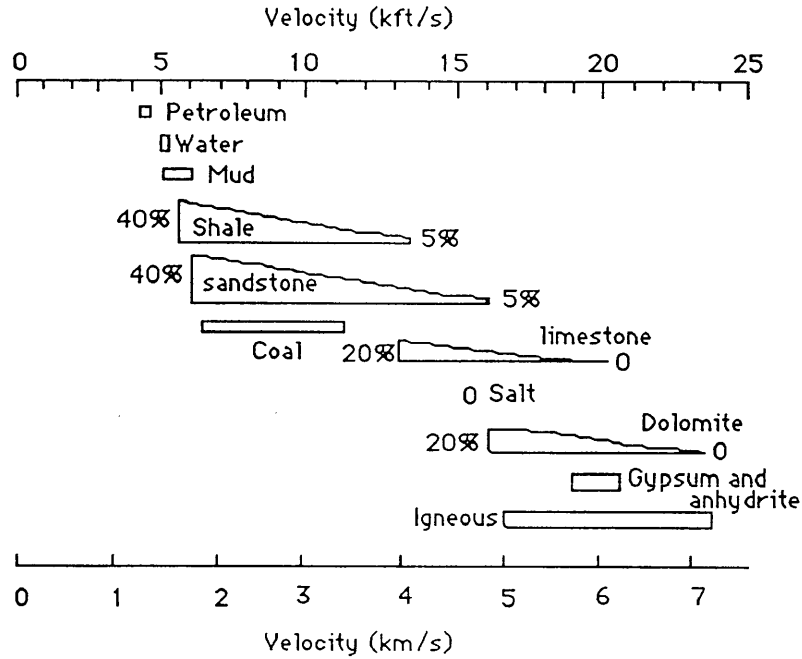


Fig 4.7 P-wave velocity for various lithologies. Adapted from Sherrif and Geldart (1983). Percentages show the porosity values.

certain kinds of soft limestones have more complex microstructures, with pore spaces between grains which may contain fluids or else softer types of solid material such as clay. For such rocks, velocity is very much dependent on the porosity and the material filling the pores. In most sedimentary rocks, the actual velocity is dependent upon the intrinsic velocity in the minerals constituting the solid rock matrix, the porosity, the pressure and the velocity of the fluid filling the pore spaces. It also depends on the compaction of any solid cementing material between the grains of the primary rock constituents. At shallow depths of burial, the velocity of most sedimentary rocks increases rapidly with increasing pressure. Beyond the depth where consolidation is reached, the influence of variation in pressure on velocity becomes small, and the porosity and

mineral composition of grains become dominant in governing velocity (Dobrin 1988).

Random packs of well-sorted particle have porosities in the range of 45-50% but under pressure the particles deform at the contact and as a result the density increases and porosity decreases (Sheriff 1977a). Porosity generally decreases with increases in depth of burial, cementation and age, and as sorting becomes poorer. Porosity is usually the most important factor in determining the velocity in the sedimentary rock (Sheriff 1983). Equations 4.4 and 4.5 show a linear relation between the reciprocal of the velocity and porosity.

$$\Delta_t = 1/V = \emptyset / V_f + (1 - \emptyset) / V_m \dots\dots\dots 4.4$$

$$\varnothing = \Delta_t - \Delta_{t_m} / \Delta_{t_f} - \Delta_{t_m} \dots\dots\dots 4.5$$

$$\emptyset = (V_f^* V_m - V_f^* V) / (V_m^* V - V_f^* V) \dots\dots\dots 4.6$$

Where

 Δ_t Formation transit time.

$V_f = 1 / \Delta t_f$ Velocity in the fluid filling the pore spaces.

$$V_m = 1 / \Delta t_m$$

Velocity in the matrix material (for sand-

stone equal 5400- 5900m/s). These figures are taken from the Schlumberger logging manual 1987).

V equals V_m at zero porosity and V_f at 100 percent porosity.

V measured formation velocity.

\emptyset porosity

In the study area equation 4.6 cannot be used to calculate the porosity in wells D7, D8, and K1-149 due to the high velocity at these wells, which show a velocity equal to or higher than the matrix velocity. El-jard (1988) shows the porosity in the Wadi field to lie between 0.03 to 0.062.

To show the effect of the low velocity layer on the calculation of the average velocity, the average velocity has been calculated in two ways:

- (a) When the depth and the time are from surface.
- (b) When the depth and time are from datum (Figs 4.2 - 4.6).

The average velocity calculated from the surface is less than the average velocity calculated from the datum, due to the effect of the low velocity layer on the travel time. The ray path in the weathered layer takes more time to reach the receiver, depending on the velocity of the weathered layer. The average velocity is the reciprocal of the travel time multiplied by the depth. That is why the average velocity calculated from surface is less than the average velocity calculated from the datum.

4.5 INTERPRETATION OF VELOCITY DATA

Velocity is usually assumed to vary from place to place in a slow systematic way, unless there is a significant structural or other change. We can expect velocities to show differences in areas separated by a fault or where there are stratigraphic changes. We expect little variation if reflectors appear to be flat and continuous. If stratigraphy is a dominant factor controlling velocity, the average velocity to the marker will be roughly constant, or may decrease slightly with depth. The change in lithology

from shale to limestone and from shale to sand and the variation in thickness as shown in Table 3.5 (Chapter 3) has affected the average velocity in the area. Wells D6 and D7-149 show a velocity decrease with depth at two reflectors top Heira (Placeocene) and top Socna (Upper Cretaceous), which suggests that the lithology is a dominant factor controlling average velocity to these two reflectors. The wells D9 and K1-149 show a velocity decrease with depth only in the Socna Formation (Upper Cretaceous) which suggests that the lithology is a dominant factor controlling average velocity to this reflector. Well D8-149 shows a velocity increase with depth for the whole sequence of the well, which may indicate that lithology is not a dominant factor controlling velocity.

The interval velocity of the Nubian quartzitic sandstone at wells D7 and D8-149 is calculated to be 6930 and 6014 m/s respectively. These two velocities are too high for quartzitic sandstone. The high velocity is due to the incorrect interval time recorded by the check shot survey between Top Gargaf and Top Nubian, the lack of information (as was mentioned in Chapter 2), and poor signal to noise ratio.

Velocity inversion suggested by the stacking velocities at CDP 1369 on line V07-85 at 1.175 and 1.488 seconds is examined by calculating the interval velocity using equation 4.7 below. The calculated interval velocity is of 3139 m/s, which is about equal to the velocity of the Heira shale. This indicates that the inversion is real and should be considered in picking the stacking velocity.

$$V_{int} = \left(\sum_{i=1}^n (V_{rms})^2 * t_i / \sum_{i=1}^n t_i \right)^{1/2} \dots\dots\dots 4.7$$

4.6 DEPTH CONVERSION

In order to convert the two-way travel time map into a depth map, we need to know the velocity distribution over the area. The sources of information on velocities are the check shot survey on the one hand and seismic stacking velocities on the other hand. Velocities derived from seismic reflection data will be unreliable, and it is necessary to rely primarily on well velocity data. In the study area velocities have been calculated in different ways:

(1) The average velocity to the the Nubian reflector is calculated from the interval velocity for each panel on the seismic lines using the relation between average and interval velocities:-

$$V_a = \sum_{i=1}^n V_i * t_i / \sum_{i=1}^n t_i \dots\dots\dots 4.8$$

Where V_i is the interval velocity for the i'th layer and t_i is the travel time for that layer. A program called Vav is used to calculate the average velocities from interval velocities. The program and the calculation results are shown in Appendix 4.

The calculated average velocity for each panel on the seismic lines is posted on the shot point base map to see the possibility of contouring

them. The velocity shows misties varying from 68 to 371 m/s at the intersections of the lines. These misties make the contouring of calculated average velocity unreliable. Figure 4.8 shows the well velocity (V_w), the average of the calculated average velocity (V_a) of the Nubian formation, and the average of the misties around the intersection of the lines (δ_m).

The average velocities calculated for each velocity analysis panel, when compared with the average velocities calculated from the wells (V_w), are different by about 350 m/s, which implies that the calculated average velocities using the relation between average and interval velocities are unreliable for depth conversion. The averages of the calculated average velocity (V_a), when compared with the well velocity (V_w), show differences of 176 to 472 m/s.

(2) Using all the wells drilled to date in the field, the average velocity is calculated using the actual depth from wells and the one way time to the formation picked from seismic sections. The average velocities calculated using the time from the seismic section will be slightly different from the average velocity calculated using the time from the well (check-shot survey). These differences are due to the phase difference between seismic lines and the wells. Tables 4.1 and 4.2 show well name, formation depth, two way time, one way time in seconds as picked from the seismic sections and the average velocity used for depth conversion for the top Nubian and top Meem reflectors. A graph of average velocity against depth for top

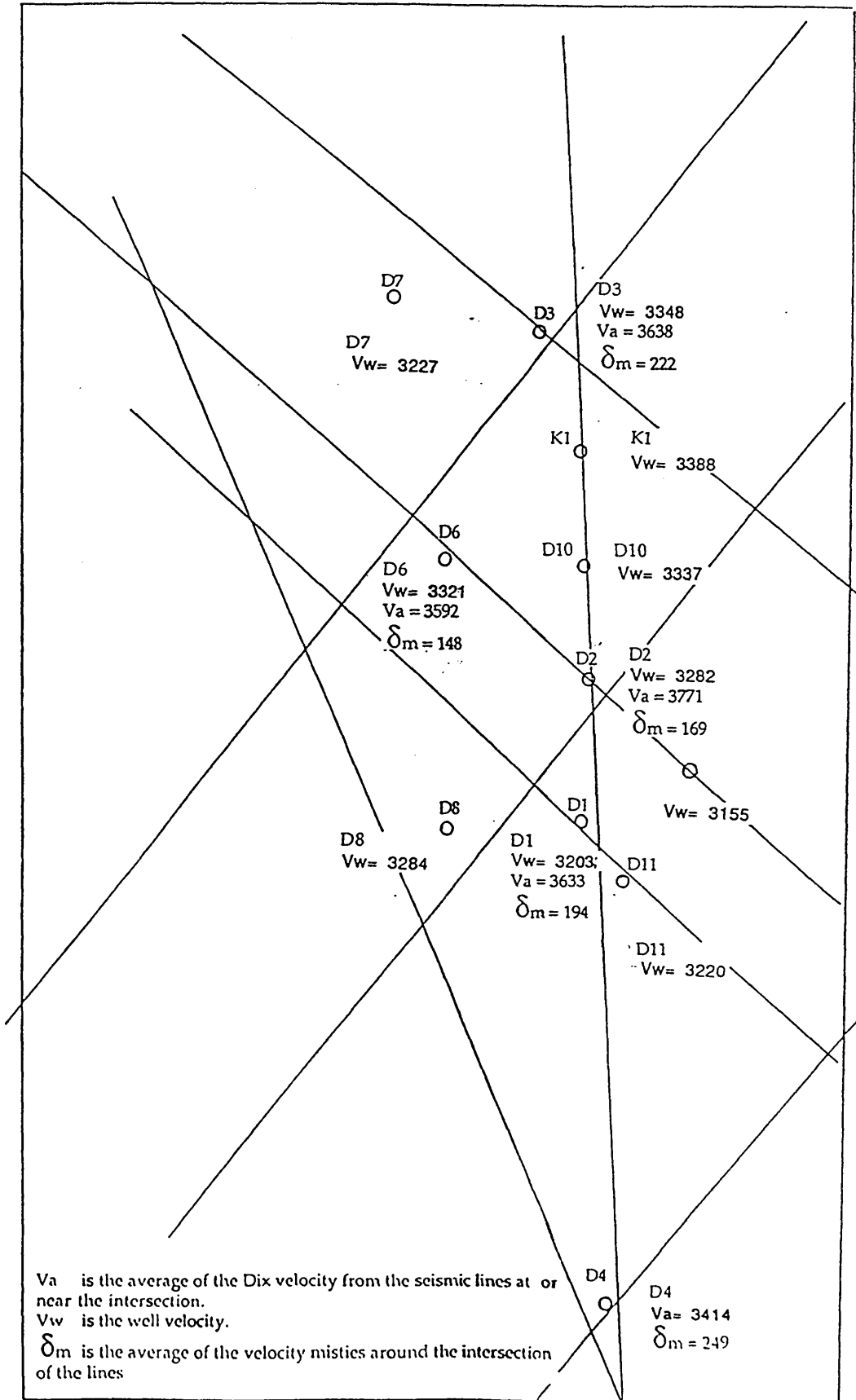


Fig 4.8 Well average velocity (V_w), average of the calculated Average velocities (V_a) and the average of the velocity misties (δ_m) to the Nubian reflector.

Table 4.1

Well name	Depth in metres	Two way time seconds	Oneway time seconds	*Velocity m/s
D1	3035	1.90	0.950	3211
D2	3217	1.96	0.980	3282
D3	3466	2.07	1.035	3348
D4	NP	-	-	-
D5	F	-	-	-
D6	2903	1.75	0.875	3317
D7	3282	2.02	1.010	3249
D8	3235	1.97	0.985	3284
D9	3581	2.27	1.135	3155
D10	3270	1.96	0.980	3337
D11	3301	2.05	1.025	3220
K1	3400	2.07	1.035	3285

Table 4.1 Well name, formation depth, two way time, one way time in seconds to the top of the Nubian Formation.

NP: Formation is not penetrated by the well.

F: Well cutting the fault at the formation.

* average velocities are calculated using one way time.

Table 4.2

Well name	Depth in metres	Two way time seconds	One way time seconds	*Velocity m/s
D1	2229	1.398	0.699	3188
D2	2159	1.360	0.680	3175
D3	2204	1.390	0.695	3171
D4	2370	1.440	0.720	3292
D5	2390	1.440	0.720	3319
D6	2204	1.350	0.675	3265
D7	2260	1.390	0.6915	3252
D8	2216	1.350	0.675	3283
D9	2225	1.375	0.6775	3236
D10	2162	1.356	0.678	3189
D11	F		-	- -
K1	2187	1.362	0.681	3211

Table 4.2 Well name, formation depth, two way time, one way time in seconds to the top of the Meem Formation.

NP: Formation is not penetrated by the well.

F: Well cutting the fault at the formation.

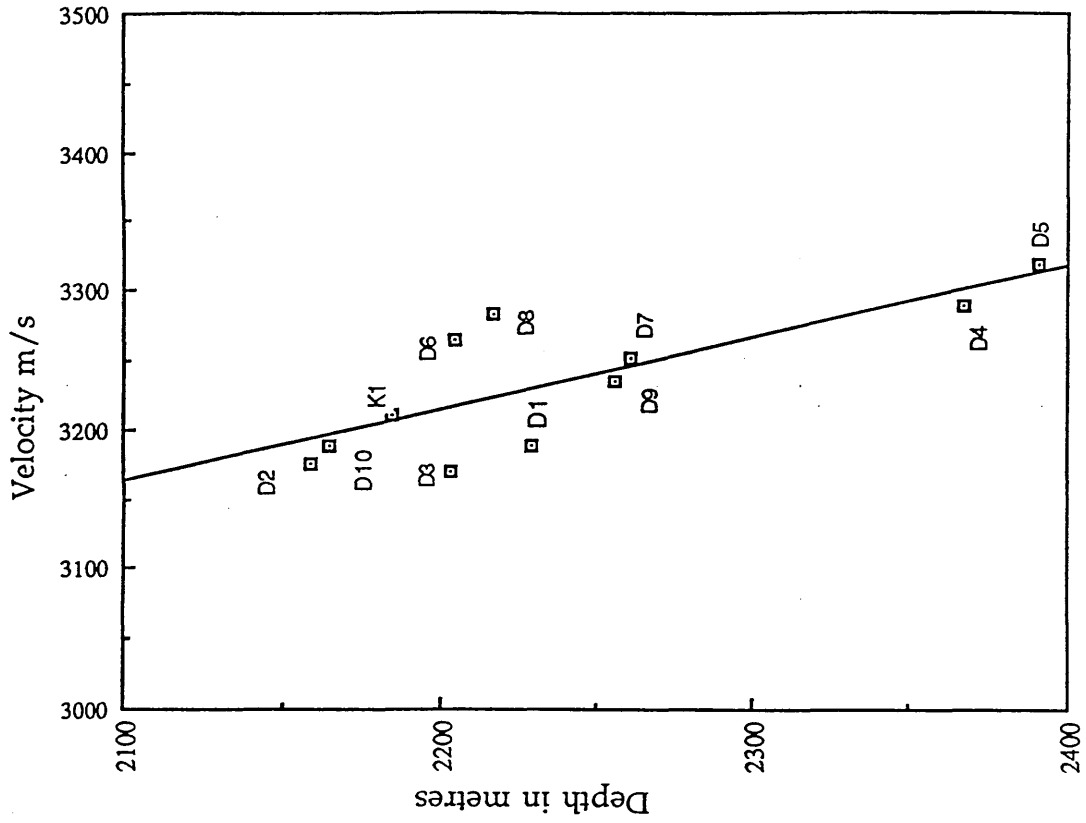
* average velocities are calculated using one way time.

Nubian (Fig 4.9a) shows that there is no systematic increase or decrease of velocity with depth. In the absence of other information we would be therefore justified in using only a constant average velocity. However, there does appear to be a systematic lateral variation of average velocity which is discussed below. The graph (Fig 4.9b) for the Top Meem shows a slight systematic increase of velocity with depth, but the best - fitted straight line clearly depends mainly on the two deep wells D4 and D5. In view of the scatter of the other points we conclude that to apply a 1-dimensional velocity - depth function for the top Meem is probably not justified.

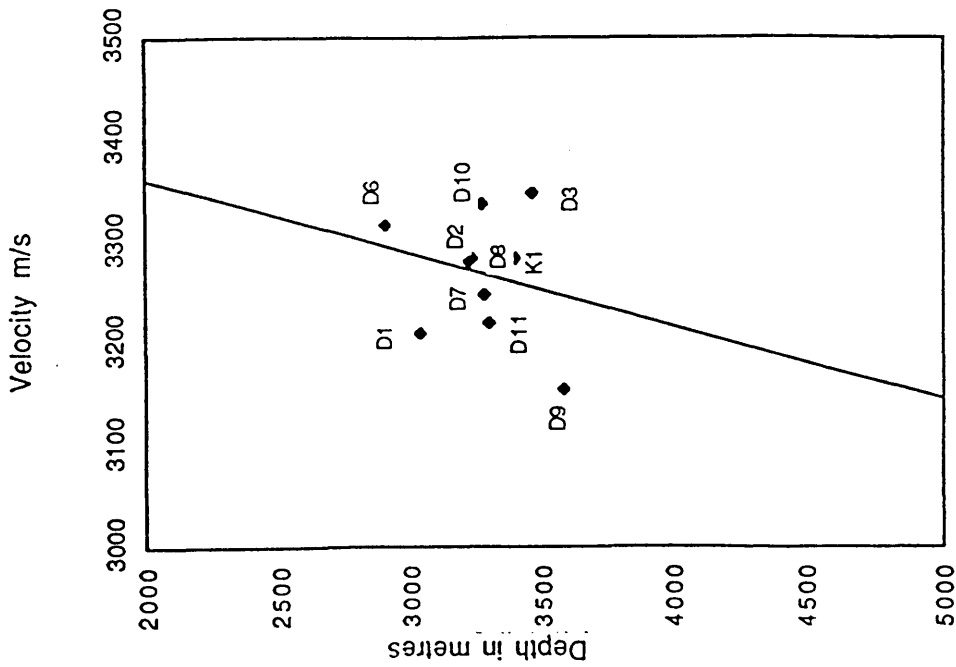
The average velocity contour maps (Figs. 4.10, 4.11) show contours representing the average velocity measured to the top of the Lower Cretaceous (Nubian equivalent) and the Palaeocene (Meem member) respectively. In the study area the average velocity calculated using the time from the seismic sections as shown in Tables 4.1 and 4.2 has been used for the depth conversion. The depth conversion has been worked in two ways:

(1) By averaging all the velocities in the area and using only one velocity for the depth conversion (3300 m/s for the Nubian and 3250 m/s for the Meem). The calculated depths using one velocity, when compared with the actual depth from the wells, show a difference of 35 to 150 m at Nubian Formation and 4 to 67 m for the Meem Formation.

(2) All the average velocities (calculated using the time from the seismic lines) are used for the depth conversion by assuming a constant rate of change of the velocity between the wells. This method will minimize the



a Top Nubian Formation



b Top Meem Formation

Fig 4.9a, b Relation between average velocity in m/s and depth in metres for all the wells, for top Nubian and top Meem.

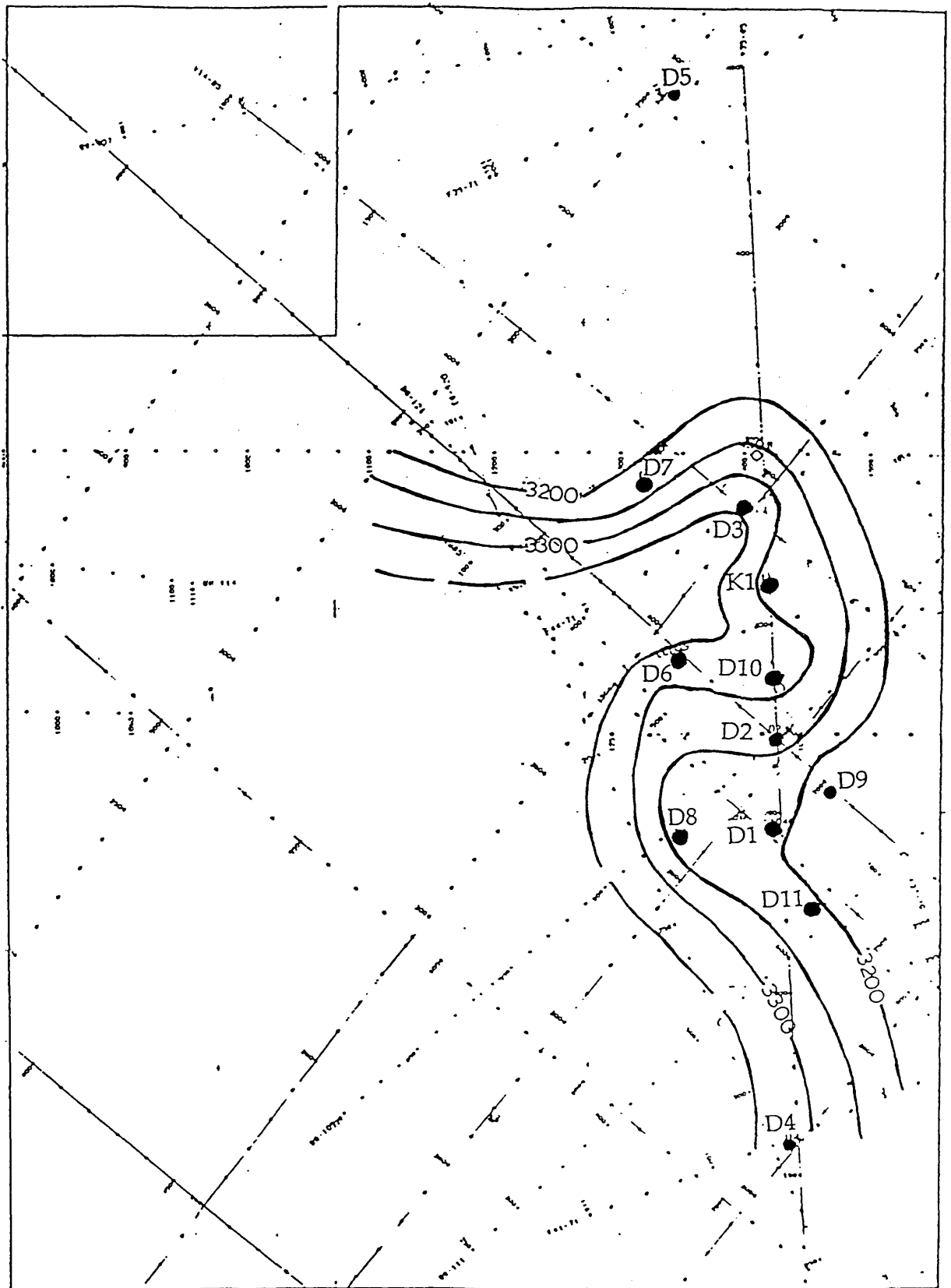


Fig 4.10 Average velocity to the top Nubian (Lower Cretaceous).

C.I 50m

Datum sea level

Scale 1:200,000

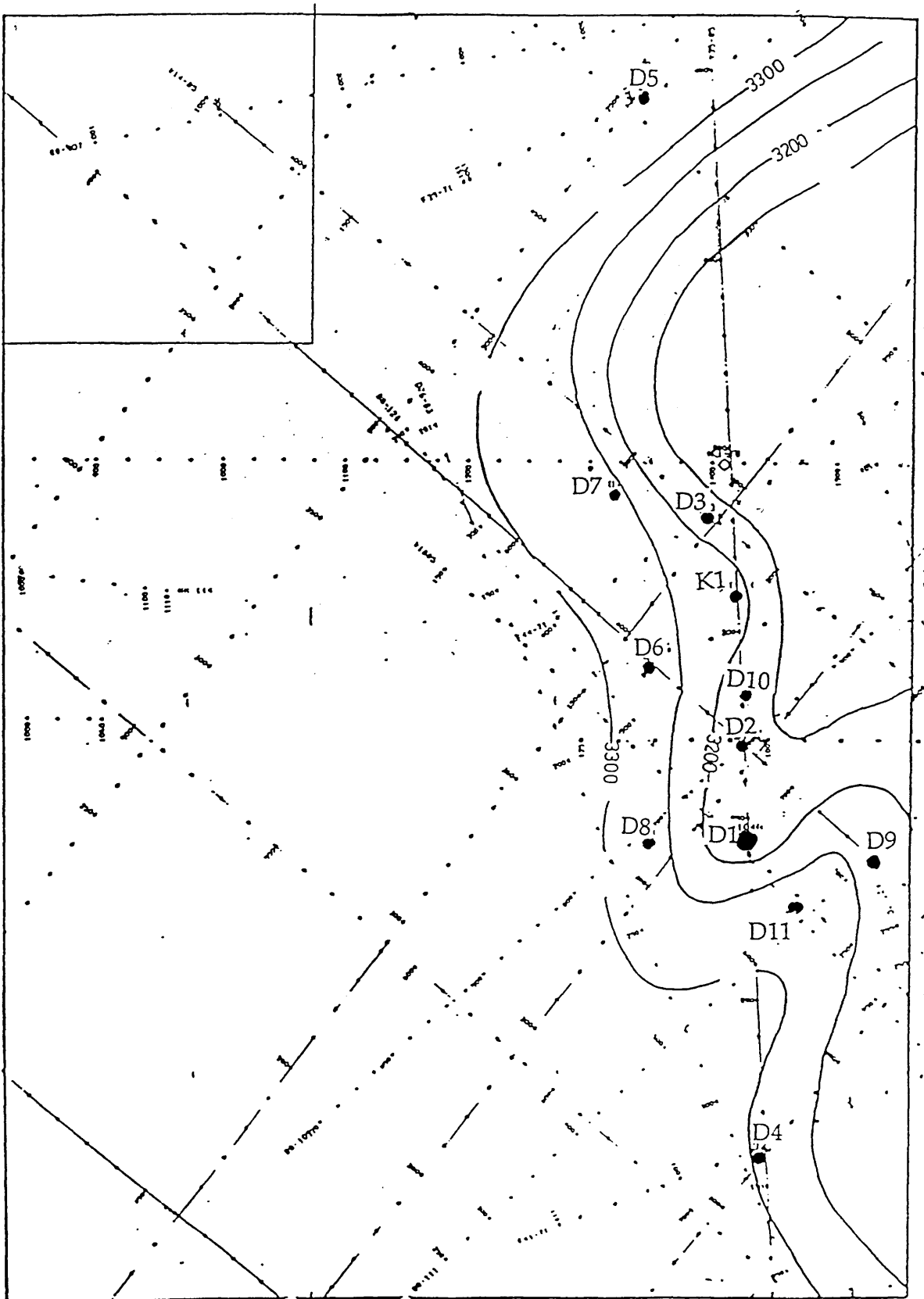


Fig 4.11 Average velocity to the top Meem (Palaeocene).
 C.I 50m Datum sea level
 Scale 1:200,000

differences between the actual depth and the calculated depth, except for the areas outside the structure where no wells have been drilled and a constant velocity has been assumed.

4.7 DEPTH MAPS

The two horizons that are of interest to oil prospectors in the Wadi field have been chosen as sample contouring horizons (Nubian equivalent and Meem member). The Nubian and Meem depth structure maps were made by converting interpreted Nubian and Meem reflection times to depth using the velocity function based on all existing wells in the field. The main exploration objectives in this area are the hydrocarbons trapped in structural closures in both the Lower Cretaceous (Nubian equivalent formation) and the Palaeocene (Meem member).

4.7.1 Nubian structure map

The structure map for the top of the Nubian formation (Fig 4.12) shows the structure bounded by two faults, with general dips towards the NE-SW and NW-SE within a major trough (the Hagfa Trough). The Wadi field is in the centre of this NE-SW trending trough (see Fig 1.1 and 1.2).

The Wadi field at Nubian formation level is mapped as one structural feature with several fault block closures. Structurally the field can be subdivided into four fault blocks as shown in the structure map on the top of the Nubian equivalent (Fig 4.12). Three of these fault blocks have been tested by drilling. Block A on the west of the field shows two dry holes D7

and D8-149, Block B, located in the middle of the study area, is the most prolific for hydrocarbon accumulation. A number of wells have been drilled within this block and tested for oil. Block C has been tested on the downthrown side of the fault by two wells D3-104 and K1-149. The fourth fault block D lies to the south of the block B and perhaps forms an extension to the fault block B, however a fault may exist on line V11-85 (Fig 3.11), separating fault block B from fault block D. No exploration drilling has been carried out in this block.

4.7.2 MEEM STRUCTURE MAP

The Meem member of the Heira shale is considered as a second reservoir in the Wadi field. The average thickness recorded is 16 m in the field, with an increase in thickness to the west and south.

The structure map for the top of the Meem member (Fig 4.13) shows a large structure dipping to the east and west to the major trough. The structure is bounded by a fault to the west of the field, with a small localized graben. Both structural and stratigraphic entrapments exist in the Wadi field and oil accumulation depends on pinching out against the downthrown side of the fault as in well D4-104 and in a local graben, as in D1-149; see the structure map for the top of the Meem Formation (Fig 4.13), line F41-70 (fig 3.15), and line V35-85 (fig 3.5). The structure in the field are controlled by the faults. There may be different levels of oil water contact in each potential fault trap. The oil water contacts in the wells are not shown in the structure maps due to the lack of information.

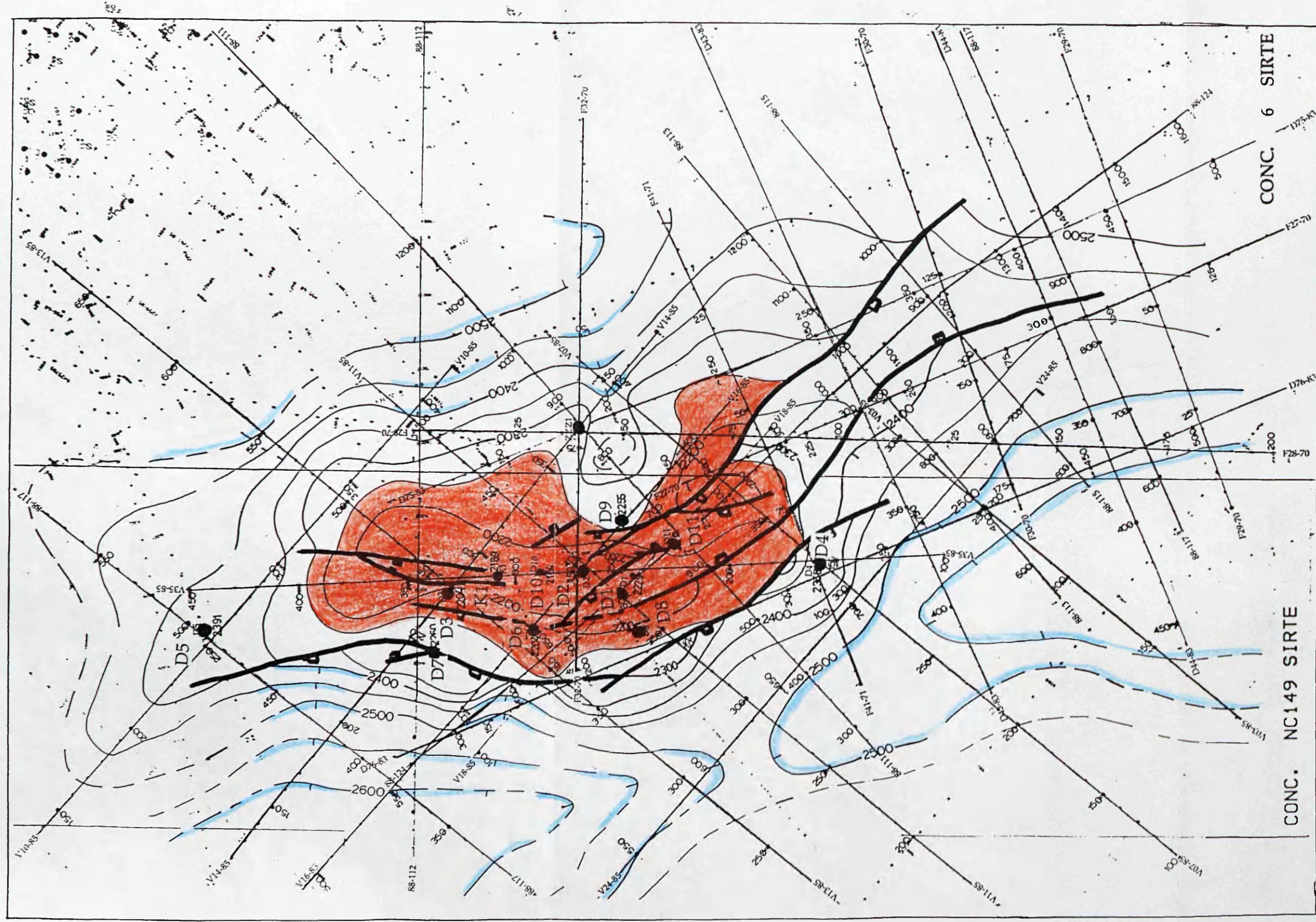


Fig 4.13 Structure map Top Meem Formation (Palaeocene).
 Contour interval 50 m. Datum Sea level.
 Red colour indicates high structure. Blue colour indicates low structure.

Chapter 5

- 5.1 Conclusions
- 5.2 Suggestions and recommendations

5.1 CONCLUSIONS

The following points are the main conclusions which were derived from the work carried out in this project.

The velocity surveys available for this study, together with the formation tops provided by Sirte Oil Company, permitted identification of the horizons on the seismic sections for interpretation and mapping. The deeper horizons (Gargaf and Nubian) are hard to identify and correlate on the seismic sections, due to the poor signal to noise ratio, whereas the shallow horizons are easily recognized strong reflectors.

The structure maps show that the structure is subdivided into a number of interlinked half-grabens separated by structurally high horsts or footwall highs, and a localized graben in the centre of the field. The faults in the Wadi field area are normal faults. The west bounding fault is interpreted as a possible growth fault characterized by thickly developed Socna shale and evaporitic salt, as shown in Figure 3.5. Using a back-stripping technique (but ignoring decompaction) with the information from the wells and seismic sections, the faults in the Wadi field have been found to have been formed at the beginning of the deposition of the Socna Formation, in Late Cretaceous (Cenomanian time). The graben around well D3-104, between K1-149 and D5-104 (see fig 3.18), is interpreted to have been formed in Eocene time, and this suggests that the faulting in the Wadi field might have been active until the Upper Eocene. Other authors writing about the Sirte Basin have concluded that the faulting in the Sirte Basin started in the Early Cretaceous (see Chapter 1).

The changes in lithology from shale to limestone and from shale to sandstone, together with the variations in thicknesses, have affected the average velocity in the area. In three wells (D6, D7, D9) the average velocity decreases with depth between two horizons (Heira (Paleocene) and top Socna (Upper Cretaceous)). This phenomenon has been found in some of the velocity analyses, where the rms velocity shows a velocity inversion (i.e. velocity decreasing with depth).

The high velocity between Top Gargaf and Top Nubian for wells D7 and D8-149 is due to the incorrect interval time recorded by the check shot survey. However the velocity inversion recorded at CDPs 1369 and 1424 (Chapter 2) is realistic and should be considered when picking the stacking velocity.

From the calculations done using the relation between average and interval velocities, it is shown that the average velocities calculated from interval velocities for each panel on the seismic section are not reliable for depth conversion, since misties appeared at the intersections of the seismic lines.

Using a single velocity to convert the time section to a depth section, shows a difference of 35 to 150 m between the actual depth from the wells and the calculated depth to the Nubian reflector, and 4 to 67 m at the Meem reflector. These suggest that the velocity is not a function of depth only, but the velocity changes laterally and is controlled by the faults. The use of all the velocities (shown in Figure 4.12 and 4.13) gives a depth very close to the actual depth at and near the wells.

The isochron maps show thinning of the sediment on the crest of the structure. This is interpreted as the deposition being contemporaneous with the growth of the structure. On the flank of the structure the contours show a trend towards increased thickness in the direction of the major faults. This suggests that the region was tilted in that direction during the time of deposition.

The depth cross section through the field (Figure 3.18) when compared with the time seismic section (Figure 3.19) shows that a structure of 40 m (which is equivalent to about 20 ms two way time) or less in amplitude are not noticeable in the shallow part of the seismic sections (e.g. Sheghega Formation). Small structures like this cannot be mapped reliably, and small elevation changes cannot be determined from the seismic section.

The structure in the Wadi field has been interpreted as four fault blocks (A, B, C, and D) as shown on the structure map for the top Nubian Formation (Fig 4.12). The map shows that the entrapment of the oil in the reservoir has been controlled by the faults downthrowing against the Socna Shale. The fault between block A and block B is a nonsealing fault (i.e because there is no closure on the downthrown side of the fault at D7 and D8 locations). This explains why wells D7 and D8-149 are dry holes. There are two leads (small prospects) against the downthrown side of the fault to the north and south of well D8-149. The fault block C shows a prospect defined by five seismic lines. Two oil wells have been drilled in this block on the downthrown side of the fault.

Another prospect is shown in fault block D to the south of fault block B, perhaps forming an extension to fault block B, which is the most prolific for hydrocarbon accumulation. However a fault may exist separating these two blocks. The prospect is only defined by three seismic lines.

From the comparison made between the time structure map and depth structure map, the structural high in time on lines F27-70 and 88-113 at shot point 200 and 900 respectively has been wiped out in depth as shown in Figure 5.1a and b. This could be due to misuse of the velocity used for depth conversion, i.e because there is no well controlling the velocity near that point.

The entrapment in the Meem member is not fully understood, because of the lack of information in well D4-104. The correlation has shown the top of the Meem member to be about 100 ms above the pinch-out as shown in line F41-71. The well shows the thickness of the Meem member to be about 16 m. The oil entrapment is interpreted to be due to pinching out against the downthrown side of the fault, or due to a structural high, as in well D4-104. The pinching out against the structural high, or the upthrown side of the fault (on the line F41-71, fig 3.15) and line V14-85, Fig 3.16 has been left without any explanation because of the lack of information available for this study from wells D4-104 and ZZZ1-6. Figure 5.2 shows part of structure map top Meem Formation with the location of D4 and ZZZ1 shown.

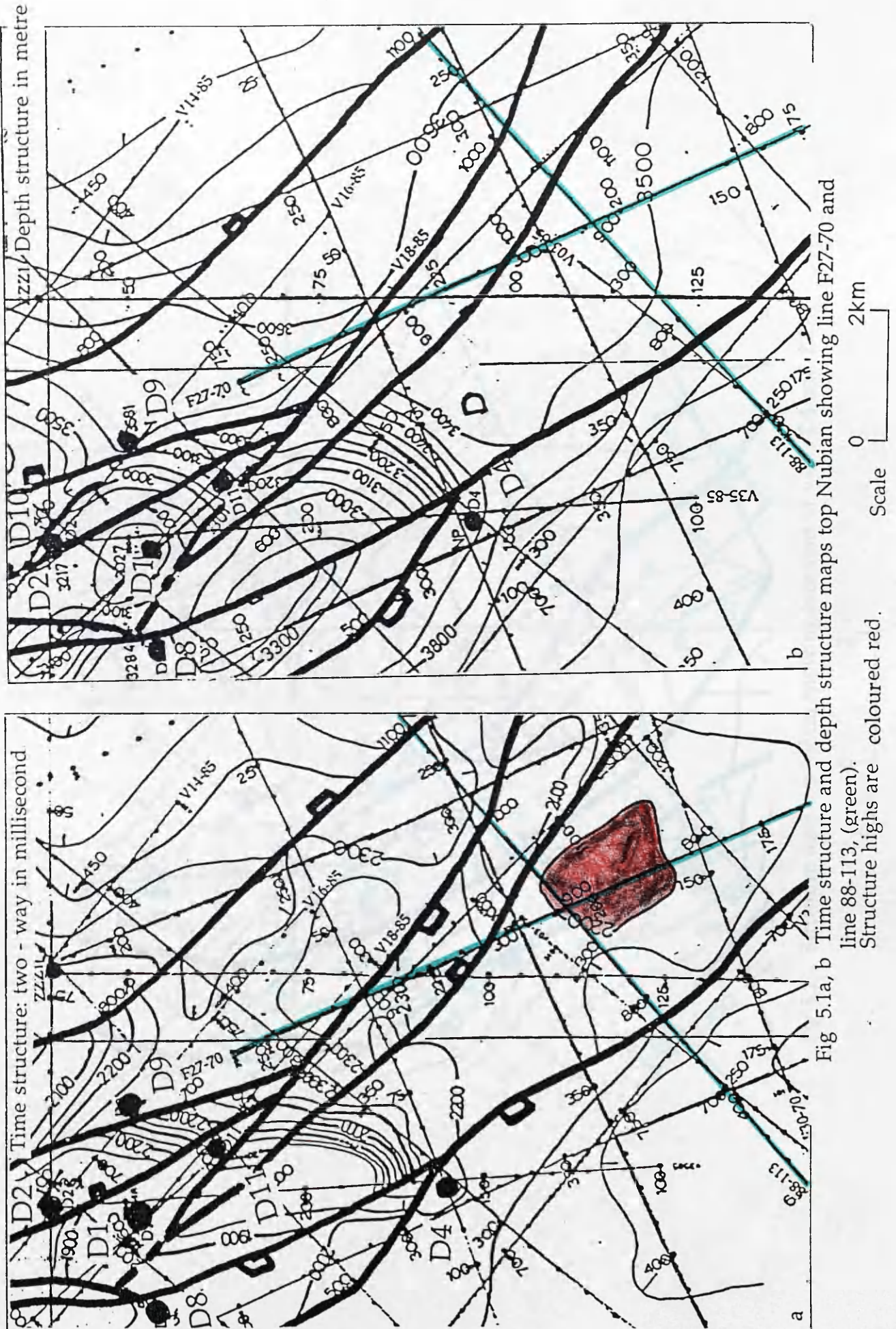


Fig 5.1a, b Time structure and depth structure maps top Nubian showing line F27-70 and line 88-113, (green). Structure highs are coloured red.

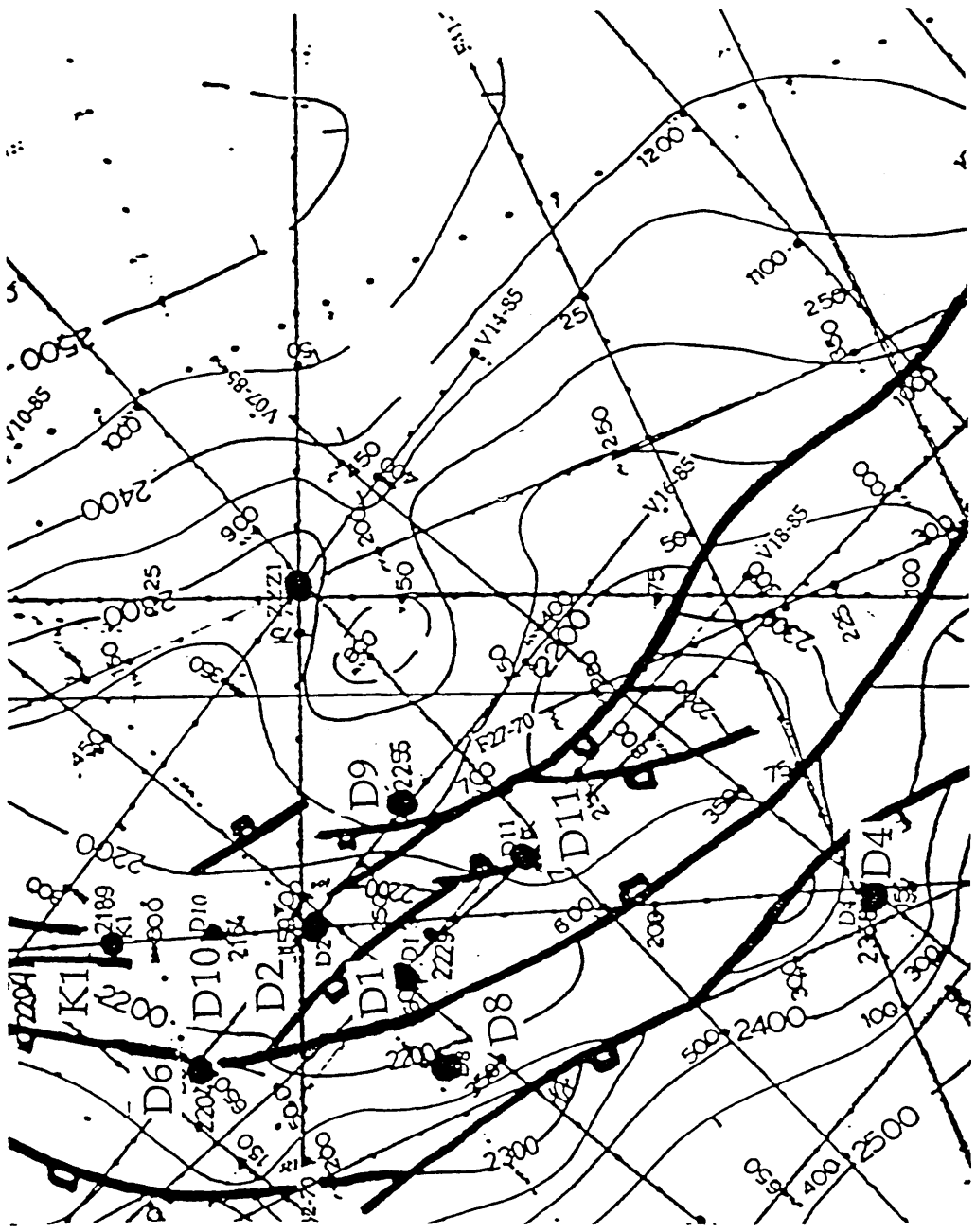


Fig 5.2 Structure map top Meem showing locations of wells D4 and ZZZ1

Using uphole static corrections to reprocess line V07-85 has solved the problem in the area where the elevation correction has been changed from "on Jabel" to "off Jabel", because there is too little uphole control. The difference in static correction times between the Sabkha formula and uphole static correction methods varied from 3 to 21 ms one way time.

Velocity spectra give a good NMO velocity indicator after residual statics are applied. Using a constant velocity function to pick velocities did not improve the stacked section. The final stacked migrated section resulted in a better defined seismic section than the original (Western Geophysical) unmigrated section.

5.2 SUGGESTIONS AND RECOMMENDATIONS

1) More upholes need to be drilled in the area to solve the static correction problem. An uphole survey needs to be done at the top and bottom of the Jabel (i.e. at the escarpment where the elevation changes). The upholes should be as close as possible to the top and bottom of the slope.

2) More care should be taken in the field about data quality control. Some noise, such as that shown in Figure 4.2a, is hard to deal with later on by processing.

3) In any reprocessing program only one static correction should be applied to all the different kinds of data that exist in the area; in particular the data shot in 1970-1971.

4) In order to correlate and tie all the wells to the seismic data, synthetic seismograms are needed for all the wells that have had a check shot survey done.

5) In order to locate the faults at their true position and to avoid misinterpretation of the faults, migration should be applied to the dip lines cutting the crest of the structure.

6) The oil lies in entrapments controlled by the faults. The seismic sections show more faults than can be shown on the structure maps. More work is needed to understand the time of faulting.

7) The oil entrapment in the Meem member needs more investigation.

8) Two wells need to be drilled to test the possibility of oil entrapment in fault block C and D.

REFERENCES

- Al-Chalabi, M.**, 1974. An analysis of stacking, rms, average, and interval velocities of a horizontally layered ground. *Geophys. Prosp.*, **22**, 458-475.
- Badley, M., E.** 1989. Practical seismic interpretation. Badley Ashton, London.
- Badley, M. E.**, 1985. Practical seismic interpretation. International Human Resources Development Corporation.
- Brady, T. J. Campbell, N. D. J., and Maher, C. E.**, 1979. Intisar "D" oil field, Libya. *Bull. Am. Ass. Pet. Geol.*, Mem 30, 543-564
- Burke, K. and Dewey. J. F.**, 1974. Two plates in Africa during the Cretaceous. *Nature*, **249**, 313-316.
- Clifford et al.**, 1980. Geology of a stratigraphic giant: Messla Oil Field, Libya. In Giant oil and gas fields of the decade 1968-1978, *Bull. Am. Ass. Pet. Geol.*, Mem 30, 507-524.
- Conant L, C., and Goudarzi, G, H.**, 1967. Stratigraphic and tectonic framework of Libya: *Bull. Am. Ass. Pet. Geol.*, **51**, 719-730.
- Conybeare, C. E. B.** 1979. Lithostratigraphic analysis of sedimentary basins. Academic Press.
- Dix, C.H.** 1955. Seismic velocities from surface measurements. *Geophysics*, **20**, 68-86.
- Dobrin, M. B and Savit, C.H.**, 1988. Introduction to geophysical prospecting (fourth edition). McGraw-Hill Book Company.
- El-jard, M.**, 1988. Geology of the Wadi field Sirte Oil Company internal report.
- Espey, H. R.**, 1983. Effective seismic data processing. Unpublished seminar, Crest hotel, Maidenhead, England.

Gumati, Y. D. and Kanes, W. H., 1985. Early Tertiary subsidence and sedimentary Facies-northern Sirte Basin, Libya: Bull. Am. Ass. Pet. Geol., 69, 39-52.

Gumati, Y. D. and Kanes, W. H., 1991. Tectonic subsidence of the Sirte Basin, Libya. J. Pet. Geol., 14, 93-102.

Harding, T. P., 1984. Graben hydrocarbon occurrences and structural style: Bull. Am. Ass. Pet. Geol., 68, 333-362.

Hatton, L. Worthington, M. H., and Makin, J., 1986. Seismic data processing: theory and practice. Oxford, Blackwell Scientific.

Hsu. K. J., 1973. Mediterranean plate tectonic and Triassic Palaeogeography. Nature, 244, 144-146.

James L. Allen and J. M. Bruso., 1989. A case history of velocity problems in the shadow of a large growth fault in the formation., Texas Gulf coast. Geophysics, 54, 426-439.

Jenyon. M. K and W. Goudswaard., 1989. Geological concepts and seismic interpretation - examples from the SEG seismic Atlas. First Break, 7, 437-446.

Kearey, P. and Brooks, M., 1991. An introduction to geophysical exploration (second edition). Blackwell Scientific Publications.

Klitzsch, E. 1971., The structural development of parts of North African since Cambrian time: Gary C. (ed) 1st Symposium Geology of Libya. Tripoli University, Faculty. Science., 253-262.

McQuillin. R, Bacon. M and Barclay. W., 1979. An introduction to seismic interpretation. Graham & Trotman Limited.

Morgan, N., 1985. Processing and interpretation. Unpublished seminar, Grand Hotel, Tripoli, Libya.

- Parson, M. G., Zagaar A. M, and Curry. J. J., 1980,** Hydrocarbon occurrences in the Sirte Basin, Libya. In: Facts and principles of the world petroleum occurrence (ed. A. Maill): Can. Soc. Pet. Geol. Mem, 6, 723-732.
- Petters. S. W., 1979.** Stratigraphic history of the south-central Sahara region. Bull. Am. Ass. Pet. Geol., 90, 753-760.
- Schlumberger, 1987.** Log Interpretation principle, Application. Schlumberger Educational Services.
- Selley, R. C. 1968.** Facies profile and other new methods of graphic data presentation: application in a quantitative study of Libyan Tertiary shoreline deposits. J. Sed. Petrol., 38, 363-372.
- Sheriff, R. E. 1978.** A first course in geophysical exploration and interpretation. International Human Resources Development Corporation.
- Sheriff, R. E. and Geldart, L. P.,1983.** Exploration seismology, volume 1, history, theory & data acquisition. Cambridge University Press.
- Sheriff, R. E. and Geldart, L. P.,1983.** Exploration seismology, volume 2, Data processing and interpretation. Cambridge University Press.
- SierraSEIS manual. 1989.** Sierra Geophysics (UK) Ltd. Heliburton House, Putney Approach London.
- Telford. W. M, Geldart. L. P, Sheriff. R. E and Keys. D. A., 1979.** Applied geophysics. Cambridge University press.
- Van Houten. F. B., 1980.** Latest Jurassic-Early Cretaceous regressive facies, Northeast Africa craton. Bull. Am. Ass. Pet. Geol., 64, 857-867.
- Van Houten. F. B., 1983.** Sirte Basin, north-central Libya: Cretaceous rifting above a fixed mantle hotspot? Geology, 11, 115-118.
- Waters, K. H., 1978.** Reflection seismology (a tool for energy resource exploration). John Wiley & Sons, Inc.

Yilmaz, O. 1987. Seismic data processing (Investigation in Geophysics, Volume 2). SEG.

Appendix 1

File	Traces zeroed	File	Traces zeroed	File	Traces zeroed	File	Traces zeroed
.1	47-96	34	80-96	160	1-96	350	1-32
2	48-96	35	81-96	183	1-96	351	1-33
3	49-96	37	83-96	225	1-96	352	1-34
4	50-96	38	84-96	321	1-04	353	1-35
5	51-96	39	85-96	322	1-05	354	1-36
6	52-96	43	89-96	323	1-06	355	1-36
7	53-96	44	90-96	324	1-07	356	1-37
8	54-96	45	91-96	32	1-08	357	1-38
9	55-96	46	92-96	326	1-09	358	1-39
10	56-96	47	93-96	327	1-10	358	1-39
11	57-96	48	94-96	328	1-11	359	1-40
12	58-96	49	95-96	329	1-12	360	1-41
13	59-96	56	58-61	330	1-13	361	1-42
14	60-96	57	59-62	331	1-14	362	1-44
15	61-96	58	60-63	332	1-15	363	1-45
16	62-96	59	61-64	333	1-16	364	1-46
17	63-96	60	62-65	334	1-17	365	1-47
18	64-96	61	63-66	335	1-17	366	1-48
19	65-96	62	64-67	336	1-18	367	1-49
20	66-96	63	65-68	337	1-19		
21	67-96	64	66-69	338	1-20		
22	68-96	65	67-70	339	1-21		
23	69-96	118	1-31	340	1-22		
24	70-96	119	1-32	341	1-23		
25	71-96	120	1-33	342	1-24		
26	72-96	121	1-34	343	1-25		
27	73-96	122	1-35	344	1-26		
28	74-96	123	1-36	345	1-27		
29	75-96	124	1-37	346	1-28		
30	76-96	125	1-38	347	1-29		
31	77-96	126	1-39	348	1-30		
32	78-96	152	1-96	349	1-31		

Table 1.1 Shot number and the edited traces.

Total number of traces 35232 trace
Number of traces edited 3177 trace

Appendix 2

```

c      This program calculates the isochron in seconds or milliseconds
c      between formations
      program isochron
      parameter (il=100)
      dimension SP(il), SH(il), Z1(il), Z2(il), N(il), G(il), T6(il)
*      T7(il), T8(il), T9(il)
c SP    shot point number
c SH    Top Sheghega Formation in ms
c Z1    Top Zelten Formation in ms
c Z2    Top Zmam Formation in ms
c N     Top Nubian Formation in ms
c G     Top Gargaf Formation in ms
c T6    the isochron time between Zelten Sheghega Formations
c T7    the isochron time between Zmam and Zelten Formations
c T8    the isochron time between Nubian and Zmam Formations
c T9    the isochron time between Gargaf and Nubian Formations

      write(6,*)'what is the number of the lines?'
      read(5,*) NL
      write(6,*)'enter the input file'
      read(5,*) ahmed1
      write(6,*)'enter the output file'
      read(5,*) isochron
      open (1, file = ahmed1)
      open (2, file = isochron)

```



```

read (1,*) INFO1, INFO2, INFO3, INFO4, INFO5, INFO6, INFO7
write (2,101) INFO1, INFO2, INFO3, INFO4, INFO5, INFO6,
INFO7
101  format (A6, 3x, 6A10)
      do 50 I= 1, NL
      read (1,*) SP(i), SH(i), Z1(i), Z2(i), UNU(i), G(i)
      write (2,*) SP(i), SH(i), Z1(i), Z2(i), UNU(i), G(i)
50   continue
      write(2,*)' -----'
      do 100 j=1, NL
      T6(j)=Z1(j)-SH(j)
      T7(j)=Z2(j)-Z1(j)
      T8(j)=UNU(j)-Z2(j)
      T9(j)=G(j)-UNU(j)
      write(2,*)INFO1, SP(j), T6(j), T7(j), T8(j), T9(j)
100  continue
      stop
      end

```

Table 2.1

S P	SH	Z	Z	NU	G
110	3850	1110	1690	2260	2470
120	3900	1115	1700	2270	2480
130	4000	1130	1705	2270	2470
140	4100	1130	1710	2280	2510
150	4100	1130	1720	2280	2580
160	4200	1130	1720	2280	2580
170	4200	1130	1720	2290	2580
180	4200	1140	1730	2290	2585
190	4200	1145	1740	2300	2590
200	4200	1150	1735	2300	2600
210	4200	1150	1730	2310	2600
220	4200	1150	1730	2330	2605
230	4200	1150	1730	2330	2610
240	4400	1160	730	2330	2640
250	4450	1160	1720	2330	2635
260	450	1160	1720	2320	2610
270	4450	1155	1720	2310	2600
280	4400	1150	1710	2310	2600
290	4350	1140	1700	2310	2600
300	4350	1130	1680	2300	2570
310	4300	1120	1670	2280	2550
320	4200	1100	1640	2190	2460
330	4100	1080	1570	2180	2450
340	4200	1090	1525	2160	2450
350	4200	1090	1520	2150	2450
360	4200	1090	1555	2150	2440
370	4400	1100	1555	2310	2450
380	4400	1110	1580	2270	2570
390	4400	1100	1560	2280	2580
400	4400	1130	1580	2280	2590
410	4500	1145	1600	2300	2590
420	4600	1170	1620	2320	2610
430	4600	1170	1620	2320	2620
460	4900	1220	1680	2400	2750

Table 2.1 Shot point number and formation tops in ms for line V07-85.

Key: SP shot point number SH Sheghega Formation
Z Zelten Formation Z Zmam Formation
NU Nubian Formation G Gargaf Formation

Table 2.2

SP	T6	T7	T8	T9
110	725	580	570	210
120	725	585	570	210
130	730	575	565	200
140	720	580	570	230
150	720	590	560	300
160	710	590	560	300
170	710	590	570	290
180	720	590	560	295
190	720	595	560	290
200	730	585	565	300
220	730	580	600	275
240	720	570	600	310
250	715	560	600	290
270	710	565	590	290
280	710	560	600	290
290	705	560	610	290
300	695	550	620	270
310	690	550	610	270
320	680	540	550	270
330	670	490	610	270
340	670	435	635	290
350	670	430	630	00.0
360	670	465	595	290
370	660	455	755	140
380	670	470	690	300
390	660	460	720	300
400	690	450	700	310
410	695	455	700	290
420	710	450	700	290
430	710	450	700	300
440	715	460	715	290
450	720	470	710	320
460	730	460	720	350

Table 2.2 Shot point number and isochron time between formation tops calculated using program Isochron for line V07-85.

Key: SP shot point number

T6 Isochron between Zelten and Sheghega

T7 Isochron between Zmam and Zelten

T8 Isochron between Nubian and Zmam

T9 Isochron between Gargaf and Nubian

Appendix 3

```

c      program Average velocity
c      This program to calculates the average, interval, and rms
c      velocities using the check shot suvery.
c      average & rms velocities refer to depth stated at start of line.
c      interval velocity refers to between THAT depth and the
c      reflector ABOVE it.
      dimension T(100), D(100), D1(100), T1(100), DD(100),
      TT(100), Va(100), Vi(100), Vrms(100)
c D      is the depth from surface.
c D1     is the subsea depth.
c DD     is the isopach.
c T      is the time from surface.
c T1     is the time from datum.
c TT     is the isochron time.
c Va     is the average velocity.
c Vi     is the interval velocity.
c Vr     is the rms velocity.
      parameter (il=100)
      character*10 ahmed1,ahmedn
      write(6,*)'WHAT IS THE NUMBER OF THE LINES ?'
      READ(5,*)NL
      WRITE(6,*)'ENTER THE INPUT FILE'
      read(5,*)ahmed1
      write(6,*)'ENTER THE OUTPUT FILE'
      READ(5,*)ahmedn

```

```

open(1,file=ahmed1)
open(2,file=ahmedn)
read(1,*)KB, ST, linenu
c KB    is the kelly bushing
c ST    static value in second or millisecond
c ln    is the line number
KB=KB*0.3048
ST=ST/1000
write(2,*)KB, ST, linenu
do 100 I=1, NL
read(1,*)D(I), T(I)
D(I)=D(I)*0.3048
T(I)=T(I)/1000
100     continue
C
WRITE(2,2000)
2000    FORMAT('average & rms vels refer to depth',
*        'at start of line',/,
*        'interval vel refers to between THAT',
*        'depth and position ABOVE it')
c       amend depths & times, calculate average velocities to each c
       depth.
do 200 j=1,NL
D1(j)=(D(j)-KB)
T1(j)=T(j)-ST
Va(j)=D1(j)/T1(j)
200     continue

```

```

c      trivially, int vel & rms vel of top layer equal average vel to first
*      depth.
      Vi(1) = Va(1)
      Vrms(1)=Va(1)
      DD(1)=D1(1)
      TT(1)=T(1)
c      calculate interval velocities for second layer onward.
      do 300 i=2,NL
      DD(i)=D1(i)-D1(i-1)
      TT(i)=T(i)-T(i-1)
      Vi(i)=DD(i)/TT(i)
300    continue
c      calculate rms velocities for second layer onward.
      SUM=Vi(1)**2*TT(1)
      SUM2=TT(1)
      do 400 m=2,NL
      SUM =SUM+Vi(m)**2*TT(m)
      SUM2=SUM2+TT(m)
      Vrms(m)=sqrt(SUM/SUM2)
400    continue
      WRITE(2,499)
499    FORMAT('  D    T    D1    T1    dD',
*           '  dT    Va    Vint  Vrms')
      do 390 K=1,NL
      write(2,500)D(K),T(K),D1(K),T1(K),DD(K),TT(K),Va(K),Vi(K),
*           Vrms(K)
500    format(f7.1,2x,f6.4,f9.1,2x,f9.4,f8.1,f8.4,1x,f8.2,1x,1x,f8.1,

```



```
*      1x,f8.1)
390    continue
      stop
      end
```

Table 3.1 Well D6-149

D	T	D1	T1	ΔD	ΔT	V _a	V _{int}	V _{rms}
635	0.3324	438.5	0.1914	438.5	0.3324	2291.00	2291.00	2291.00
1153	0.4720	956.7	0.3310	518.2	0.1396	2890.00	3711.00	2787.00
1917	0.6630	1720.2	0.5220	763.5	0.1910	3295.00	3997.00	3183.00
2068	0.7020	1871.4	0.5610	151.2	0.0390	3335.00	3876.00	3226.00
2665	0.8850	2468.5	0.7440	597.1	0.1830	3173.00	3262.00	3233.00
2749	0.9020	2552.6	0.7610	84.1	0.0170	3354.00	4948.00	3274.00
3101	1.0080	2904.0	0.8670	351.4	0.1060	3349.00	3315.00	3278.00
3668	1.1300	3471.6	0.9890	567.5	0.1220	3510.00	4651.00	3453.00

Table 3.2 Well D7-149

D	T	D1	T1	ΔD	ΔT	V _a	V _{int}	V _{rms}
644	0.3654	458.7	0.2294	458.7	0.3654	1999.00	1999.0	1999.00
1168	0.5040	982.0	0.3680	523.3	0.1386	2668.00	3775.0	2611.00
1964	0.7071	1778.4	0.5710	796.4	0.2030	3114.00	3923.0	3046.00
2101	0.7369	1915.9	0.6009	137.5	0.0299	3188.00	4597.0	3124.00
2724	0.9330	2538.9	0.7970	623.0	0.1961	3185.00	3177.0	3135.00
2918	0.9730	2732.2	0.8370	193.2	0.0400	3264.00	4831.0	3222.00
3468	1.1550	3282.9	1.0190	550.8	0.1820	3221.00	3026.0	3192.00
3947	1.2240	3761.2	1.0880	478.2	0.0690	3456.00	6930.0	3510.00

Key

D Depth from surface (metres) T Time from surface (seconds)

D1 subsea depth (metres) T1 Corrected time (seconds)

 ΔD Isopach ΔT Isochron time (seconds)V_a Average velocity (m/s) V_i Interval velocity (m/s)V_{rms} Rms velocity (m/s)

Table 3.1 and 3.2 Average, interval, and rms velocities calculated from check shot survey using program Average velocity.

Table 3.4 Well D8-149

D	T	D1	T1	ΔD	ΔT	Va	Vint	Vrms
671	0.3860	441.2	0.2240	441.2	0.3860	1969.00	1969.0	1969.00
1182	0.5230	952.6	0.3610	511.5	0.1370	2638.00	3733.0	2552.00
1960	0.7216	1730.8	0.5596	778.2	0.1986	3092.00	3918.0	2991.00
2111	0.7540	1881.7	0.5920	150.9	0.0324	3178.00	4656.0	3081.00
2713	0.9415	2483.0	0.7795	601.4	0.1875	3185.00	3207.0	3106.00
2903	0.9830	2673.5	0.8210	190.5	0.0415	3256.00	4590.0	3183.00
3465	1.1486	3235.0	0.9866	561.4	0.1656	3278.00	3390.0	3214.00
3599	1.1710	3369.7	1.0090	134.7	0.0224	3339.00	6014.0	3290.00

Table 3.3 Well D9-149

D	T	D1	T1	ΔD	ΔT	Va	Vint	Vrms
646	0.3780	444.5	0.2350	444.5	0.3780	1891.00	1891.0	1891.00
1168	0.5180	966.3	0.3750	521.8	0.1400	2576.00	3727.0	2523.00
1959	0.7160	1757.3	0.5730	791.0	0.1980	3066.00	3994.0	3003.00
2106	0.7440	1904.5	0.6010	147.2	0.0280	3168.00	5257.0	3117.00
2633	0.9090	2431.5	0.7660	527.0	0.1650	3174.00	3193.0	3131.00
2822	0.9530	2620.8	0.8100	189.3	0.0440	3235.00	4301.0	3195.00
3771	1.2510	3569.0	1.1080	948.2	0.2980	3221.00	3182.0	3191.00

Key

D Depth from surface (metres) T Time from surface (seconds)

D1 subsea depth (metres) T1 Corrected time (seconds)

 ΔD Isopach ΔT Isochron time (seconds)

Va Average velocity (m/s) Vi Interval velocity (m/s)

Vrms Rms velocity (m/s)

Table 3.3 and 3.4 Average, interval, and rms velocities calculated from check shot survey using program Average velocity.

Table 3.5 Well K1-149

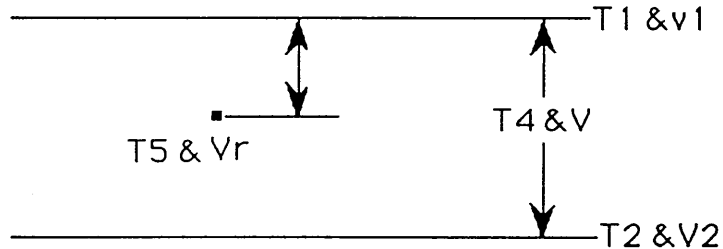
D	T	D1	T1	ΔD	ΔT	Va	Vint	Vrms
639	0.3640	448.2	0.2280	448.2	0.2280	1965.00	1965.0	1965.00
1169	0.5045	978.2	0.3685	784.6	0.1925	2654.00	3772.0	2598.00
1953	0.6970	1762.8	0.5610	784.6	0.1925	3142.00	4075.0	3078.00
2086	0.7260	1895.1	0.5900	132.3	0.0290	3211.00	4561.0	3150.00
2622	0.8900	2628.4	0.7958	536.8	0.1640	3225.00	3272.0	3173.00
2918	0.9318	2684.4	0.7958	775.4	0.2375	3302.00	4703.0	3257.00
3594	1.1693	3403.8	1.0333	775.4	0.2375	3294.00	3264.0	3259.00
4160	1.2750	3969.2	1.1390	565.4	0.1057	3484.00	5349.0	3480.00

Key
D Depth from surface (metres) T Time from surface (seconds)
D1 subsea depth (metres) T1 Corrected time (seconds)
 ΔD Isopach ΔT Isochron time (seconds)
Va Average velocity (m/s) Vi Interval velocity (m/s)
Vrms Rms velocity (m/s)

Table 3.5 Average, interval, and rms velocities calculated from check shot survey using program Average velocity.

Appendix 4

- c Program to calculate average velocity from interval velocity for
- c each panel on the seismic section.
- c The program will search for the velocity analysis if it's picked at
- c the reflector
- c If the velocity is not picked at the reflector
- c then the program will interpolate between the velocities above
- c and below the
- c reflector to calculate that velocity at the reflector as shown in the
- c diagram below.



- c Diagram showing velocity above and below the reflector

program avelocity.f

parameter(il=100)

dimension SP(il), T1(il), T2(il), T3(il), T4(il), T5(il), v1(il),

* v2(il), v(il), vr(il)

- c SP is the shot point number
- c T1 is the time where the velocity analysis are picked
- c T2 is the time where the velocity analysis are picked
- c T3 is the time where the velocity is need to be calculated.

- c T4 is the difference above and below reflector
- c T5 is the difference in time between the reflector and time above it.
- c v1 is the velocity above the reflector
- c v2 is the velocity below the reflector
- c v is the difference between the velocities above and below the reflector.
- c Vr is the calculated velocity at the reflector

```

character*60 ahmed1,avelocity,info1,info2,info3,info4,info5,
* info6,info7
write(6,*)'what is the number of the lines?'
read(5,*) NL
write(6,*)'enter the input file'
read(5,*) ahmed1
write(6,*)'enter the output file'
read(5,*)avelocity
open(1,file= ahmed1)
open(2,file= avelocity)
read(1,*)info1, info2, info3, info4, info5, info6, info7
write(2,101) info1, info2, info3, info4, info5, info6, info7
101 format(A6, 3x, 6A10)
do 50 I=1,NL
read(1,*) SP(i), T1(i), T2(i), T3(i), v1(i), v2(i)
write(2,*)SP(i), T1(i), T2(i), T3(i), v1(i), v2(i)
50 continue
write(2,*)'-----'
do 100 j=1, NL

```



```

T4(j)=T2(j)-T1(j)
T5(j)=T3(j)-T1(j)
v(j)=v2(j)-v1(j)
write(2,*)T4(j), T5(j), v(j)
100  continue
      write(2,*)'.....'
      do 300 k=1, NL
        v3(k)=T5(k)*v(k)/T4(k)
        vr(k)=v1(k)+v3(k)
        write(2,*)T5(k), v3(k), vr(k)
300  continue
      stop
      end

```

Table 4.1

SP	T1	T2	T3	V1	V2
140	0.0	630	410	1500	1651
180	0.0	640	420	1500	1711
230	240	630	420	1591	1795
270	0.0	630	445	1500	1731
180	0.0	640	420	1500	1711
230	240	630	420	1591	1795
270	0.0	630	445	1500	1731
310	0.0	620	430	1500	1741
330	0.0	590	410	1500	1825
350	0.0	710	420	1500	1952
390	0.0	730	440	1500	2022

Table 4.1 Time and interval velocity as shown in the seismic section (V07-85) for top Nubian Formation reflector

Table 4.2

T4	T5	V
630	410	151
640	420	211
390	80	204
630	445	231
640	420	211
390	180	204
630	445	231
620	430	241
590	410	325
710	420	452
270	300	597
730	40	522

Table 4.3

T5	V3	Va
410	98	598
420	138	1638
180	94	1685
445	163	1663
420	138	1638
180	94	1685
445	163	1663
430	167	1667
410	225	1725
420	267	1767
30	66	1748
440	314	1814

Table 4.2 and 4.3 Average velocities calculated from the interval velocities for top Nubian reflector using program Avelocity.